Review

Recent progress on magnetic iron oxide nanoparticles: synthesis, surface functional strategies and biomedical applications

Wei Wu[1,2,4], Zhaohui Wu[3,4], Taekyung Yu[3], Changzhong Jiang[2] and Woo-Sik Kim[3]

[1] Laboratory of Printable Functional Nanomaterials and Printed Electronics, School of Printing and Packaging, Wuhan University, Wuhan 430072, People's Republic of China
[2] Key Laboratory of Artificial Micro- and Nano-structures of Ministry of Education, School of Physics and Technology, Wuhan University, Wuhan 430072, People's Republic of China
[3] Department of Chemical Engineering, Kyung Hee University, Korea

E-mail: weiwu@whu.edu.cn, czjiang@whu.edu.cn and wskim@khu.ac.kr

CrossMark

Abstract

This review focuses on the recent development and various strategies in the preparation, microstructure, and magnetic properties of bare and surface functionalized iron oxide nanoparticles (IONPs); their corresponding biological application was also discussed. In order to implement the practical *in vivo* or *in vitro* applications, the IONPs must have combined properties of high magnetic saturation, stability, biocompatibility, and interactive functions at the surface. Moreover, the surface of IONPs could be modified by organic materials or inorganic materials, such as polymers, biomolecules, silica, metals, etc. The new functionalized strategies, problems and major challenges, along with the current directions for the synthesis, surface functionalization and bioapplication of IONPs, are considered. Finally, some future trends and the prospects in these research areas are also discussed.

1. Introduction

Iron oxides are common compounds, which are widespread in nature and can be readily synthesized in the laboratory. Magnetic iron oxides have served humans for centuries, for example, the application of small iron oxide nanoparticles

[4] The authors contributed equally to this work.

(IONPs) as a contrast agent for *in vitro* diagnostics has been practiced for nearly half a century [1–3]. In the past decade, the synthesis of magnetic IONPs has been intensively developed not only for its fundamental scientific interest but also for its many technological applications, such as targeted drug delivery, magnetic resonance imaging (MRI), magnetic hyperthermia and thermoablation, bioseparation, and biosensing [4–7]. Particularly, bioapplications based on magnetic nanoparticles (NPs) have received considerable attention because NPs offer unique advantages over other materials. For example, magnetic IONPs are inexpensive to produce, physically and chemically stable, biocompatible, and environmentally safe [8].
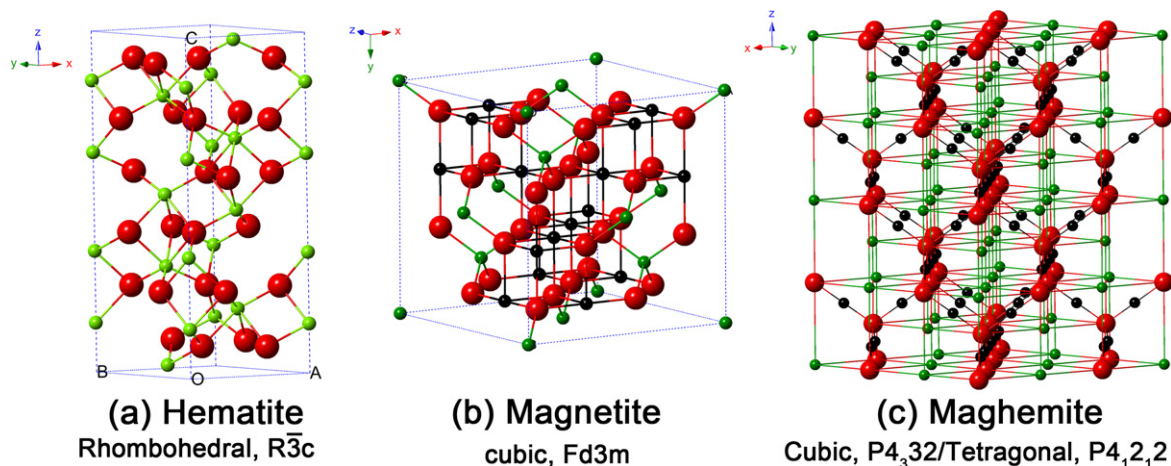
Figure 1. Crystal structure and crystallographic data of the hematite, magnetite and maghemite (the black ball is Fe^{2+}, the green ball is Fe^{3+} and the red ball is O^{2-}).

1.1. Iron oxides

Eight iron oxides are known [9], among these iron oxides, hematite (α-Fe_2O_3), magnetite (Fe_3O_4) and maghemite (γ-Fe_2O_3) are very promising and popular candidates due to their polymorphism involving temperature-induced phase transition. Each of these three iron oxides has unique biochemical, magnetic, catalytic, and other properties which provide suitability for specific technical and biomedical applications.

1.1.1. Hematite (α-Fe_2O_3).

As the most stable iron oxide and *n*-type semiconductor under ambient conditions, hematite (α-Fe_2O_3) is widely used in catalysts, pigments and gas sensors due to its low cost and high resistance to corrosion. It can also be used as a starting material for the synthesis of magnetite (Fe_3O_4) and maghemite (γ-Fe_2O_3), which have been intensively pursued for both fundamental scientific interests and technological applications in the last few decades [10]. Hematite is an *n*-type semiconductor with a band gap of 2.3 eV, where the conduction band (CB) is composed of empty d-orbitals of Fe^{3+} and the valence band (VB) consists of occupied 3d crystal field orbitals of Fe^{3+} with some admixture from the O 2p non-bonding orbitals [11]. As shown in figure 1(a), Fe^{3+} ions occupy two-thirds of the octahedral sites that are confined by the nearly ideal hexagonal close-packed O lattice.

1.1.2. Magnetite (Fe_3O_4).

As shown in figure 1(b), Fe_3O_4 has the face centered cubic spinel structure, based on 32 O^{2-} ions and close-packed along the [111] direction. Fe_3O_4 differs from most other iron oxides in that it contains both divalent and trivalent iron. Fe_3O_4 has a cubic inverse spinel structure that consists of a cubic close packed array of oxide ions, where all of the Fe^{2+} ions occupy half of the octahedral sites and the Fe^{3+} are split evenly across the remaining octahedral sites and the tetrahedral sites. In stoichiometric magnetite $Fe^{II}/Fe^{III} = 1/2$, and the divalent irons may be partly or fully replaced by other divalent ions (Co, Mn, Zn, etc). Thus, Fe_3O_4 can be both an *n*- and *p*-type semiconductor. However,
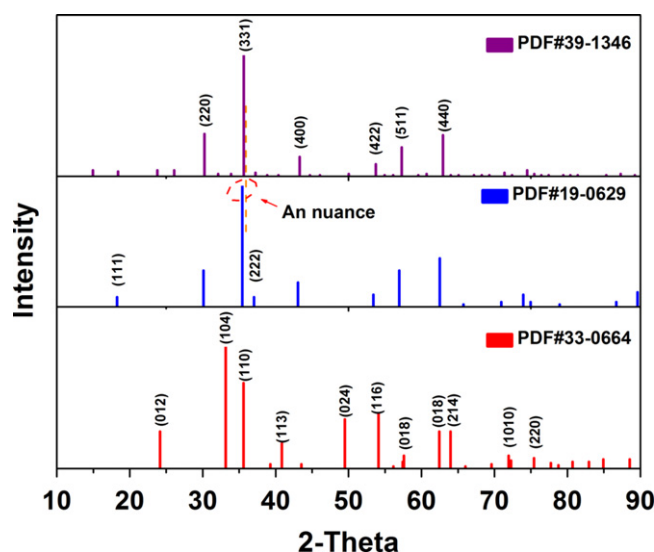

Figure 2. The XRD peak lines from standard powder diffraction files of α-Fe_2O_3 (33–0664), Fe_3O_4 (19–0629) and γ-Fe_2O_3 (39–1346).

Fe_3O_4 has the lowest resistivity among iron oxides due to its small bandgap (0.1 eV) [12].

1.1.3. Maghemite (γ-Fe_2O_3).

As shown in figure 1(c), the structure of γ-Fe_2O_3 is cubic; each unit of maghemite contains 32 O^{2-} ions, 21⅓ Fe^{3+} ions and 2⅓ vacancies. Oxygen anions give rise to a cubic close-packed array while ferric ions are distributed over tetrahedral sites (eight Fe ions per unit cell) and octahedral sites (the remaining Fe ions and vacancies). Therefore, the maghemite can be considered as fully oxidized magnetite, and it is an *n*-type semiconductor with a bandgap of 2.0 eV.

Figure 2 shows the x-ray diffraction (XRD) peak lines from the standard powder diffraction files of α-Fe_2O_3 (33–0664), Fe_3O_4 (19–0629) and γ-Fe_2O_3 (39–1346), and it can be found that γ-Fe_2O_3 has a crystal structure similar to that of Fe_3O_4. The diffractogram of the cubic form of γ-Fe_2O_3 is identical to that of Fe_3O_4 with some line shift towards higher angles. It is noteworthy that the annealing treatment is

a key step in most synthesis of different crystalline phase iron oxides. Any type of iron oxide can be obtained from the other types by oxidizing or reducing the annealing treatment. Thus, the XRD patterns are a basic characterization technique for determining the crystal structure and types of magnetic IONPs.

1.2. Size, shape and magnetic properties

Understanding the correlation between the magnetic properties and the size and shape of IONPs is a prerequisite for widespread applications of magnetism in data storage and bio-separation areas [13]. Generally, α-Fe_2O_3 has weak ferromagnetism at room temperature, while the saturation magnetization is often smaller than 1 emu g^{-1}. However, γ-Fe_2O_3 and Fe_3O_4 exhibit ferrimagnetism at room temperature, with the saturation magnetization reaching to 92 emu g^{-1} [14]. It is noteworthy that many properties of IONPs depend on their size and shape. For example, Levy *et al* studied the magnetic properties of IONPs from 6 to 18 nm, the results revealed that magnetic disorder was particularly evident for 13–18 nm IONPs due to a drastic loss of their hyperthermia performance [15]. Guardia *et al* reported that pseudospherical and faceted IONPs with a narrow size distribution (4–20 nm) and a high saturation magnetization ($M_s \approx 80$–85 emu g^{-1} at 5 K) were obtained by thermal decomposition using oleic acid as a surfactant. In contrast, decanoic acid yields much larger pseudocubic IONPs (45 nm) with a broader size distribution and a larger saturation magnetization ($M_s = 92$ emu g^{-1} at 5 K), which is close to the expected value for bulk magnetite [16]. One-dimensional iron oxide nanostructures are very appealing, owing to their many unique physicochemical properties based on high intrinsic anisotropy and surface activity. Recently, we showed a comparative study of the magnetic behavior of single and tubular clustered Fe_3O_4 NPs. The results revealed that the competition of the demagnetization energy of shape and the magnetocrystalline anisotropy energy of small IONPs would increase the coercivity, and the magnetic properties are strongly influenced by the morphology of the Fe_3O_4 NPs [17]. In general, IONPs become superparamagnetic at room temperature when the size of IONPs is below about 15 nm, meaning that the thermal energy can overcome the anisotropy energy barrier of a single nanoparticle. However, aggregation among superparamagnetic IONPs is a common phenomenon. Hence, for protecting bare IONPs against aggregation, the magnetic properties can be tailored by the coating materials, such as Au, Ag and Co_3O_4.

There are a number of magnetic properties for characterization of IONPs. The most decisive properties are the response type to the magnetic field (including ferromagnetic, paramagnetic, antiferromagnetic and ferrimagnetic) and magnetization, which can be measured from the hysteresis loops (M–H) and zero-field cooled/field cooled (ZFC/FC, M–T) curves. As shown in figure 3(a), the saturation magnetization (M_s), remanence magnetization (M_r) and coercivity (H_C) can be obtained from the hysteresis loops. When the IONPs are superparamagnetic, the M–H curve should show

no hysteresis, and the forward and backward magnetization curves overlap completely and are almost negligible [17, 18]. As shown in figure 3(b), in ZFC measurements, the samples were cooled from 300 to 10 K without applying an external field. After reaching 10 K, an external field was applied, and the magnetic moments were recorded as the increased temperature. Conversely, for FC measurements, the samples were cooled from 300 K under an applied external field, and then the magnetic moments were recorded as the increased temperature. When the IONPs are cooled to the zero magnetic field temperature, the total magnetization of the IONPs will be zero since the magnetization of the individual IONPs is randomly oriented. An external magnetic field energetically favors the reorientation of the moments of the individual particle along the applied field at low temperatures. Thus, upon increasing the temperature, all ZFC magnetic moments increase and reach a maximum, where the temperature is referred to as the blocking temperature (T_B). T_B is defined as the temperature at which NPs' moments do not relax (known as blocked) during the time scale of the measurement [19, 20]. The high field can lower the energy barriers between the two easy axis orientations, therefore, lowering the blocking temperature. Moreover, if the applied field reaches a critical value, the blocking temperature will disappear [13].

2. Synthesis methods of magnetic IONPs

To date, a variety of synthetic methods such as co-precipitation, thermal decomposition, hydrothermal and solvothermal syntheses, sol–gel synthesis, microemulsion, ultrasound irradiation and biological synthesis have been applied to produce magnetic IONPs. These methods can be divided into aqueous and non-aqueous routes. Aqueous approaches are attractive in terms of their low cost and sustainability; there is, however, a generic challenge in directly obtaining water-soluble monodisperse magnetic IONPs without size selection. Non-aqueous routes generally obtained IONPs which only dissolved in nonpolar solvents. Various magnetic nanostructures with different morphologies have been synthesized, including particles, wires, and rods.

2.1. Co-precipitation

As the most conventional method, the co-precipitation method consists of mixing ferric and ferrous ions in a 1:2 molar ratio in very basic solutions at room temperature or at elevated temperature. The reaction mechanism can be simplified as: $Fe^{2+} + 2Fe^{3+} + 8OH^- \leftrightarrows Fe(OH)_2 + 2Fe(OH)_3 \rightarrow Fe_3O_4\downarrow + 4H_2O$. Usually, the reaction undergoes gas protection. The nucleation of the Fe_3O_4 nucleus is easier when the solution pH is lower than 11, while the growth of the Fe_3O_4 nucleus is easier when the solution pH is higher than 11.

After the pioneering work prepared by Massart [21], co-precipitation was widely studied in preparing Fe_3O_4 NPs for its extraordinary advantages, such as gram-scale production
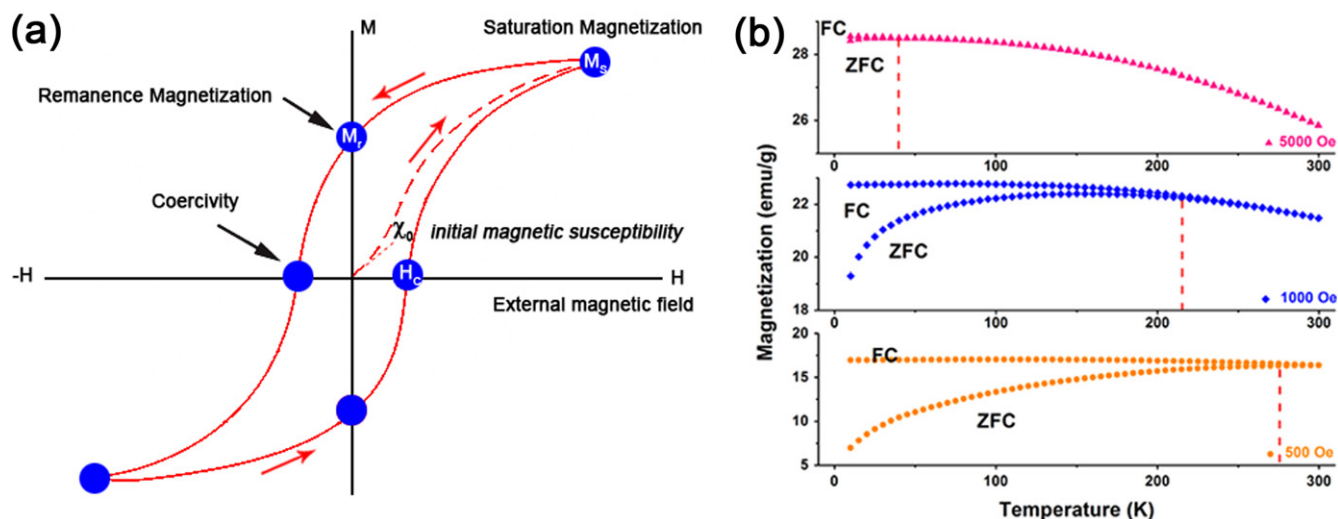
Figure 3. Schematic presentation of the typical hysteresis loops of IONPs (a); the ZFC/FC curves of γ-Fe$_2$O$_3$ at the different applied field (b).
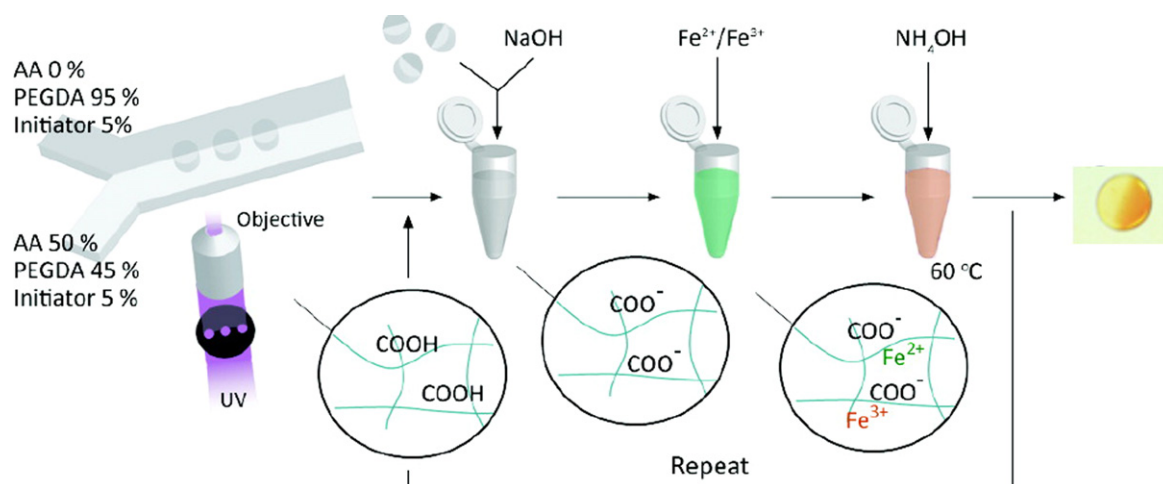

Figure 4. Schematic showing the *in situ* co-precipitation synthesis process of IONPs in polymer. (Reprinted with permission from S K Suh *et al* 2012 *J. Am. Chem. Soc.* **134** 7337. Copyright 2012 American Chemical Society.)

and facility. We have reported the large-scale co-precipitation synthesis of Fe$_3$O$_4$ NPs, where their corresponding morphology, structure, and magnetic properties at different reaction temperatures were investigated [22]. Recently, several modified co-precipitation methods have been developed; for example, as reported by Wu *et al*, magnetic Fe$_3$O$_4$ nanopowders with an average diameter of 15 nm were synthesized by ultrasonic-assisted chemical co-precipitation utilizing high purity iron separated from iron ore tailings by an acidic leaching method [23]. The present synthesis method of Fe$_3$O$_4$ NPs easily yields SPIONPs without a protecting gas. Recently, superparamagnetic Fe$_3$O$_4$ NPs with sizes of 4.9–6.3 nm were synthesized by a one-step aqueous co-precipitation route based on the use of alkanolamines as the base, the reported methodology provides a simple, versatile, and cost-effective route for the high-yield synthesis of IONPs featuring improved magnetic properties and small particle sizes [24]. Typically, small size leads to low magnetic properties; the above results showed improved magnetic properties while keeping their small size.

Currently, the problems of aggregation and biocompatibility of IONPs perhaps hinder the applications in biomedical fields. Therefore, many surfactants and biomolecules have been introduced directly in the co-precipitation process. For instance, Salavati-Niasari *et al* have reported Fe$_3$O$_4$ NPs with a size range of 25 nm that were prepared by a facile chemical co-precipitation method; the surfactant octanoic acid was present in the reaction system to improve the dispersity [25]. Liu *et al* have prepared magnetic chitosan coated Fe$_3$O$_4$ NPs by the co-precipitation method under 0.45 T static magnetic fields, which assisted the glutaraldehyde cross-linking reaction; the water was replaced by 2% chitosan in an acetic acid solution during the reaction process. The resulting NPs were used to immobilize lipase [26]. Recently, Suh *et al* have reported an *in situ* synthesis of nonspherical magnetic IONPs in a carboxyl functionalized polymer matrix, in which the iron ions diffused into the polymer particles and they were allowed to chelate with the deprotonated carboxyl groups, nucleated and finally grew to the IONPs in the polymer particles (figure 4) [27]. This method can be used to add multiple

functionalities, such as the addition of biomolecules after subsequent reactions.

However, control over particle size, morphology and composition in the co-precipitation route is limited as particle kinetically controlled growth. The size, shape and composition of the IONPs depend on the experimental parameters, such as the types of iron salts (chlorides, perchlorates, sulfates, nitrates, etc), Fe(II)/Fe(III) ratio, pH value and ionic strength of the medium. For example, Blanco-Andujar *et al* have synthesized uncoated IONPs by using sodium carbonate as a co-precipitating agent; the reaction proceeded sufficiently slowly to enable a detailed study of both the reaction pathway and products [28]. Pereira *et al* have synthesized superparamagnetic ferrite NPs (MFe_2O_4, where M = Fe, Co, Mn) through a novel one-step aqueous co-precipitation method on the basis of using a new type of alkaline agent, including alkanolamines isopropanolamine and diisopropanolamine. Remarkably, the resulting NPs exhibited smaller particle sizes (up to 6 times) and enhanced saturation magnetization (up to 1.3 times) relative to those prepared with NaOH [24]. We also investigated the effect of the drying method on the change of the morphology and magnetic properties of IONPs, and the results revealed that NPs obtained by vacuum drying tend to be agglomerated more easily when the average diameter of the grain decreased in pace with the evaporation of the surface adsorptive water and inner containing water, though the structure and morphology are maintained better by ambient air drying. Among all the drying treatments, the highest saturation magnetization was obtained after drying in a vacuum at 70 °C. This finding is instructive to elucidate in depth some relationship between structure and magnetic property [22].

Although the co-precipitation method is one of the successful and classical techniques for synthesizing IONPs with high saturation magnetization, more attention should be paid to overcoming the shortcomings of this method, such as the broad particle size distribution of products, and the utilization of a strong base in the reaction process.

2.2. High-temperature thermal decomposition

The above co-precipitation method involves fast particle formation rates and therefore, particle size and size distribution are hardly controlled. To avoid the limitations of this method, different alternative strategies have been developed, such as nonaqueous thermal decomposition strategies. In principle, the thermal decomposition strategies can be subdivided into hot-injection approaches, where the precursors are injected into a hot reaction mixture, and conventional reaction strategies where a reaction mixture is prepared at room temperature and then heated in a closed or open reaction vessel.

Due to the fact that most of the reactions are carried out at room temperature in co-precipitation, the obtained IONPs often exhibit low crystallinity. In contrast, higher monodisperse, narrow size distribution and highly crystalline magnetic IONPs are obtained from high-temperature thermal decomposition of organometallic or coordinated iron
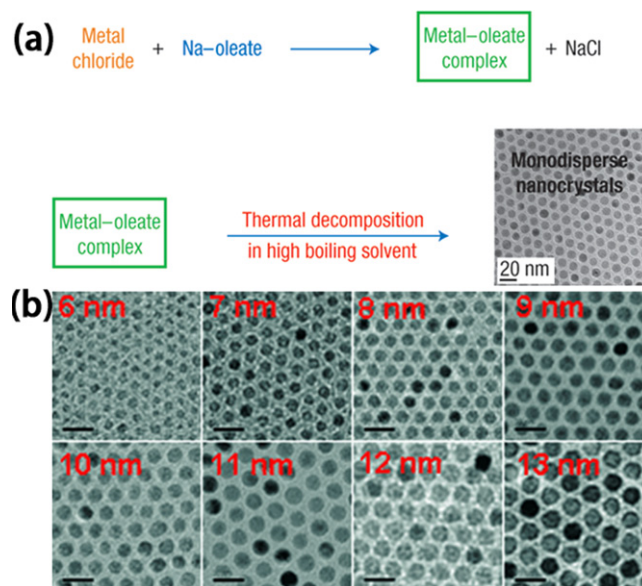

Figure 5. Metal–oleate precursors were prepared from the reaction of metal chlorides and sodium oleate. The thermal decomposition of the metal–oleate precursors in the high boiling solvent produced monodisperse nanocrystals (a). (Reprinted with permission from J Park *et al* 2004 *Nat. Mater.* **3** 891. Copyright 2004 Nature Publishing Group.) Transmission electron microscopy (TEM) images of 6, 7, 8, 9, 10, 11, 12, and 13 nm-sized air-oxidized IONPs showing the one nanometer level increments in diameter (b). (Reprinted with permission from J Park *et al* 2005 *Angew. Chem. Int. Edn* **44** 2872. Copyright 2005 John Wiley and Sons.)

precursors in organic solvents, which display superior properties to those obtained by co-precipitation, since nucleation can be separated from growth and complex hydrolysis reactions can be avoided [29, 30]. The as-used ferric salts include $Fe(CO)_5$ [31], $Fe(acac)_3$ (acac = acetylacetonate) [32], iron oleate [33], $Fe(Cup)_3$ (Cup = N-nitrosophenylhydroxylamine) [34, 35], Prussian blue ($Fe_4[Fe(CN)_6 \cdot 14H_2O]$) [36, 37], Fe–urea complex ($[Fe(CON_2H_4)_6](NO_3)_3$) [38], ferrocene (Fe$(C_5H_5)_2$) [39], and $Fe_3(CO)_{12}$ [40]. To obtain monodisperse IONPs, various organic molecules including oleic acid, 1-octadecene, 1-tetradecene, and oleylamine, are often added in the reaction process as stabilizers. The stabilizer can slow down the nucleation process and it affects the adsorption of additives on the nuclei and the growing nanocrystals, which may inhibit the growth of the IONPs, and favor the formation of small IONPs. The as-obtained products are usually spherical NPs with sizes of below 30 nm and their size-distribution can only be controlled to a small extent.

As shown in figure 5, Hyeon *et al* have reported a synthetic method of obtaining monodisperse IONPs by using inexpensive and nontoxic iron chloride rather than toxic and expensive iron pentacarbonyl. An organic solvent dispersion containing the iron–oleate complex and a surfactant was slowly heated to the boiling point of the solvent to produce monodisperse IONPs. In a single reaction, as much as 40 g of monodisperse IONPs was generated without any size-selection process [41]. The size of the IONPs was controlled by changing the aging temperature and other parameters. This concept of continuous growth without additional nucleation
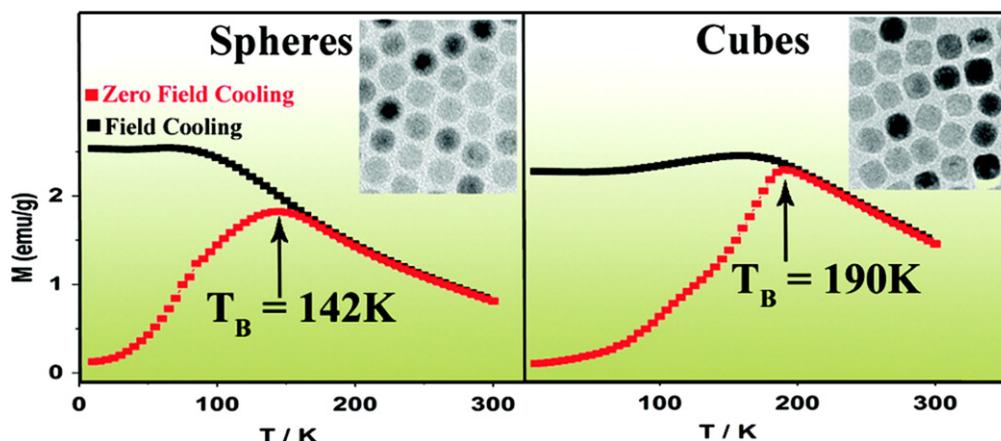
Figure 6. Monodisperse IONPs with spherical and cubic morphologies are prepared by the thermal decomposition of FeOOH, and exhibit very different blocking temperatures. (Reprinted with permission from R Chalasani and S Vasudevan 2011 *J. Phys. Chem.* C **115** 18088. Copyright 2010 American Chemical Society.)

could be applicable to other materials, and the synthetic procedure is highly reproducible.

Moreover, the thermal decomposition method is often used to prepare iron oxide with different shapes, such as nanocubes and nanospheres. For example, Amara *et al* synthesized Fe_3O_4 nanocubes and nanospheres by solventless thermal decomposition of various mixtures of ferrocene and polyvinylpyrrolidone (PVP). The described method offered a new simple, single-step process for the preparation of magnetite nanocubes/spheres [42]. As shown in figure 6, Chalasani and Vasudevan have reported monodisperse iron oxide nanocrystals with spherical and cubic morphologies that were prepared by the thermal decomposition of FeOOH. The higher T_B values in particles of cubic morphology are shown to be a consequence of exchange bias fields. The results reveal that the exchange bias fields originate from the presence of trace amounts of wustite, FeO [43]. In fact, the magnetic properties of IONPs are also associated with the shape and size of the NPs [16, 44, 45].

Additionally, the shape and size of IONPs can also be tailored by the use of different precursors, additives and solvents during the thermal decomposition process. Shavel and Liz-Marzán have reported a detailed overview on the effect of various synthesis parameters during the synthesis process of IONPs with different shapes, through high-temperature decomposition of a preformed iron oleate complex. While this procedure has been previously shown to produce monodisperse magnetite spheres, the use of specific additives is demonstrated to allow for the preparation of strongly faceted iron oxide nanocrystals, with either cubic or octahedral shapes. Additionally, using squalene or octadecene as the solvent was found to induce the reduction of the iron precursors and thereby lead to the formation of NPs with core–shell (in the case of nanocubes) or island-like structures (in the case of octahedrons) of Fe^0/iron oxide [46]. Demortière *et al* reported a fine control of IONP diameters from 2.5 to 14 nm by using different types of solvents, including eicosene (14 nm), di-*n*-octyl ether (11 nm), dibenzyl ether

(9 nm), di-*n*-octyl ether (5 nm), hexadecene (3.5 nm), and di-*n*-hexyl ether (2.5 nm) [47].

Hyeon's method is commonly used for the synthesis of monodisperse and reproducible IONPs with a tailored size [41, 48]. However, the nucleation of IONPs in thermal decomposition involves boiling the solvents, so the accurate shape of the IONPs is not fully reproducible. Recently, Lynch *et al* conducted a mechanistic study on the synthesis of colloidal IONPs by thermal decomposition; gas bubbles were generated by boiling solvents or artificial Ar bubbling, and the results illustrated that gas bubbles had a stronger effect on the nucleation of IONPs than on their growth [49]. It is noteworthy that the IONPs resulting from the thermal decomposition method are usually dissolved in nonpolar solvents.

2.3. Hydrothermal and solvothermal synthesis

The aqueous solution route is used for the fabrication of α-Fe_2O_3 and Fe_3O_4 NPs; the solution synthesis for γ-Fe_2O_3 usually involved the controlled oxidation of Fe_3O_4 and the direct mineralization of Fe^{3+} ions. Subsequently, other non-aqueous solution methods have also been developed to synthesize highly crystalline, monodisperse, and shape-controlled γ-Fe_2O_3 NPs, in which organometallic compounds were always used as precursors. However, hydrothermal or solvothermal synthesis includes various wet-chemical techniques of crystallizing the substance in a sealed container from the high temperature aqueous or non-aqueous solution (generally in the range 130–250 °C) under high vapor pressure (generally in the range 0.3–4 MPa) [1]. This method has also been used to grow dislocation-free single crystal particles, and grains formed in this process could have a better crystallinity than those from other processes, and hence hydrothermal and solvothermal synthesis are prone to obtaining highly crystalline IONPs, including α-Fe_2O_3, γ-Fe_2O_3, and Fe_3O_4 NPs.

Possible advantages of the hydrothermal method over other types of crystal growth include the ability to create crystalline phases which are not stable at the melting point. In addition, materials which have a high vapor pressure near
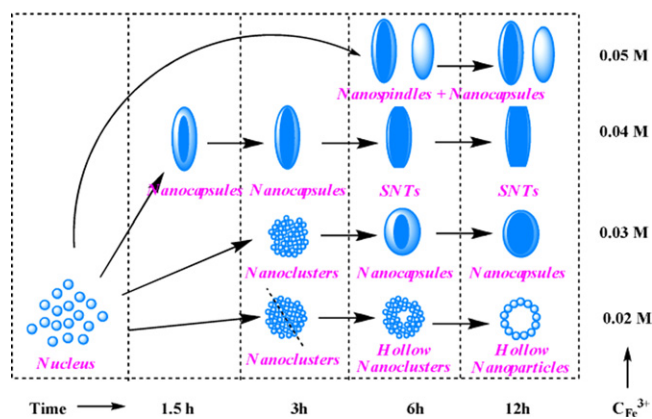
Figure 7. Schematic illustration of the shape evolution for hematite nanostructures at different reaction times and different ferric concentrations. (Reprinted with permission from W Wu *et al* 2010 *J. Phys. Chem.* C **114** 16092. Copyright 2010 American Chemical Society.)

their melting points can also be grown by the hydrothermal method [50]. The method is also particularly suitable for the growth of good-quality iron oxide nanocrystals while maintaining good control over their composition. It has to be pointed out that the concepts embodied in the hydrothermal process have already been extrapolated to non-aqueous systems, and the so-called 'solvothermal process' has emerged, in which an organic solvent is used as the reaction medium instead of water. See [51] for an overview of the current state-of-the-art of hydrothermal synthesis routes for the synthesis of a rich family of IONPs with different shapes or assembled complex nanostructures.

Moreover, the hydrothermal and solvothermal route is a facile and conventional method for obtaining hollow IONPs. In a typical procedure, using Fe^{3+} as the iron resource, acetate, urea, and sodium citrate are mixed in ethylene glycol under stirring, then the resultant homogeneous dispersion is transferred to a Teflon-lined stainless steel autoclave and sealed to heat at about $200\,°C$ for 8–24 h [52–55]. Furthermore, the hydrothermal and solvothermal synthesis route has been developed to prepare IONPs with controllable size and shape [56–59]. For example, Ma *et al* developed a facile template-free synthetic route for the controlled fabrication of various α-Fe_2O_3 nanostructures, such as small NPs, nanopolyhedra, and NP-aggregated microcubes, by simply controlling the synthesis parameters such as reaction time and solvent [60]. Recently, Tian *et al* reported a facile solvothermal approach to synthesize ultrasmall monodisperse Fe_3O_4 NPs with a precise size control of 1 nm, in which Fe(acac)$_3$ acted as an iron source, *n*-octylamine as a reductant, and *n*-octanol as a solvent [61].

In addition, the hydrothermal and solvothermal route is beneficial to obtaining shape-controlled IONPs. We present a facile approach for the production of magnetic iron oxide short nanotubes (SNTs) and other shapes (NPs, nanorings) employing an anion-assisted hydrothermal route by using phosphate and sulfate ions. As shown in figure 7, the size, morphology, shape, and surface architecture control of the iron oxide SNTs are achieved by simple adjustments of ferric

ion concentration without any surfactant assistance. Investigation of the formation mechanism reveals that the ferric ion concentrations, the amount of anion additive, and the reaction time contribute significantly to SNT growth. The shape of the SNTs is mainly regulated by the adsorption of phosphate ions on faces parallel to the long dimension of elongated α-Fe_2O_3 NPs (axis) during nanocrystal growth, and the hollow structure is given by the preferential dissolution along the *c*-axis due to the strong coordination of the sulfate ions. Moreover, the as-synthesized hematite (α-Fe_2O_3) SNTs can be converted to magnetite (Fe_3O_4) and maghemite (γ-Fe_2O_3) ferromagnetic SNTs by a reducing atmosphere annealing process while preserving the same morphology [10].

2.4. Sol–gel reactions and polyol method

The sol–gel process is a classical wet-chemical technique widely used in the fields of materials science and ceramic engineering. Such a method is used primarily for the fabrication of materials (typically metal oxides). Generally, it involves starting from a colloidal solution that acts as the precursor for an integrated network of either discrete particles or network polymers. In this system, a sol is a stable dispersion of colloidal particles or polymers in a solvent. A gel consists of a three dimensional continuous network, which encloses a liquid phase. In a colloidal gel, the network is built from the agglomeration of colloidal particles. In a polymer gel, the particles have a polymeric sub-structure made by aggregation of sub-colloidal particles. Generally, sol particles may interact by Van der Waals forces or hydrogen bonds, and a gel may also form from linking polymer chains. In most gel systems used for materials synthesis, the interactions are of a covalent nature and the gel process is irreversible. The gelation process may be reversible if other interactions are involved. Typical precursors for the synthesis of IONPs are iron alkoxides and iron salts (such as chlorides, nitrates and acetates), which undergo various forms of hydrolysis and polycondensation reactions [62]. These reactions are performed at room temperature, and further heat treatments are needed to acquire the final crystalline state. By this method, the IONPs will form through at least a two-step phase transformation: $Fe(OH)_3 \rightarrow \beta$-$FeOOH \rightarrow \gamma$-$Fe_2O_3$ [63]. The final properties of IONPs are highly dependent upon the structure created during the sol stage of the sol–gel process. For example, Lemine *et al* reported Fe_3O_4 NPs with an average particle size of 8 nm were successfully prepared by the sol–gel method. The saturated magnetization could be up to $47\,emu\,g^{-1}$ at room temperature, and it was expected that these NPs were promising materials for biomedical applications [64]. Recently, Qi *et al* reported Fe_3O_4 NPs in the interval of $9 \sim 12$ nm that were synthesized by a non-alkoxide sol–gel method. Through this technique, sol–gel materials were prepared from ethanolic solutions of metal chlorides without the need for alkoxides, polymeric gel agents, or elaborate reaction schemes [65].

The different organic precursors are the crucial roles in controlling the shape and crystal structure of IONPs. For

example, Woo *et al* have described a sol–gel mediated synthesis of Fe_2O_3 nanorods with controlled phase depending on the conditions. The diameter and length of the nanorods could be controlled by the H_2O/oleic-acid ratio in the gelation process, and the phase of the nanorods could be controlled by the temperature, atmosphere, and hydrous state of the gels during crystallization [66]. In our previous report, water-soluble hollow spherical Fe_3O_4 nanocages (about 100 nm) with high saturation magnetization were prepared by applying glutamic acid as an additive in a one-pot sol–gel process and subsequent annealing to synthesize γ-Fe_2O_3 nanocages with similar nanostructures. The results indicated that glutamic acid played an important role in the formation of the cage-like nanostructures [18, 67].

The polyol method is also understood as an inversed sol–gel method (the sol–gel method uses an oxidation reaction but polyol synthesis uses a reduction reaction), which is well suited for the preparation of IONPs with various shapes and sizes [68]. In the polyol synthesis process, the polyols not only serve as solvents but also reducing agents, which apply as stabilizers to control particle growth and prevent interparticle aggregation. In the typical reaction process, an iron precursor compound is suspended in a liquid polyol. The suspension is stirred and heated to a given temperature that can reach the boiling point of the polyol. Compared to the hydrothermal method, this reaction does not require high pressure, thus, it is unnecessary to operate in the Teflon-lined stainless steel autoclave. For example, Cai and Wan fabricated monodisperse Fe_3O_4 NPs by utilizing four types of polyols to reduce $Fe(acac)_3$ in a similar reaction procedure, including ethylene glycol (EG), diethylene glycol (DEG), triethylene glycol (TREG) and tetraethylene glycol (TEG). Only the TREG can yield non-agglomerated Fe_3O_4 NPs with uniform shape and narrow size distribution. The result illustrates that the polyol solvent plays a crucial role in determining the morphology and colloidal stability of the resulting particles [69]. Indeed, the polyol solvent also plays an important role in determining the size and magnetic properties of IONPs: different polyols will generate IONPs with different sizes [70, 71].

In comparison with the co-precipitation method, the sol–gel and polyol methods for IONPs have several advantages. For example, the IONPs can be easily dispersed in aqueous media and other polar solvents because the surface of IONPs contain many hydrophilic ligands. Also the relatively high reaction temperature of these two methods favors IONPs with higher crystallinity and saturation magnetization. Nevertheless, the disadvantages of the sol–gel process are the relatively high cost of the metal alkoxides and the release of large amounts of alcohol during the calcination step, requiring safety considerations during the sol–gel process.

2.5. Microemulsion

Microemulsions are clear, stable, and isotropic liquid mixtures of oil, water and surfactant, frequently in combination with a co-surfactant. The surfactant molecules may form a monolayer at the interface between the oil and water, with the hydrophobic tails of the surfactant molecules dissolved in the oil phase and the hydrophilic head groups in the aqueous phase, and vice versa. In this system, the aqueous phase may contain metal salts and/or other ingredients, and the 'oil' may actually be a complex mixture of different hydrocarbons and olefins. The two basic types of microemulsions are direct (oil dispersed in water, o/w) and reversed (water dispersed in oil, w/o), which have all been used to synthesize IONPs with tailored shape and size. Common surfactants including bis(2-ethylhexyl) sulfosuccinate (AOT), sodium dodecyl sulfate (SDS), cetyltrimethylammonium bromide (CTAB), and PVP have been widely used in the fabrication of magnetic IONPs [72–74]. Generally, the size control and the dynamics of IONP formation can be achieved by varying, for instance, the droplet size, the initial concentration of reactants and the nature of surfactants.

Recently, Darbandi *et al* reported that uniformly sized and crystalline IONPs with a spinel structure and mean diameters of about 3, 6 and 9 nm were synthesized in high yield using the microemulsion route at room temperature. During this process, the capping agent (polyoxyethylene (5) non-ylphenylether as surfactant) was capable of preventing the agglomeration effect, which can occur in case of direct particle contact [75]. Okoli *et al* synthesized magnetic IONPs for protein binding and separation using w/o and o/w microemulsions, respectively. The potential of both approaches for the production of nanocrystalline magnetic IONPs with high surface area for protein binding/protein purification are investigated and compared. The average specific surface areas of the IONPs are 147 $m^2 g^{-1}$ for w/o and 304 $m^2 g^{-1}$ for o/w microemulsions. A higher specific surface area seen in o/w microemulsions is attributed to the small size of the nanoparticle. The protein bound IONPs exhibited a significant reduction of the removal rate of clay particles in suspension as compared to bare IONPs, evidencing a significant interaction between the magnetic IONPs and the protein [76, 77].

However, despite the presence of surfactants, the aggregation of the produced magnetic IONPs usually requires several washing processes and further stabilization treatments for them to be used in biomedical applications.

2.6. Sonolysis or sonochemical method

The sonolysis (sonochemical or ultrasound irradiation) method uses the chemical effects of ultrasound arising from acoustic cavitation. High intensity ultrasound is used for the production of novel structures and provides an unusual route to known materials without bulk high temperatures, high pressures, or long reaction times [78]. Under ultrasound irradiation, the alternating expansive and compressive acoustic waves create bubbles (i.e., cavities) and make the bubbles oscillate. The oscillating bubbles can accumulate ultrasonic energy effectively while growing to a certain size (typically tens of mm). Under the right conditions, a bubble can overgrow and subsequently collapse, releasing the concentrated energy stored in the bubble within a very short time (with a heating and cooling rate of $>10^{10} K s^{-1}$). This cavitational implosion is really localized and transient with a
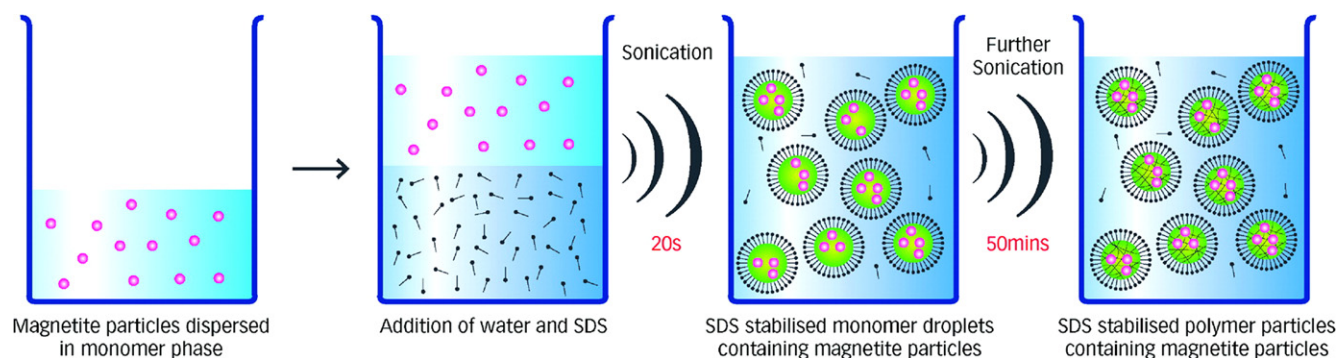
Figure 8. Schematic diagram of the procedure for the encapsulation of Fe_3O_4 NPs and monomer droplet to latex particle conversion by the sonochemically driven miniemulsion polymerization pathway. (Reprinted with permission from B M Teo *et al* 2009 *Langmuir* **25** 2593. Copyright 2009 American Chemical Society.)

temperature of 5000 K and a pressure of 1000 bar [1, 79, 80]. Therefore, the sonolysis method is employed to prepare various forms of bare and functionalized IONPs by the sonication of an aqueous ferro or ferrous salt solution, and the experimental process is often carried out under ambient conditions (usually in the presence of air) [81–85].

The sonolysis method can be used to synthesize biocompatible IONPs. For instance, Theerdhala *et al* reported on the binding of a semi-essential amino acid, L-arginine, onto the surface of Fe_3O_4 NPs, creating a stable aqueous suspension by a one-step method through sonochemical synthesis. These surface-functionalized IONPs could become a promising vehicle for drug delivery [86]. Recently, Zhu *et al* synthesized Fe_3O_4 NPs of 30–40 nm by a sonochemical method, and these NPs were uniformly dispersed on reduced graphene oxide sheets (Fe_3O_4/RGO). The composite Fe_3O_4/RGO was immobilized with hemoglobin to fabricate a biosensor for detecting H_2O_2. The biosensor demonstrated a fast response to H_2O_2 (within 10 s) and displayed an excellent linear relationship at 4×10^{-6} to 1×10^{-3} M with the detection limit of 2×10^{-6} M (S/N = 3) [87].

In addition, the ultrasound-initiated procedure, as a technology, represents an effective and innocuous means of producing a range of nanocomposites, consisting of multiple combinations of different polymers and encapsulated materials. Teo *et al* have developed a simple and efficient method for preparing 100 nm latex beads loaded with a high content of Fe_3O_4 NPs; the formation procedure of Fe_3O_4 NPs under the ultrasound-initiated effect is well illustrated in figure 8. The NPs exhibited excellent colloidal stability (remained suspended stably in an aqueous solution for more than 12 months with no noticeable degradation) and strong magnetic properties (superparamagnetic with a saturated magnetization of 24 emu g^{-1}), and were of the desired size to be technologically relevant [88]. The sonochemical method has some advantages, including uniformity of mixing and reduction of crystal growth, which can also lead to an acceleration effect in chemical dynamics and rates of the reactions. However, the sonolysis method is not beneficial to realize the fabrication of IONPs with controllable shapes and dispersity.

2.7. Microwave-assisted synthesis

It has long been known that molecules undergo excitation with electromagnetic radiation. This effect is utilized in household microwave ovens to heat food. However, microwave-assisted synthesis has only been used as a reaction methodology by chemists for a few years. Excitation with microwave radiation results in the molecules aligning their dipoles within the external field. Strong agitation, provided by the reorientation of molecules, in phase with the electrical field excitation, causes an intense internal heating. Therefore, microwave-assisted synthesis can significantly reduce the processing time and energy cost, due to its almost instantaneous 'in core' heating of materials in a homogeneous and selective manner, different from the classical ones.

The microwave-assisted synthesis method has been widely used to prepare magnetic IONPs with controllable size and shapes recently [89–92]. For example, Sreeja and Joy reported the fabrication of superparamagnetic γ-Fe_2O_3 NPs with an average diameter of 10 nm using the microwave-assisted method at 150 °C, in a short time-duration of 25 min. Their work showed that lower temperature and less reaction time were required to obtain comparable results by microwave heating [93]. Jiang *et al* have reported cubic IONPs that were prepared via the microwave-assisted method followed by Ostwald ripening procedures. The results illustrated the phase and magnetic properties of IONPs would change by varying the experimental conditions [94]. Indeed, the phase of IONPs by the microwave-assisted synthesis could be slightly different depending on the experimental conditions. For instance, Hu *et al* synthesized three major iron oxide phases: magnetite, maghemite and hematite, under microwave treatment in an autoclave, from alcohol/water solutions of chloride salts in the presence of NaOH. The results revealed that the pure hematite phase can be obtained in the presence of single precursor $FeCl_3$. When $FeCl_2$ was used as the single precursor, magnetite or maghemite NPs were produced depending on the drying process used [95]. Additionally, the microwave-assisted synthesis method is often employed to prepare biocompatible magnetic IONPs. Recently, Osborne reported a rapid and straightforward microwave-assisted synthesis of superparamagnetic dextran-coated IONPs. The
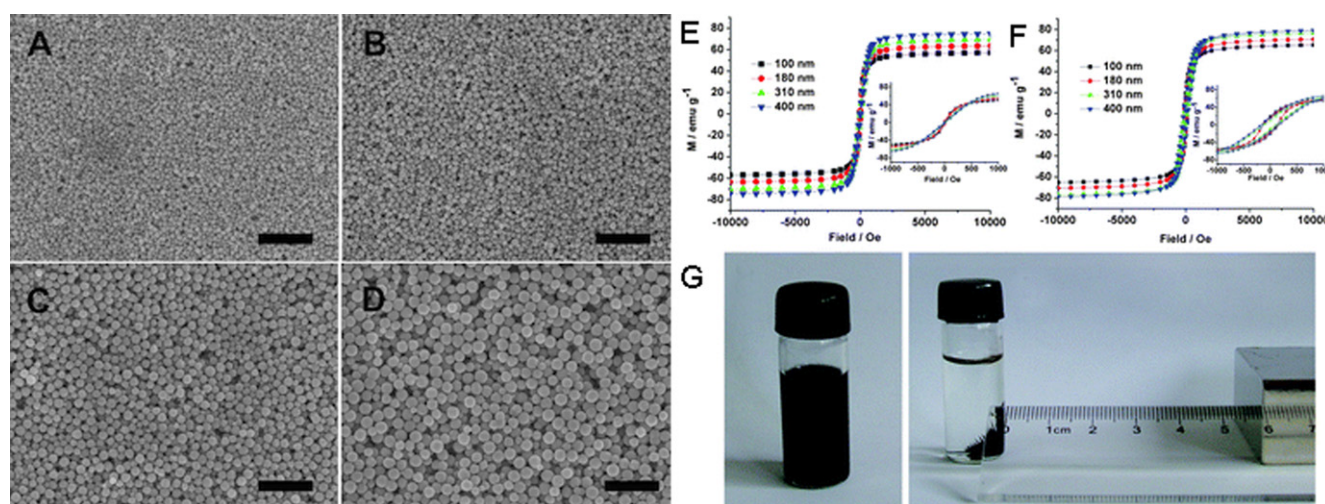
Figure 9. Typical SEM images of the polyacrylic acid-Fe$_3$O$_4$ hybrid nanostructure synthesized using different initial iron amounts of 0.7 mmol (A), 1.5 mmol (B), 3.0 mmol (C), and 5.0 mmol (D). All of the scale bars are 2 μm. Magnetization curves of the hybrid nanostructure with different sizes at a temperature of 300 K and 1.8 K. Insets show the data around zero field with an expanded scale ranging from −1000 to 1000 Oe (E), (F). Photographs of a solution of the hybrid nanostructure with the diameter of 400 nm in the absence and presence of a magnet (G). (Reprinted with permission from S Liu *et al* 2011 *CrystEngComm* **13** 2425. Copyright 2011 Royal Society of Chemistry.)

NPs were produced in two hydrodynamic sizes with differing core morphologies by varying the synthetic process. The IONPs are found to be superparamagnetic and exhibit properties consistently in MRI. In addition, the dextran coating imparts the water solubility and biocompatibility necessary for *in vivo* utilization [96]. As shown in figure 9, Zhu *et al* reported polyacid-conjugated Fe$_3$O$_4$ superparamagnetic hybrid nanostructures that were conveniently fabricated by the introduction of a microwave-assisted method. The hybrid nanostructure was composed of superparamagnetic magnetite nanograins and presented a cluster-like structure; and its size range can be tuned from about 100–400 nm by varying the amount of FeCl$_3$ in the system. The hybrid nanostructure exhibits excellent magnetic responsibility and good biocompatibility, which offers advantageous functionality due to the preferential exposure of uncoordinated carboxylate groups on its surface [97]. Compared to the thermal decomposition method, the stabilization of the IONPs prepared by the microwave-assisted synthesis route in organic solvents can be easily dispersed in water without laborious ligand exchange or purification steps. Such characteristics can be considered as attractive for fabrication of large-scale IONPs [98].

2.8. Biosynthesis

Biosynthesis of IONPs is a kind of bottom-up approach where the main reaction occurring is reduction/oxidation. The microbial enzymes or the plant phytochemicals with antioxidant or reducing properties are usually responsible for the reduction of salts into their respective NPs [99]. Generally, the biosynthesis method is a green chemical and eco-friendly route, and the obtained products exhibit a good biocompatibility. In the traditional biosynthesis for magnetic IONPs, magnetotactic bacteria and iron reducing bacteria are used,

such as *Geobacter metallireducens*, *M. gryphiswaldense*, etc [100–102].

Recently, new types of bacteria have been employed to synthesize magnetic IONPs. For example, Bharde *et al* have reported that the bacterium *Actinobacter* sp. was capable of synthesizing maghemite NPs under aerobic conditions when reacted with a ferric chloride precursor. Moreover, maghemite NPs showed superparamagnetic characteristics as expected. Compared to the earlier reports of synthesis of magnetite NPs by magnetotactic bacteria and iron reducing bacteria, which took place strictly under anaerobic conditions, the present procedure offered a significant advance since the reaction occurred under aerobic conditions [103]. Recently, Sundaram *et al* reported the ability of *Bacillus subtilis* strains isolated from rhizosphere soil to produce IONPs. This successful synthesis of stabilized Fe$_3$O$_4$ NPs, which was capped by organic molecules, indicates the applicability of the isolated *Bacillus subtilis* strain for the bulk synthesis of IONPs [104].

Currently, how to control the size and shape of magnetic IONPs during biosynthesis processes, and the elucidation of the exact mechanism of IONPs production using living organisms, require much more experimentation.

2.9. Other methods

Except for the above-mentioned methods, numerous chemical or physical methods can also be used to synthesize magnetic IONPs, such as electrochemical methods [105–107], flow injection synthesis [108], and aerosol/vapor methods [109–111].

The electrochemical methods for IONPs present some advantages over other methods, the crucial one being the high purity of the product, and the control of particle size is achieved by adjusting the current or the potential applied to the system. Cabrera *et al* prepared Fe$_3$O$_4$ NPs with sizes
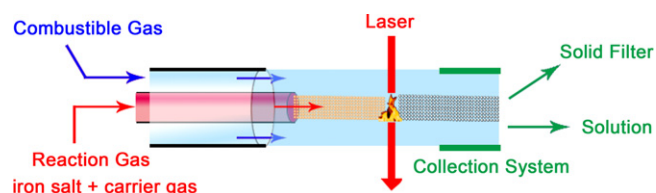
Figure 10. Detail of the reaction area where the laser interacts with the gas reactants and the influence of the collection system to obtain larger aggregates (solid filter) or well-dispersed ultrasmall IONPs (solution, the size is below 5 nm) under similar experimental conditions.

between 20 and 30 nm by Fe electro-oxidation in the presence of an amine surfactant, which acted as a supporting electrolyte and coating agent for particle size and aggregation control during the synthesis process. The distance between electrodes is critical for the successful synthesis of IONPs [112]. Recently, Rodríguez-López *et al* reported magnetic IONPs with controlled size distribution were electrochemically synthesized by applying a dissymmetric pattern of potential pulses to iron-based electrodes in aqueous media. It was found that Fe_3O_4 NP formation was favored, while avoiding the formation of metallic Fe particles with more anodic potentials and the longest time [113].

In fact, flow injection synthesis is a modified co-precipitation method. In the reaction process, different precursors can be added by pumping with a controllable flow rate. Therefore, this method showed some advantages, such as high reproducibility, high mixing homogeneity, and an opportunity for a precise external control of the process [108].

Spray and laser pyrolysis are the main aerosol technologies for fabricating magnetic IONPs. In spray pyrolysis, fine IONPs are produced by the evaporation of ferric salts, drying, and pyrolysis reaction of liquid drops (a reducing agent in organic solvent) inside a high temperature atmosphere, especially the flame-spray. Particle size and size distribution depend on the size and size distribution of liquid drops, and the evaporation process of a solvent and the property of the starting material. Recently, Abid *et al* reported IONPs with variable oxidation states by flame-spray pyrolysis, revealing that the different flame configurations are an important factor of the morphology and size control of the final IONPs [114]. For reducing the reaction volume, laser became the energy resource and heated a gaseous mixture of iron precursor and a flowing mixture of gas producing small, narrow size, and non-aggregated NPs in the pyrolysis process (as shown in figure 10). Importantly, laser pyrolysis can produce well-dispersed fine IONPs. For example, Costo *et al* have synthesized very high crystallinity, and ultrasmall NPs (<5 nm) with a rather spheroid morphology and exceptionally narrow particle size distributions through an optimized acid treatment. The dissolution of the disordered layer from the particle surface and further recrystallization of an iron polymer activated the surface and prepared the particles for further functionalization with bioactive ligands [115]. However, the final IONPs made by this process had a very broad size distribution

due to the difficulty of obtaining a uniform size of initial droplets or gaseous mixture.

The characterization of the above mentioned synthetic methods are briefly summarized in table 1. In terms of simplicity of synthesis, classical co-precipitation is the preferred route. In terms of size and morphology control of IONPs, thermal decomposition seems the best method to develop IONPs smaller than 20 nm, and the hydrothermal or solvothermal method seems to be the most suitable for producing IONPs larger than 20 nm. As an alternative, the other methods can also be used to synthesize magnetic IONPs with a narrow size distribution and controllable morphology. However, the major difficulties in the synthesis of IONPs are still to control the size, shape, composition and size distribution on the nanoscale due to the fact that the aggregation and/or continuous growth of IONPs to minimize the overall surface free energy and magnetic interactions. The current methods often involve a number of different steps with multiple microstructural problems that may have a pernicious influence on the magnetic performance. Therefore, searching for a facile and flexible fabricated method to produce IONPs with the desired morphologies without aggregation is of extreme importance to realize the full potential of these materials in biomedical applications. Thus, looking for new routes of large-scale synthesis and improvement of the known ones should be continued.

3. Surface functionalization of magnetic IONPs

An unavoidable problem associated with magnetic IONPs in the size range is their intrinsic instability over longer periods, which manifests in two main ways: (1) loss of dispersibility, where small NPs tend to aggregate and form large particles to reduce the surface energy; and (2) loss of magnetism, where bare IONPs are easily oxidized in air due to their high chemical activity, especially Fe_3O_4 and γ-Fe_2O_3 NPs. Therefore, it is crucial to develop a proper protection strategy to chemically stabilize bare IONPs against damage during or after the subsequent application. For biomedical applications, it is necessary to obtain water dispersible NPs, because most biological media are nearly neutral aqueous solutions.

In view of the many strategies and their subsequent application, efforts have been devoted to fabricating four types of IONP-based materials, including the core–shell structure, matrix dispersed structure, Janus-type heterostructures and shell–core–shell structure (figure 11).

3.1. Core–shell structure

In this structure, the iron oxide core was encapsulated in an inorganic or an organic coating that renders the whole particle stable and biocompatible, and may serve as a support for biomolecules. Generally, IONPs are not located at the center of the functional coating material; this structure is also known as a yolk structure. Indeed, the magnetic composite nanomaterials not only provide the material with an improved

Table 1. Summary comparison of the synthetic methods for producing magnetic IONPs.

| Method	Reaction and conditions	Reaction temp. [°C]	Reaction period	Size distribution	Shape control	Yield
Co-precipitation	Very simple, ambient	20–150	Minutes	Relatively narrow	Not good	High/scalable
Thermal decomposition	Complicated, insert atmosphere	100–350	Hours-days	Very narrow	Very good	High/scalable
Hydro- or solvothermal synthesis	Simple, high pressure	150–220	Hours-days	Very narrow	Very good	High/scalable
Sol–gel and polyol method	Complicated, ambient	25–200	Hours	Narrow	Good	Medium
Microemulsion	Complicated, ambient	20–80	Hours	Narrow	Good	Low
Sonolysis or sonochemical method	Very simple, ambient	20–50	Minutes	Narrow	Bad	Medium
Microwave-assisted synthesis	Very simple, ambient	100–200	Minutes	Medium	Good	Medium
Biosynthesis	Complicated, ambient	Room temp.	Hours-days	Broad	Bad	Low
Electrochemical methods	Complicated, ambient	Room temp.	Hours-days	Medium	Medium	Medium
Aerosol/vapor methods	Complicated, insert atmosphere	>100	Minutes-hours	Relatively narrow	Medium	High/scalable
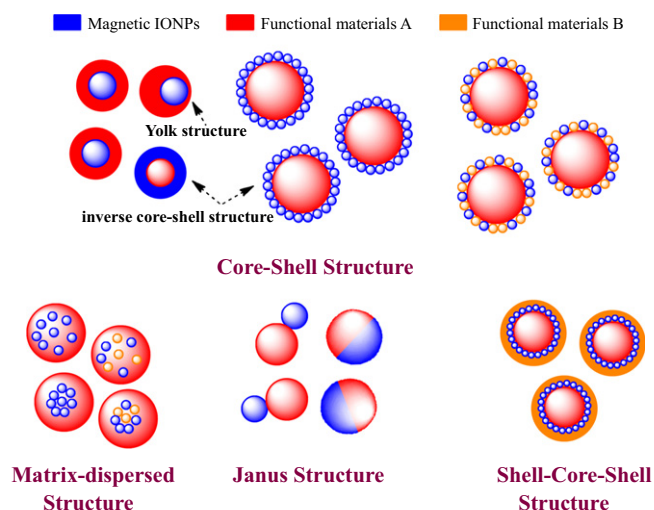
Figure 11. Typical morphologies of magnetic composite nanomaterials. Blue spheres represent magnetic IONPs, and the nonmagnetic entities and matrix materials are displayed in other colors. The nonmagnetic entity may provide the composite material with further functionalities and properties, providing multifunctional hybrid systems.

stability of the nanoparticulate building blocks, but also further introduce new physical and biological properties, and multifunctional behaviors. Thus, in the inverse core–shell structure, the magnetic IONPs will coat the surface of nonmagnetic functional materials. Moreover, magnetic IONPs can combine one or more functional materials and further coat with another functional material on the functionalized surface. The above structures are collectively called core–shell structures.

However, some literature has reported 'shell–core' structures in magnetic nanomaterials; in this structure, the iron oxide will coat the surface of core materials [116–118]. For example, Zhan and Zhang have reported the synthesis of CdSe@Fe$_2$O$_3$ core–shell NPs by a one-step seeded-growth approach. These NPs not only retain their individual semiconducting and magnetic functionalities, but also exhibit some new properties that are affected by the coating components. These bi-functional CdSe@Fe$_2$O$_3$ NPs might find potential applications in biosensing and biomedical research [119].

3.2. Matrix-dispersed structure

Magnetic IONPs are dispersed in a matrix to prevent the superparamagnetic NPs from aggregating into large ferromagnetic species. Matrix-dispersed NPs can be created in a variety of different states, e.g. dispersed in a continuous amorphous matrix, grafted on larger, mesoscale particles, or well defined, three-dimensional superstructures of NPs [120].

3.3. Janus structure

In Janus structure, one side is magnetic IONPs, and the other side is functional materials. Anisotropic surface chemical compositions are interesting for applications even if one is not concerned with self-assembly. For example, Sun *et al* developed dumbbell-like Au-Fe$_3$O$_4$ and Pt- Fe$_3$O$_4$ NPs, where the sizes of the particles are tuned from 2 to 8 nm for Au and Pt, and 4 nm to 20 nm for Fe$_3$O$_4$ [121, 122]. This Janus particle can be used in target-specific platin delivery [123]. Zhao and Gao have prepared magnetic γ-Fe$_2$O$_3\|$SiO$_2$ Janus particles by flame synthesis. The highly uniform γ-Fe$_2$O$_3\|$SiO$_2$ presents excellent aqueous dispersibility, consequently providing different choices for further manipulation of Janus particles to form interesting assembled structures [124].

3.4. Shell–core–shell structure

In this structure, the location of magnetic IONPs is between the two functional materials. Most applications require magnetic IONPs to be embedded in the nonmagnetic layers to avoid aggregation and sedimentation of magnetic IONPs as well as to endow them with particular surface properties for specific applications. For example, luminescent layers, magnetic IONPs and biocompatible polymer layers are combined into bimodal nanocomposite materials, allowing manipulation by an external magnetic field and real time optical visualization at the same time.

A prerequisite for every possible applied structure is the proper surface protection or functionalization of such magnetic composite NPs, which determines their interaction with the environment. These interactions ultimately affect the colloidal stability of the composite particles, and may yield a controlled assembly or the delivery of NPs to a target, especially by appropriate functional organic materials or inorganic materials on the IONP surface [125].

3.5. Organic materials

IONPs with any organic material coating are used mainly for magnetic recording, electromagnetic shielding, MRI, and especially in the biological field for specific drug targeting, magnetic cell separation, etc. The stability of magnetic NPs under an external high applied magnetic field is very important for *in vivo* biological application as well as in other fields. Several approaches have been developed to functionalize IONPs, including *in situ* coatings and post-synthesis coating, which are the common routes for organic material coating on the IONP surface [126–128]. Furthermore, to stabilize the particles against aggregation and with good biocompatibility, the IONPs are coated with different organic materials, such as dextran, starch, poly(ethylene glycol) (PEG), poly (D, L-lactide) (PLA), polyethylenimine (PEI), especially for hydrophilic organic materials.

3.5.1. Small molecules and surfactants.
With proper surface modification, magnetic IONPs can be functionalized by special groups (e.g. –OH, –COOH, –NH$_2$, –SH), which are suitable for further modifications by the attachment of different bioactive molecules for various applications.

As a small molecule, silane is often used to modify and endow the functionalized end groups to the surface of bare

IONPs directly for post-connecting with metal ions, polymers, biomolecules or other biological entities. Significantly, silane modified magnetic IONPs still maintain the saturation magnetization values of the bare IONPs, where the decreased value is often less than 5 emu g^{-1}; this character illustrates that the magnetic separation is not affected after silane modification. 3-aminopropyltriethyloxysilane (APTES), *p*-aminophenyltrimethoxysilane (APTS) and mercaptopropyl-triethoxysilane (MPTES) agents are the most common silanes for anchoring the –NH$_2$ and –SH, respectively. For instance, Shen *et al* reported a facile approach to synthesize APTES-coated magnetic IONPs (Fe$_3$O$_4$@APTES) with tunable surface functional groups for potential biomedical applications. The cytotoxicity and hemolytic assay results demonstrated that acetylation of the amine groups on the surfaces of IONPs would significantly improve the particles' cytocompatibility and hemocompatibility [129]. Furthermore, as seen in our previous study, APTES was beneficial to maintaining the morphology of the Fe$_3$O$_4$ NPs, whereas MPTES modification caused a slight decrease in the saturation magnetization [130]. Additionally, the silane ligand-exchange reaction can make the hydrophobic IONPs change into water-dispersible NPs.

However, fabrication of oil-soluble type IONPs is very important for obtaining monodisperse IONPs. The most common organic compounds are oleic acid and oleyamine, which have a C18 tail with a cis-double-bond in the middle, forming a kink. Such kinks have been postulated as being necessary for effective stabilization, which can be a reasonable explanation for why stearic acid cannot stabilize IONPs (with no double-bond in its C18 tail) [1]. Moreover, oleic acid is widely used in IONP synthesis because it can form a dense protective monolayer, thereby producing highly uniform IONPs. Generally, the oleic acid and oleyamine are often used in the high-temperature thermal decomposition reaction process. For instance, Fe$_3$O$_4$ was synthesized via facile thermal decomposition of Fe(acac)$_3$ in the presence of oleic acid or/and oleyamine. In a typical procedure, Fe(acac)$_3$ is added to oleic acid and/or other organic compound (such as phenyl ether, 1, 2-hexadecane diol, etc) at room temperature. The reaction mixture was heated to >100 °C under a nitrogen atmosphere with vigorous stirring, and then kept at that temperature for a certain time. The above well-mixed solution was then heated to >300 °C, and the solution color gradually became black, indicating that the magnetic NPs were being formed in the presence of oleic acid and another organic compound [41, 131–133]. Salas *et al* have shown that the high temperature decomposition of an iron oleate complex can be used to obtain superparamagnetic nanocrystals with sizes over 10 nm, where the as-obtained IONPs exhibited high saturation magnetization. The results concerning the size of the IONPs as a function of the oleic acid added to the reaction medium showed a complex behavior that can be qualitatively explained in terms of the nucleation and growth rates. Broader size distributions lead to worse magnetic properties either in large (15 or 18 nm) or in small IONPs (9 nm) [134]. Moreover, oleic acid coating Fe$_3$O$_4$ NPs resulted in no appreciable changes in the overall magnetic

behavior of the samples. These Fe$_3$O$_4$ NP systems with high values of M_S, corresponding to 80% of the bulk value, are suitable for technological applications [135]. The final shape of the IONPs could be readily tuned from sphere to cube by adjusting the experimental parameters, such as reaction time, temperature, and surfactants [44].

Indeed, the magnetic IONPs resulting from high-temperature decomposition of an organic iron precursor are capped with nonpolar endgroups on their surface and are usually stable in nonpolar solvents (such as hexane). The capping molecules (also called ligands) are typically long-chain alkanes with polar groups binding to the IONPs' surface. Hence, to take advantage of their high-quality properties in biological applications, it is necessary to transfer IONPs from organic phase to aqueous phase, and the hydrophobic surfactant coating needs to be replaced by a hydrophilic, biocompatible, and functional coating that allows controlled interaction with biological species.

To synthesize water-soluble magnetic IONPs directly, one way is to use small molecules (such as amino acid, citric acid, vitamin, cyclodextrin, etc) in the reaction process [136–138]. For example, Gao *et al* synthesized highly charged hydrophilic superparamagnetic Fe$_3$O$_4$ colloidal nanocrystal clusters with an average diameter of 195 nm by using a modified one-step solvothermal method. Anionic polyelectrolyte poly (4-styrenesulfonic acid-co-maleic acid) sodium salt (PSSMA) containing both sulfonate and carboxylate groups was used as the stabilizer. The PSSMA-stabilized IONP clusters could be well dispersed in water, phosphate buffered saline (PBS), and ethanol. Moreover, silica shells could be directly coated onto these clusters by the Stöber method. The colloidal nanocrystal clusters remained negatively charged in the experimental pH ranges from 2 to 11, and also showed high colloidal stability in PBS and ethanol [139]. Recently, Majeed *et al* reported a one-step protocol for the preparation of fairly monodisperse and highly water-soluble magnetic IONPs through a co-precipitation method using a novel multifunctional, biocompatible and water-soluble polymer ligand dodecanethiol-polymethacrylic acid (DDT-PMAA). The as-prepared IONPs were conjugated with the anti-cancer drug doxorubicin (DOX) and its efficacy, as a model drug delivery system, was determined using HepG2 cells. The efficiency of the drug-NP conjugates i.e., covalently bound DOX-IONPs and electrostatically loaded DOX/IONPs, was found to be significantly higher than that of the free drug (DOX). Indeed, owing to the several intrinsic properties of DDT-PMAA, it not only efficiently controls the size of the IONPs but also gives them excellent water solubility, long time stability against aggregation and oxidation, biocompatibility, and a multifunctional surface rich in thioether and carboxylic acid groups [140]. Obviously, these highly colloidal stable IONPs have potential applications in biotechnology.

Another way is to use a ligand exchange procedure to change the polarity of the hydrophobic layer to being hydrophilic [141–143]. It involves adding an excess of ligand to the nanoparticle solution, resulting in the displacement of the original ligand on the surface of NPs. For instance, Dong
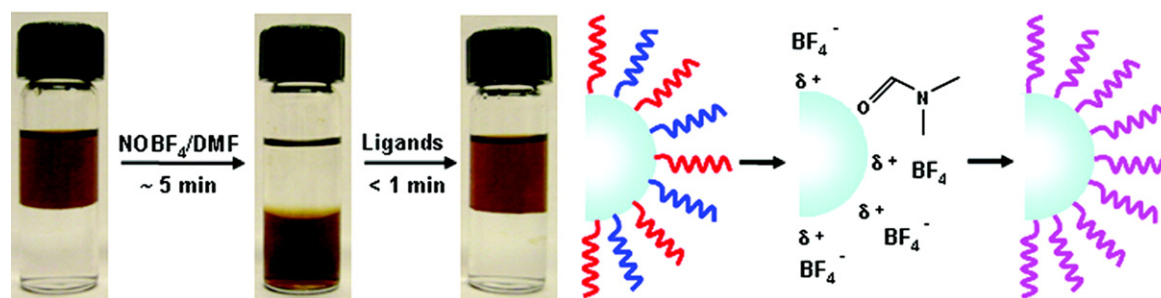
Figure 12. A facile ligand-exchange approach, which enables sequential surface functionalization and phase transfer of colloidal NCs while preserving the NC size and shape. (Reprinted with permission from A Dong *et al* 2010 *J. Am. Chem. Soc.* **133** 998. Copyright 2010 American Chemical Society.)

et al reported a facile ligand-exchange approach, which is enabled for sequential surface functionalization and phase transfer of colloidal IONPs while preserving the NPs' size and shape. Nitrosonium tetrafluoroborate (NOBF$_4$) is used to replace the original organic ligands attached to the NPs' surface, stabilizing the NPs in various polar and hydrophilic media for years, without aggregation or precipitation (shown in figure 12). Significantly, as illustrated in figure 12, the hydrophilic NPs obtained by NOBF$_4$ treatment can readily undergo secondary surface modification due to the weak binding affinity of BF$_4^-$ anions to the surface of NPs, allowing fully reversible phase transfer of NPs between hydrophobic and hydrophilic media [144]. Ninjbadgar and Brougham have reported a novel and efficient method to produce water dispersible superparamagnetic Fe$_3$O$_4$ NPs by ring opening coupling reactions. Fe$_3$O$_4$ NPs prepared by non-hydrolytic organic phase methods were subsequently functionalized with (3-glycidyloxypropyl) trimethoxysilane, the linker between the Fe$_3$O$_4$ NPs and organic molecule prevent aggregation, and it also is available for subsequent coupling reactions with a wide range of polymers and biomolecules. Ring opening coupling reactions were used to coat the epoxy-functionalized Fe$_3$O$_4$ NPs with aminated polymers (polyetheramines) or small molecules (arginine). The obtained NPs, with hydrodynamic size of 13 nm, are found to be very stable over extended periods in water or PBS due to the presence of a dense stabilizer layer covalently anchored onto the surface. Exceptionally high spin-lattice relaxivity, low r_2/r_1 ratios were exhibited in the clinical MRI frequency range, irrespective of the molecule selected for nanoparticle stabilization. As a result, the dispersions are excellent candidates for incorporation into multifunctional assemblies or for use as a positive contrast agent for MRI [145].

3.5.2. Polymers. Compared with small molecules and surfactants, polymer functionalization not only provides multifunctional groups and more colloid stability, but also plays a significant role regarding its biological fate (i.e., pharmacokinetics and biodistribution) [146]. Furthermore, a large number of natural and synthetic biodegradable polymers, such as polyaspartate [147], polysaccharides [148–150], gelatin [151–153], starch [154–156], alginate [157–159], poly(acrylic acid) [160–162], PEG [163, 164],

poly(D,L-lactide) (PLA) [165–167], chitosan [168, 169], and polymethylmethacrylate (PMMA) [170–172], are currently under evaluation for the functionalized materials of IONPs.

Several approaches have been developed to functionalize IONPs with polymers, where the common approaches include *in situ* and post-synthesis coating. In the *in situ* approach, the conventional routes are mini/micro-emulsion polymerization and the sol–gel process for polymer functionalizing IONPs (polymer@IONPs) during the synthesis process [173, 174]. The organic molecules capped the IONPs and formed a capping layer during the emulsion polymerization process; the conventional structure is a core–shell structure or matrix dispersed structure [75, 175]. Unfortunately, these direct surface modification strategies are often unsuccessful in maintaining colloidal stability and the thickness of the shell is not easy to control.

Consequently, the prevalent routes for polymer@IONPs is post-synthesis functionalization, which is based on the pre-prepared IONPs for further polymer functionalization via a one-pot route, self-assembly, or heterogeneous polymerization (such as inverse mini/emulsion polymerization and dispersion polymerization) [171]. Particularly, the one-pot method is a facile route for obtaining polymer@IONP composite nanomaterials [176]. The physical adsorption and functional groups anchoring on the surface of IONPs are the common mechanism in this strategy, the resulting structure of complex NPs is prone to form a core–shell structure. Furthermore, the covalent bonding is a wide and commonly used functional technique and the cross-linking is made by using the alkyl chain or carboxylic acid functionalized thiol and hydrogen bonding [177]. In addition, various heterogeneous polymerizations with water-soluble monomers have been explored to prepare well-defined core–shell or matrix dispersed structure polymer@IONPs for biomedicine applications [178, 179]. For instance, an all-in-one NP platform with a size-range of 30 nm–100 nm was developed based on an oil-in-water emulsion method. The hydrophobic layer coated IONPs were included in the soybean oil core of the emulsions. Subsequently, these oil droplets are stabilized by a PEGylated lipid mixture to favor the formation of small particles, which increased the longevity of the complex particles in circulation, so the complex NPs are enabled for MRI detection. The emulsions allowed loading high quantities of iron oxide nanocrystals, and the resulting complex
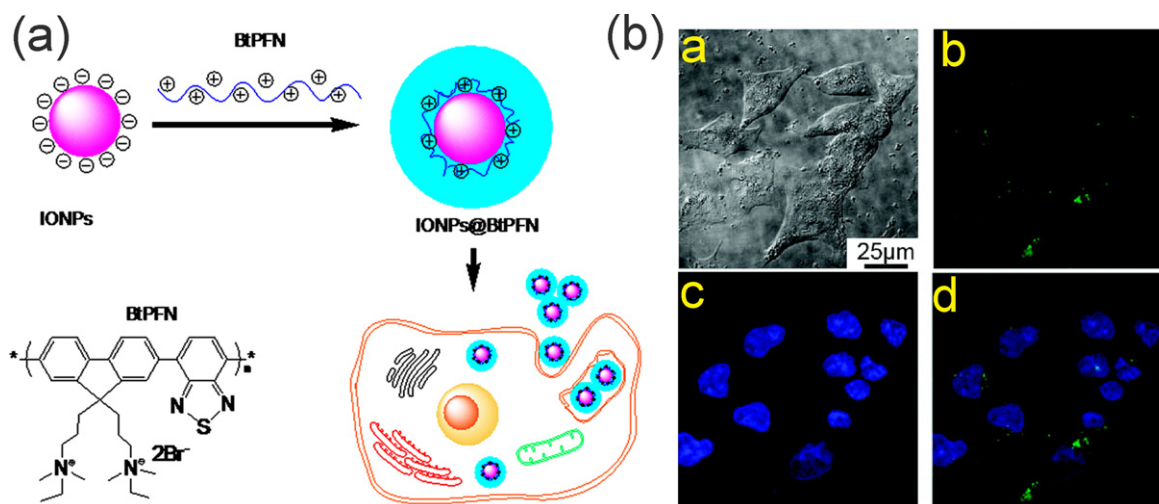
Figure 13. Schematic of the preparation of IONP@conjugated polymer (BtPFN) and internalization by cancer cells; confocal laser scanning microscopy (CLSM) images of Bel-7402 cells incubated with MP/BtPFN (green color) for 4 h at 37 °C, whereas cell nuclei are stained by Hoechst 33342 dye (blue color). (a) Bright-field image. (b)–(d) Fluorescence images of the green (b) and blue (c) channels, and a merged image (d). (Reprinted with permission from B Sun *et al* 2010 *Macromolecules* **43** 10348. Copyright 2010 American Chemical Society.)

particles caused a remarkably high transverse relaxivity (r_2) [180].

The stability of IONPs can be enhanced and the application field extended by introducing polymers with multiple functional groups. For example, conjugated polymers, which are characterized by a delocalized electronic structure, exhibited efficient coupling between optoelectronic segments, thereby the conjugated polymer functionalized IONPs can be applied in imaging, diagnosis, and therapy [181, 182]. Wang *et al* used the fluorescent conjugated polyelectrolyte (BtPFN) to coat the surface of magnetic IONPs and form IONP/BtPFN composite NPs with a positively charged fluorescent shell by electrostatic adsorption (as shown in figure 13). The organic/inorganic hybrid NPs display a simultaneous response toward light excitation and external magnetic fields. Furthermore, these nanocomposites can be used as robust fluorescent probes in cell imaging, and if optimized, as multicolor probes to detect interactions of tremendous NPs with living cells. The long-term effects of IONP/BtPFN NPs in cell indicated most MP/BtPFN NPs were clearly in the cytoplasm, whereas a few of them migrated to the region very close to the outer nuclear membranes of the cells [183].

Presently, the fashionable trend for polymer functionalized IONPs in biomedicine is functionalizing with smart polymers, which endow special properties to IONPs for a stimulus response environment, such as pH, temperature, light, etc [184, 185]. Generally, pH-sensitive polymers are polyelectrolytes that bear in their structure weak acidic or basic groups that either accept or release protons in response to changes in environmental pH. Thermo-sensitive polymers can be classified into different groups depending on the mechanism and chemistry of the groups. The functional groups of polymers have a crucial role in stimulus response properties and comprehensive application in biomedicine such as drug delivery, MRI, and biosensors; some typical polymers and functional groups are listed in table 2 [186–188].

Additionally, considerable interest has been attracted to functionalizing IONPs with amphiphilic block copolymers, which incorporate more functional groups into the polymers for multifunctional applications [189]. The self-assembly method is the common route to design and prepare stable complex IONPs with amphiphilic block copolymers in the liquid phase. Furthermore, this technique is used to prepare film platforms, drug carriers and MRI [190]. For instance, novel multifunctional nanocomposites were successfully prepared through a simple self-assembly process for the controlled release of anticancer drug and MRI. The SPIONPs were 'fixed' between the hydrophobic segment of the pH-sensitive amphiphilic polymer (HAMAFA-b-DBAM) and the surface of hollow mesoporous silica NPs (HMS), which were modified by the long-chain hydrocarbon octadecyltrimethoxysilane. The amphiphilic polymer was further conjugated with a folic acid (FA) group; the nanocomposites could target the FA receptor of over-expressed tumor cells efficiently. The loaded drug can be released from the HMS core triggered by the mildly acidic pH environment in the cancer cells due to the hydrolysis of the pH-sensitive polymer shell. The targeting process of the nanocomposites could be easily tracked by MRI due to the magnetism of the SPIONPs [191].

However, it is worth noting that, in some cases, the presence of polymer or copolymer layers may negatively influence the magnetic properties of the IONPs. Thus, great caution has to be exercised during the selection of polymeric materials for the stabilization of magnetic colloids.

3.5.3. Biomolecules. Recently, biomolecule functionalized magnetic IONPs have become a common and effective strategy in the biological separation, detection, sensor and other bio-applications due to their higher biocompatibility. The various biomolecules, including

Table 2. Examples of smart polymer functionalized IONPs.

Type of stimulus	Polymers	Functional groups	Clinical products and examples	Refs.
pH	Polypropylacrylic acid (PPAA), polyethacrylic acid (PEAA); Poly(methyl methacrylate) (PMMA) Poly (acrylic acid) (PAA)	—C(=O)—O—		[192, 193]
	Chitosan	–NH$_2$ –OH		[194]
	Poly(L-lysine), Poly(ethyleneimine) (PEI),	N (triethylamine structure) –NH– –NH$_2$		[195, 196]
	Poly(4-vinylpyridine), poly(2-vinylpyridine) (PVP) and poly(vinylamine) (PVAm)	pyridine ring; pyrrolidone ring structures		[197, 198]
Temperature	Poly(N-isopropylacrylamide) PNIPAAm	–NH—C(=O)—	Pluronics® F127 Poloxamers® 407, Tetronics®	[199, 200]
	Poly(N,N′-diethyl acrylamide), Poly(dimethylamino ethyl methacrylate)	N—C(=O)— ; —C(=O)—O— ; N	PEG/PLGA, Regel ®	[201]
Light	Polyethylene glycol (PEG)	–O–, –OH	T$_1$ MR Contrast Agent	[202]
	Polyethylene glycol (PEG)	–O–		[203]
	Poly (lactic acid)	—C(=O)—O—		[204]

enzymes, antibodies, proteins, biotin, bovine/human serum albumin, avidin and polypeptides have been bound onto the surface of IONPs [7, 205–209].

For instance, Magro *et al* reported on the surface characterization, functionalization, and application of stable water suspensions of novel surface active maghemite NPs by avidin. Bound avidin was determined by measuring the disappearance of free avidin absorbance at 280 nm, as a function of increasing nanoparticle concentration, showing the presence of 10 ± 3 avidin molecules per nanoparticle. Fe_2O_3@avidin was applied for the large scale purification of recombinant biotinylated human sarco/endoplasmic reticulum Ca^{2+}-ATPase (hSERCA-2a), expressed by *Saccharomyces cerevisiae*. The protein was magnetically purified, and about 500 μg of a 70% pure hSERCA-2a were recovered from 4 L

of yeast culture, with a purification yield of 64% [210]. As shown in figure 14, Bhattacharya *et al* demonstrated a rapid, sensitive, specific and efficient method for the detection of *Staphylococcus aureus* (*S. aureus*) as the model analyte at ultra-low concentrations using antibody labeled multifunctional Au-Fe_3O_4 nanocomposites. Fluorescence/confocal as well as optical microscopy could detect a total count of *S. aureus* within concentrations of 10^2–10^7 CFU mL^{-1} in 30 min and the detection limit is 10^2 CFU mL^{-1}. These antibody targeted NPs are a potent probe for a broad application in detecting specific bacteria, *S. aureus*, in various biodetection systems [211]. The biological molecule functionalized IONPs will greatly improve the particles' biocompatibility. Such magnetic IONPs can be very useful to assist an effective separation of proteins, DNA, cells, biochemical products, etc.

Figure 14. Schematic demonstration of pathogen detection by antibody-modified-fluorescent-MPA–Au–Fe$_3$O$_4$ nanocomposites. (Reprinted with permission from D Bhattacharya *et al* 2011 *J. Mater. Chem.* **21** 17273. Copyright 2011 Royal Society of Chemistry.)

3.6. Inorganic materials

Inorganic materials can possess a number of different properties such as high electron density and strong optical absorption (e.g. noble metal particles, in particular Au and Ag), photoluminescence in the form of fluorescence (semiconductor quantum dots, e.g. CdSe or CdTe) or phosphorescence (doped oxide materials, e.g. Y$_2$O$_3$), or magnetic moment (e.g. manganese or cobalt oxide NPs) [212–215]. These coatings not only provide stability to the NPs in solution but are also widely used for the improvement of semiconductor efficiency, information storage, optoelectronics, catalysis, quantum dots, optical bioimaging, biological labeling, and so on. Especially, some inorganic materials help in binding various biological ligands to the IONP surface, such as silica, Au, metal oxides, etc [216–218].

3.6.1. Silica. Silica-coated IONPs (IONP@silica) is a classical and important composite material for both fundamental study and bio-applications. Silica coating can enhance the dispersion in solution because the silica layer could screen the magnetic dipolar attraction between magnetic IONPs. Additionally, the silica coating would increase the stability of IONPs and protect them in an acidic environment. Finally, owing to the existence of abundant silanol groups on the silica layer, IONP@silica could be easily activated to provide the surface of NPs with various functional groups. For practical applications, it is required that each IONP should be coated with a homogeneous silica layer without core-free silica particles, regardless of the size of the NPs. For instance, as a heating source and magnetic guidance, IONPs play an important role in hyperthermia and targeted drug delivery, and the existence of core-free silica particles will lead to a loss in the effective dose of IONPs. The major reason causing uneven heating in

hyperthermia and tissue distribution of the targeted drugs can be attributed to the unequal core number and silica shell thickness.

Three different approaches have been explored to generate IONP@silica nanomaterials. The first method relied on the well-known Stöber process [219], in which silica was formed *in situ* through the hydrolysis and condensation of a sol–gel precursor, this is a prevailing choice for preparing IONP@SiO$_2$. Generally, the IONPs were homogeneously dispersed in the alcohol, then the silane was added, and finally the water or ammonia aqueous solution was dropped into the mixed solution and IONP@SiO$_2$ formed. Tetraethoxysilane (TEOS), vinyltriethoxysilane (VTEOS), octadecyltrimethoxy silane are the most common used silanes, which easily bind on the surface of IONPs through OH groups [220–222]. For example, Xuan *et al* synthesized monodispersed γ-Fe$_2$O$_3$@meso-SiO$_2$ by this method, and the size of the magnetic core and the thickness of the porous shell were controlled by tuning the experimental parameters. The magnetic property of the γ-Fe$_2$O$_3$ porous core enabled the microspheres to be used as a contrast agent in magnetic resonance imaging with a high r_2 (76.5 s^{-1} mM^{-1} Fe) relaxivity. The biocompatible composites possess a large BET surface area (222.3 m^2 g^{-1}); the composite NPs have been used as a bi-functional agent for both MRI and drug carriers [223]. In our previous report, the ultrafine hollow Fe$_3$O$_4$/silica NPs (the diameter of about 32 nm) with a high surface area were synthesized by using CTAB and AOT as co-templates and subsequent annealing treatment. The composite NPs can be magnetic separated by the external magnetic field [224]. The iron oxide@SiO$_2$ NPs are often used in MRI; it is noteworthy that the increase of the silica coating thickness will cause a significant decrease of the r_1 and r_2 relaxivities of their aqueous suspensions [225]. In this method, the amount of silane used is a key factor for tuning the silica shell thickness, and the adequate silica shell thickness can therefore be tuned to allow for both a sufficiently high response as a contrast agent, and adequate grafting of targeted biomolecules [226].

The second method was based on microemulsion synthesis, in which micelles or inverse micelles were used to confine and control the coating of silica on core NPs [227]. It is noteworthy that this method requires much effort to separate the core–shell NPs from the large amount of surfactants associated with the microemulsion system. Recently, Ding *et al* reported the coating regulations of Fe$_3$O$_4$ NPs by the reverse microemulsion method to obtain Fe$_3$O$_4$@SiO$_2$ core–shell NPs. As shown in figure 15, the regulation produces core–shell NPs with a single core and with different shell thickness and especially it can be applied to different sizes of Fe$_3$O$_4$ NPs and avoid the formation of core-free silica particles. The small aqueous domain was suitable to coat ultrathin silica shell, while the large aqueous domain was indispensable for coating thicker shells. To avoid the formation of core-free silica particles, the thicker silica shells were achieved by increasing the content of either TEOS through the equivalently fractionated drops or ammonia with a decreased one-off TEOS [228]. The advantage of this
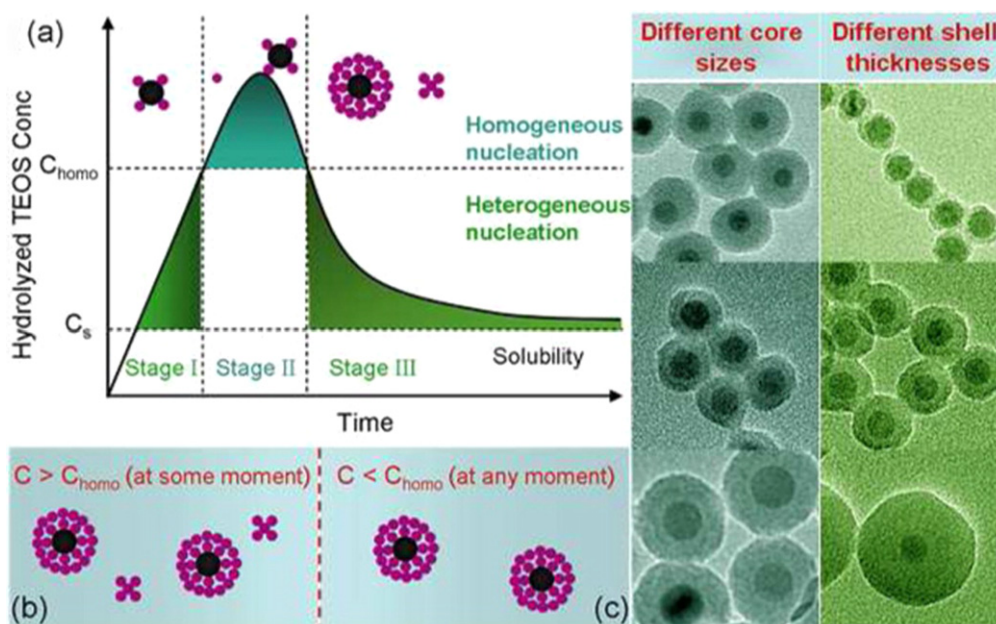
Figure 15. (a) La Mer-like diagram: hydrolyzed TEOS (monomers) concentration against time on homogeneous nucleation and heterogeneous nucleation, (b) the existence of $Fe_3O_4@SiO_2$ core/shell NPs and SiO_2 NPs in the reaction production when $C > C_{homo}$ at some moment, (c) only the existence of $Fe_3O_4@SiO_2$ core/shell NPs in the reaction production when $C < C_{homo}$ at any moment. (Reprinted with permission from H L Ding *et al* 2012 *Chem. Mater.* **24** 4572. Copyright 2012 American Chemical Society.)
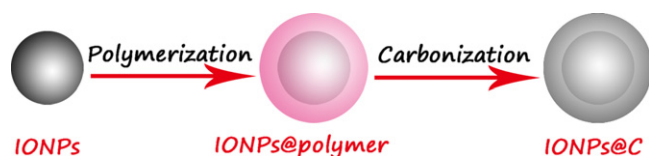

Figure 16. Schematic illustration of the fabrication of IONP@C composites.

method is that uniform silica shells with controlled thickness on the nanometer scale can be realized.

The third method is aerosol pyrolysis, in which IONP@SiO$_2$ were prepared by aerosol pyrolysis of a precursor mixture composed of silicon alkoxides and metal compound in a flame environment [229]. For instance, Basak *et al* have reported the controlled synthesis of a core–shell type γ-Fe$_2$O$_3$/SiO$_2$ nanocomposite, which is demonstrated in a single step in a furnace aerosol reactor using premixed precursors. The result reveals that the synthesis of a silica-coated γ-Fe$_2$O$_3$ nanocomposite depends on the choice of proper precursors as proposed in the generalized mechanism [230].

3.6.2. Carbon. Carbon protected IONPs have recently triggered enormous research activities due to their good chemical and thermal stability, and intrinsic high electrical conductivity. The carbon coating provides an effective oxidation barrier and prevents corrosion in magnetic core materials. Hydrophilic carbon coating on iron oxide nanoparticle cores endows better dispersibility and stability than those shown by bare IONPs [231].

Various approaches have been developed for synthesizing IONP@C core–shell nanostructures. As shown in figure 16, the common approach is a three-step process: firstly, magnetic IONPs are prepared as seeds by various methods, and then the polymer is coated through the polymerization process, finally forming IONP@C composite materials by annealing treatment. For example, Lei *et al* demonstrated that through a controlled coating of a thin layer of polydopamine on the surface of α-Fe$_2$O$_3$ in the dopamine aqueous solution, followed by subsequent carbonization, N-doped carbon-encapsulated magnetite has been synthesized and displayed excellent electrochemical performance as an anode material for lithium-ion batteries [232]. Li *et al* reported for the first time for the selected-control, large-scale synthesis of monodispersed Fe$_3$O$_4$@C core–shell spheres, chains, and rings with tunable magnetic properties based on structural evolution from eccentric Fe$_2$O$_3$@poly(acrylic acid) core–shell NPs [233].

Recently, much attention has been paid to the synthesis of Fe$_3$O$_4$/graphene as a new kind of hybrid material, owing to its wide-ranging applications in lithium-ion batteries, ion removal, sensors, catalysts, etc [234–237]. The unique properties of Fe$_3$O$_4$/graphene hybrids, combining effects from graphene, which has high conductivity and a large surface-to volume ratio, and Fe$_3$O$_4$ NPs, with their high magnetism, low price, and environmentally benign nature, have opened a new window for fabricating highly stable multifunctional nanomaterials [238]. Many approaches can be used to synthesize the Fe$_3$O$_4$/graphene hybrid materials. For example, Liu *et al* reported a superparamagnetic reduced graphene oxide-Fe$_3$O$_4$ hybrid composite (rGO-Fe$_3$O$_4$), which was prepared by the solvothermal reaction of Fe(acac)$_3$ and graphene oxide (GO) in ethylenediamine (EDA) and water [239]. Zhang *et al* have described a facile approach to control the assembly of monodisperse Fe$_3$O$_4$ NPs on chemically rGO.
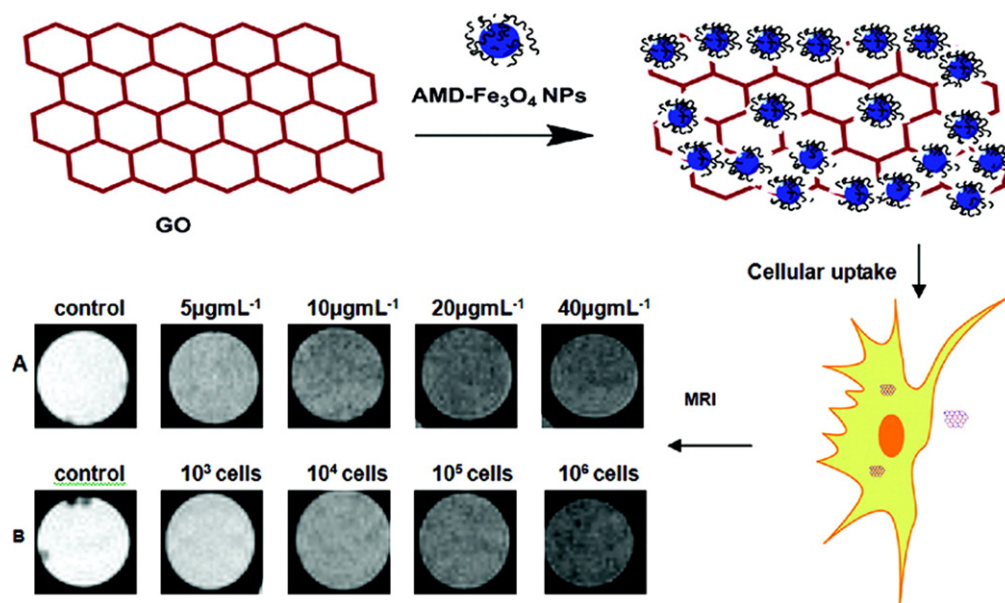
Figure 17. Schematic diagram showing preparation of Fe_3O_4–GO composites and using for cellular MRI. (Reprinted with permission from W H Chen *et al* 2011 *ACS Appl. Mater. Interfaces* **3** 4085. Copyright 2011 American Chemical Society.)

First, reduction and functionalization of GO by PEI were achieved simultaneously by simply heating the PEI and GO mixture at 60 °C for 12 h. Meso-2,3-dimercaptosuccinic acid (DMSA)-modified Fe_3O_4 NPs were then conjugated to the PEI moiety which was located on the periphery of the GO sheets via the formation of amide bonds between COOH groups of DMSA molecules bound on the surface of the Fe_3O_4 NPs and amine groups of PEI [240].

Moreover, Fe_3O_4/graphene hybrid materials have been used in biological fields, such as targeted drug delivery and MRI [241–243]. For example, Chen *et al* have reported that the fabricated composites of aminodextran-coated Fe_3O_4 NPs and GO were efficient for cellular MRI. As shown in figure 17, the *in vivo* study showed that the internalization of Fe_3O_4–GO composites has no effect on the cellular viability and proliferation. Compared to the bare Fe_3O_4 NPs, the Fe_3O_4–GO composites exhibit a significantly improved T_2 weighted MRI contrast, which is explained by the fact that the Fe_3O_4 NPs formed aggregates on the GO sheets, resulting in a considerable enhanced T_2 relaxivity [244].

3.6.3. Metal. Metallic NPs (e.g., Au, Ag, Cu, Pd, Co, Pt, etc) possess a range of fascinating properties (localized surface plasmon resonance (LSPR) and surface-enhanced Raman scatting (SERS)) [245] and many anisotropic metallic NPs have been applied in catalysis [246], contrast imaging [247], medicine [248], and sensing [249]. The combination of metallic NPs and magnetic IONPs has also attracted increasing interest to materials scientists due to their combined physicochemical properties and potential properties in catalysts [250], biotechnology [251], and biomedicine [252, 253]. Generally, monodispersed iron oxide/metal nanostructures, such as core–shell, core–satellites, and dumbbell structures, exhibit binary/polynary properties. Moreover, these structures can be

modified with different charges, functional groups or moieties on the surface of IONPs to improve stability and compatibility [254–256]. One of the most efficient and facile functionalization methods is the sequential growth of metallic components (e.g., Ag or Au) onto the surface of the IONP core in a one-pot reaction. The core–shell, core–satellites and dumbbell structures can be formed by microemulsion and thermal decomposition methods [257, 258]. However, it was found that the direct coating of IONPs with metal (or coating metal with IONPs) is very difficult in thermal decomposition, due to the dissimilar nature of the two surfaces and lattice [259]. Gold and silver seem to be ideal coatings owing to their low reactivity with IONPs. Furthermore, the introduction of surfactants and additives to the synthesis can alter the stability and surface property of IONPs or metallic NPs. Oleylamine (OA) is the common agent acting as capping agent, stabilizer and reductant [260]. For instance, OA and oleic acid capped 10 nm Fe_3O_4 NPs were synthesized via thermal decomposition of iron (III) oleate and were used for the synthesis of Fe_3O_4–Au NPs. Subsequently, core–shell Fe_3O_4–Au and Fe_3O_4–Au–Ag NPs are prepared by depositing Au and Ag on the surface of Fe_3O_4 NPs. Furthermore, the tunable plasmonic property of the core–shell structure was adjusted by shell thickness to be either red-shifted (to 560 nm) or blue-shifted (to 501 nm), which has great potential for nanoparticle-based diagnostic and therapeutic applications [261].

Another common route to synthesize IONP/metal composites involves multi-step methods including the seed-mediated method and emulsion method, resulting in core–shell, aggregated, and multilayers or hybrid IONP/metal structures. The most commonly reported structure in the literature is the core–shell Fe_3O_4@Au structure. For instance, monolayer-capped core–shell Fe_3O_4@Au was prepared by using the prepared Fe_3O_4 NPs as the seed and subsequently

reducing Au ions. The Fe_3O_4 NP seeds displayed high efficiency of gold coating on the Fe_3O_4 NP seeds for formatted Fe_3O_4@Au core–shell NPs with controllable surface properties [262]. Layer-by-layer self-assembly is another feasible multi-step method for preparing multilayers or hybrid IONP/metal structures [258, 263]. The self-assembly approach renders NPs or other discrete components to spontaneously organize into ordered structures by molecular interactions [264], and the chemistry conjugation, organic surfactants with aliphatic/hydrophobic tail groups, and/or hydrocarbon solvents are the primary interactions for the formation of hybrid IONP/metal structures [258, 265]. For example, FeOOH–Au hybrid nanorods were synthesized by a layer-by-layer technique and subsequently those hybrid nanorods can be transformed into Fe_2O_3–Au and Fe_3O_4–Au hybrid nanorods via the controllable annealing process. The homogenous deposition of Au NPs onto the surface of FeOOH nanorods is attributed to the strong electrostatic attraction between metal ions and polyelectrolyte-modified FeOOH nanorods [266]. Recently, Truby *et al* prepared hybrid plasmonic–superparamagnetic NPs (gold nanorods–superparamagnetic IONPs, Au NR–SPIONs) with unique optical and magnetic properties by a facile aqueous-based, self-assembly approach. In this process, although only Au NRs were functionalized by carboxyl-bearing surface ligands, the hybrid Au NR–SPION nanostructures were produced upon simple mixing of the components owing to the chemisorption between the carboxyl groups and SPION surface. This hybrid SPION–Au NP structure maintained similar plasmonic properties to COOH–Au NPs according to the extinction spectra [190].

In all the above mechanisms, the formation of IONP/metal structures was via molecular or charged links between IONPs and metal, whereas the dumbbell IONP/metal structures interfacial interaction originate from electron transfer across the nanometer contact at the interface of IONPs and metal NPs, inducing new properties that are not present in the individual component [267]. Sun *et al* developed a series of dumbbell IONP/metal structures through controlling the nucleation and growth of only one Fe_3O_4 on each Au (or Pt, or Pd) seeding NPs under the current synthetic conditions, which was attributed to the possible electron transfer between Au and Fe, and applied for enhanced catalysis, target-specific imaging and delivery [121, 123, 268, 269]. Furthermore, they based this on the understanding of the formation mechanism and took insight from the mechanical property of dumbbell-like Au–Fe_3O_4 NPs by overgrowing Au_2 on Au_1–Fe_3O_4 NPs. The 'tug-of-war' mechanism between Au_2 and Fe_3O_4 was attributed to the formation of a Au_2–Au_1–Fe_3O_4 ternary nanostructure after Au_2 growing on the preformed Au_1–Fe_3O_4 NPs. The strain energy between Au_1 and Fe_3O_4 played an important role, which not only decided their structure stability, but might also affect their functional performance. The reduced compressive stress in Au_1 NP will result in possibly unbalanced stress across the interface. As a result, Au_2 extracted Au_1 out from the Au_1–Fe_3O_4 conjugation, generating a new dumbbell-like Au_2–Au_1 and a dented Fe_3O_4 NP [270, 271]. As shown in figure 18, Buck *et al* have developed a total-synthesis framework for the construction of hybrid nanoparticle architectures that include M–Pt–Fe_3O_4 (M = Au, Ag, Ni, Pd) heterotrimers, M_xS–Au–Pt–Fe_3O_4 (M = Pb, Cu) heterotetramers and higher-order oligomers based on the heterotrimeric Au–Pt–Fe_3O_4 building block. This synthetic framework conceptually mimics the total-synthesis approach used by chemists to construct complex organic molecules. The reaction toolkit applies solid-state nanoparticle analogues of chemoselective reactions, regiospecificity, coupling reactions and molecular substituent effects to the construction of exceptionally complex hybrid nanoparticle oligomers [272].

However, taking into account what the application requires and the relatively limited chemical stability of the metal-coated IONP core–shell, aggregated, and dumbbell, most studies have focused on the development of multi-layer IONP/metal components. Affinity via amine/thiol terminal groups, surfactants and biocompatibility multi-layers are applied to further enhance protecting the core from oxidation and corrosion, and to exhibit good biocompatibility [273–275]. Generally, co-polymers and branched polymers with biocompatibility are selected as effective stabilizers for metal–iron oxide composites. For instance, Lim *et al* utilized three different macromolecules, Pluronic F127, cationic polyelectrolyte poly(diallyldimethylamonium chloride) (PDDA), and PEG, to coat the preformed core–shell iron oxide/Au particles and promote colloidal stability in elevated ionic strength media. The results demonstrated that the co-polymer Pluronic F127 or PDDA coatings yielded longer stable dispersions (up to 20 h) than single polymer PEG [276]. Encapsulation is another effective route for the promotion of safety and stability of IONP/metal components and the formation of a new structure (such as the rattle structure) [277], and inorganic material SiO_2 is a universal material. The Fe_3O_4–Au hybrid nanocrystal encapsulated in a silica nanosphere was synthesized via reducing $AuCl_4^-$ and the preferential nucleation of Au at the Fe_3O_4 surface. Then Fe_3O_4 was selectively dissolved through a reductive process. As a result, a nanorattle structure consisting of a hollow or porous silica nanoshell and Au nanocrystals can be generated [278].

3.6.4. Metal oxides and sulfides. More and more metal oxides or sulfides have been used to protect or functionalize IONPs, mainly because of the fantastic magnetic properties of IONPs and other unique physical or chemical properties of metal oxides and sulfides.

Oxide and sulfide semiconductors are the most common compounds that are used to functionalize magnetic IONPs, such as TiO_2 [279–281], ZnO [282], SnO_2 [283, 284], WO_3 [285], Cu_2O [286], CdS [287–289], ZnS [290, 291], PbS [292], Bi_2S_3 [293], etc. For example, the spindle-like IONP@SnO_2, IONP@TiO_2 and IONP@ZnO composite NPs were synthesized successively by different wet-chemical routes; their composite NPs exhibited enhanced photocatalytic abilities for organic dyes, mainly owing to the synergistic
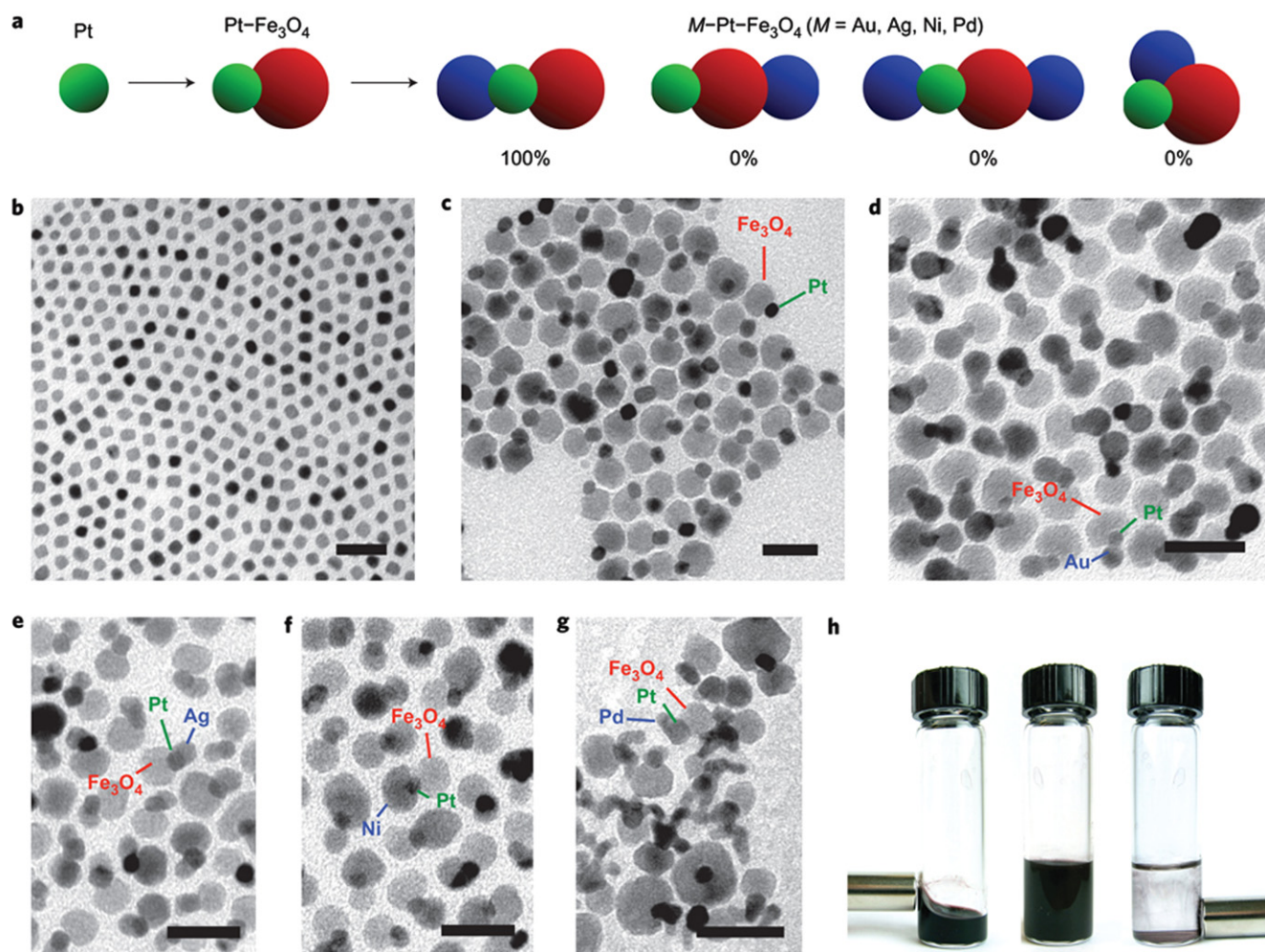
Figure 18. Stepwise construction of M–Pt–Fe_3O_4 heterotrimers (M = Ag, Au, Ni, Pd). a, Schematic showing the multistep synthesis of M–Pt–Fe_3O_4 heterotrimers, along with the most significant possible products and their observed frequencies (expressed as the percentage of observed heterotrimers, not total yield). Representative TEM images show Pt nanoparticle seeds (b), Pt–Fe_3O_4 heterodimers (c) and Au–Pt–Fe_3O_4 (d), Ag–Pt–Fe_3O_4 (e), Ni–Pt–Fe_3O_4 (f) and Pd–Pt–Fe_3O_4 (g) heterotrimers. All scale bars are 25 nm. (h) Photographs of a vial that contains Au–Pt–Fe_3O_4 heterotrimers in hexane (left), which responds to an external Nd–Fe–B magnet, the same vial with Au–Pt–Fe_3O_4 heterotrimers in a larger volume of hexanes (middle) and the same vial after precipitation of the heterotrimers with ethanol (right). The precipitated heterotrimers collect next to the external magnet. (Reprinted with permission from M R Buck *et al* 2011 *Nat. Chem.* **4** 37. Copyright 2011 Nature Publishing Group.)

effect between the narrow and wide bandgap semiconductors and effective electron-hole separation at the interfaces of iron oxides/semiconductors [281–284]. As shown in figure 19, Lee *et al* developed a sol–gel reaction of tantalum (V) ethoxide in a microemulsion containing Fe_3O_4 NPs that was used to synthesize multifunctional Fe_3O_4/TaO_x core–shell NPs recently, which were biocompatible and exhibited a prolonged circulation time. When the NPs were intravenously injected, the tumor-associated vessel was observed by using computed tomography (CT), and MRI revealed the high and low vascular regions of the tumor [294]. Wu *et al* have presented a very simple strategy for the synthesis of superparamagnetic and fluorescent Fe_3O_4–ZnS hollow nanospheres by a combining of corrosion and the Ostwald ripening process. These hollow nanospheres with diameters smaller than 100 nm are not only nontoxic with a highly porous shell but also exhibit very good magnetic resonance and fluorescence [295]. Indeed, semiconductors are common used as a

functionalized layer to coat IONPs for obtaining bi-functional composite NPs, such as fluorescence and magnetic [212], photocatalyst and magnetic, etc.

Magnetic materials coated on magnetic IONPs usually have a dramatic influence on the final magnetic properties, including the iron oxide itself [296], Co_3O_4 [297, 298], NiO [299], Mn_xO_y [300, 301], $CoFe_2O_4$, $MnFe_2O_4$, etc. The combination of two different magnetic phases will generate new magnetic composites with many possible applications. For example, Manna *et al* have reported the magnetic proximity effect in a ferrimagnetic Fe_3O_4 core–ferrimagnetic γ-Mn_2O_3 shell nanoparticle system. As shown in figure 20, the magnetization of core–shell NPs is clearly greater than that of the bare core NPs [302]. Liu *et al* have developed the manufacture of a series of multifunctional magnetic core–shell hetero-nano-architectures (designated as Fe_3O_4@NiO and Fe_3O_4@Co_3O_4) by an *in situ* solvothermal-coating/decomposition approach. The resulting core–shell NPs
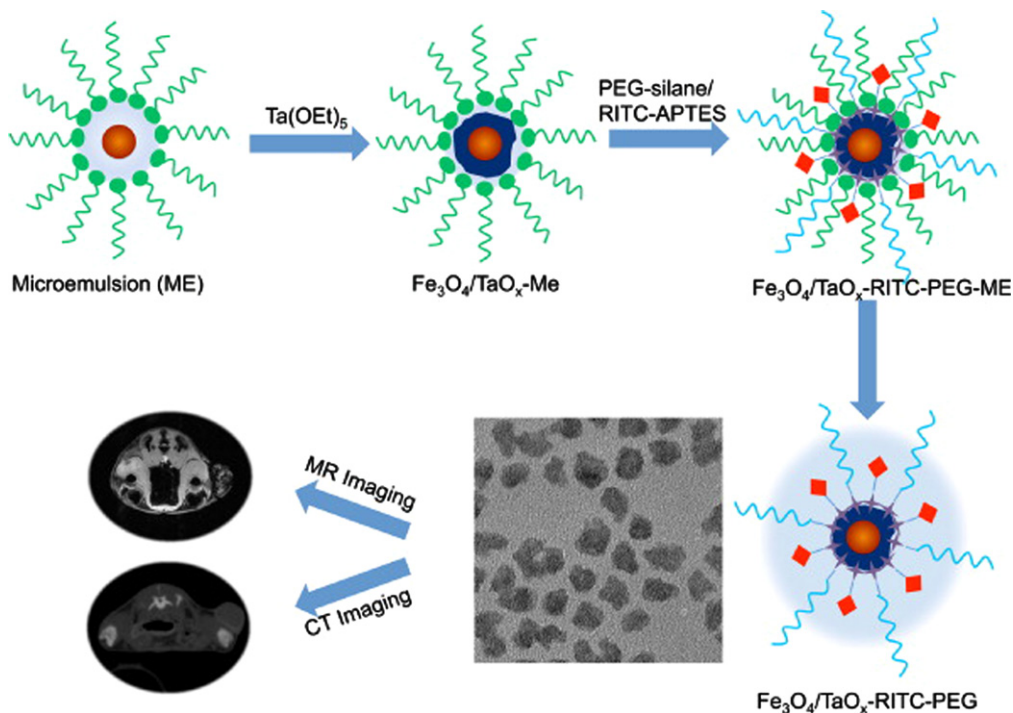
Figure 19. Schematic illustration of synthesis and modification of Fe_3O_4–TaO_x core–shell NPs, and application for simultaneous MRI and CT. (Reprinted with permission from N Lee *et al* 2012 *J. Am. Chem. Soc.* **134** 10309. Copyright 2012 American Chemical Society.)
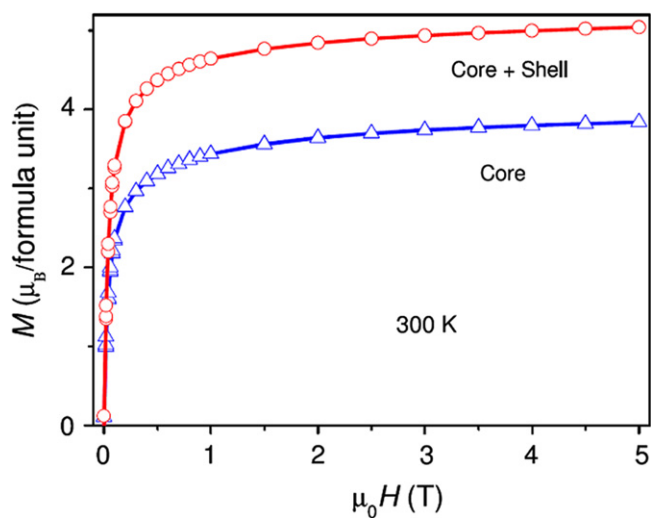

Figure 20. Magnetization versus field plots of bare core Fe_3O_4 and core–shell Fe_3O_4–γ-Mn_2O_3 NPs at 300 K. (Reprinted with permission from P Manna *et al* 2011 *J. Phys. Condens. Matter* **23** 506004. Copyright 2011 Institute of Physics.)

presented a number of important characteristics, such as controllable shell thickness, excellent magnetism, stable recyclability as well as a large surface-exposure area. By taking advantage of the high affinity of the metal ion on the shell surface toward biomolecules and rapid response toward an assistant magnet, the Fe_3O_4@NiO can be applied to magnetically separate His-tagged proteins from a cell lysate and efficiently enrich peptides with different molecular weights from complex sample systems for mass spectrometry analysis [303].

4. Biomedical applications

The biocompatibility and toxicity of IONPs are important criteria to take into account for their biomedical applications. Parameters determining biocompatibility and toxicity are the nature of the magnetically responsive component, and the final size of the composite particles including their core and the coatings (shell). Ideally, composite IONPs must also have a high magnetization so that their movement in the blood can be controlled with an external magnetic field until it is immobilized close to the targeted pathologic tissue [153]. Magnetic IONPs with a long blood retention time, biodegradability and low toxicity have emerged as one of the primary nanomaterials for biomedical applications *in vitro* and *in vivo*. Some biomedical applications require surface functionalized, especially core–shell type, magnetic IONPs.

4.1. In vivo applications

IONPs have a large surface area and can be engineered to provide a large number of functional groups for cross-linking to tumor-targeting ligands such as monoclonal antibodies, peptides, or small molecules for diagnostic imaging or the delivery of therapeutic agents [304]. Especially, the magnetic properties of IONPs can be used in numerous *in vivo* applications, which can be divided into three main groups: (i) magnetic vectors that can be directed by means of a magnetic field gradient towards a certain location, such as in the case of targeted drug delivery; (ii) magnetic contrast agents in MRI; and (iii) hyperthermia or thermoablation agents, where the
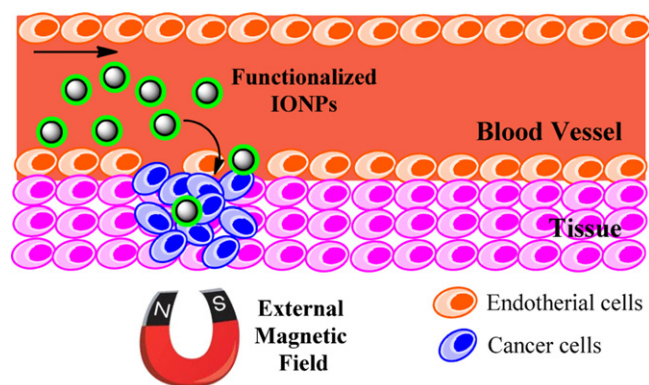
Figure 21. Schematic representation of magnetic nanoparticle-based drug delivery system: these magnetic carriers concentrate at the targeted site using an external high-gradient magnetic field. After accumulation of the magnetic carrier at the target tumor site *in vivo*, drugs are released from the magnetic carrier and effectively taken up by the tumor cells.

magnetic particles are heated selectively by application of a high-frequency magnetic field [305].

4.1.1. Targeted drug delivery. In traditional drug delivery systems, such as oral ingestion or intravascular injection, the medication is distributed throughout the body through systemic blood circulation. For most therapeutic agents, however, only a small portion of the medication reaches the affected organ and there is reduced drug diffusion through biological barriers causing a high incidence of adverse effects. Targeted drug delivery (TDD) seeks to concentrate the medication in the tissues of interest while reducing the relative concentration of the medication in the remaining tissues and crossing the biological barriers by active accumulation or an active targeting strategy [306]. Furthermore, magnetic IONP-based drug targeting (figure 21) is a promising cancer treatment method for avoiding the side effects of conventional chemotherapy by reducing the systemic distribution of drugs and lowering the doses of cytotoxic compounds [307]. Functionalized IONPs as a carrier can deliver a wide range of drugs to all areas in the body. Hence the efficient intracellular delivery of NPs is one of the main factors in enhancing the efficacy of the encapsulation therapeutic agent. Generally, magnetic IONPs are used as the core and biocompatible components act as a functionalized shell to form the core–shell structure for TDD carriers, and the drugs are bound or encapsulated into the polymer matrix. In a drug carrier system, the sizes, surface properties, and stability are the crucial features. Partially, the IONPs should be small enough to penetrate through the capillary bed. However, if the diameter of the IONPs is smaller than 10 nm, they will be rapidly removed through extravasations and renal clearance. Therefore, IONPs with a diameter ranging from 10 to 100 nm are optimal for intravenous injection and have the most prolonged blood circulation times [68]. Additionally, IONPs with a positive charge are better internalized by human breast cancer cells than those IONPs with negative charge. However, intake of

these IONPs also depends upon cell type. IONPs with a hydrophobic surface are easily adsorbed at the protein surface and show a low circulation time [308]. Hence, many biocompatibility materials have been used to functionalize IONPs for TDD, such as biocompatible organic polymers (PEG, chitosan, dextran, etc), liposomes, silica, and bioceramics [182].

Nanostructure-mediated TDD, a key technology for the realization of nanocarriers, has the potential to enhance drug bioavailability, improve the timed release of drug molecules, easily functionalize with targeting ligands, and enable precision drug targeting (sensitivity to an external magnetic field). In particular, magnetic composite IONPs are currently recognized as one of the most promising modalities of such drug carriers [309–311]. Furthermore, nanostructure targeted IONPs carriers can not only serve as a vehicle for drug delivery, but also for gene delivery [312]. For instance, Qiu *et al* have developed an MRI visible gene delivery system Stearic-LWPEI-SPIO for the delivery of minicircle DNA (mcDNA). These Stearic-LWPEI-SPIOs possess a high mcDNA binding capability for the protection of mcDNA from enzymatic degradation and the controlled release of mcDNA in the presence of polyanionic heparin. Furthermore, Stearic-LWPEI-SPIO NPs loaded with mcDNA can enhance expression of luciferase in MCF-7 cells without evidently exhibiting cellular toxicity [313].

A high drug loading efficiency and drug-release rate are essential parameters for therapy, while mesoporous functional layers (such as SiO_2 and C) and IONPs with hollow or mesoporous structure are enabling the promotion of drug loading [314, 315]. For example, Zhang *et al* reported the development of a magnetic drug carrier composed of doxorubicin-conjugated Fe_3O_4 nanoparticle cores and a PEG-functionalized porous silica shell (Fe_3O_4–DOX/$pSiO_2$–PEG). The DOX loading capacity of the porous drug carrier system is 16.3 μg mg^{-1}. Fe_3O_4–DOX/$pSiO_2$–PEG NPs can be internalized by cells through an endocytosis process, and can also be easily functionalized with a targeting ligand via a silicone coupling agent for increased and specific uptake of the drug carrier in tumor cells over-expressing the folate receptor, such as MCF-7 and HeLa cells [316]. Recently, Kayal and Ramanujan have reported the DOX loading and release profiles of PVA coated IONPs, which showed that they can release 45% of the adsorbed drug in 80 h; the results illustrated that composite NPs are promising magnetic drug carriers to be used in magnetically targeted drug delivery [317].

Moreover, carriers comprising coated magnetic IONPs loaded with an anti-cancer drug are injected into the patient's body via the human circulatory system. An external magnetic field is used to localize the drug loaded carriers at the target site and the drug can then be released from the carriers either via enzymatic activity or changes in physiological conditions such as pH, osmolality, or temperature, and be taken up by target cells. Smart control release systems have been developed to meet the changed physiological conditions, enhance accumulation, and control drug release at the intended sites. The stimulus pH-/thermo-/photo-magnetic

TDD systems are the common smart control release systems [318]. Generally, the pH of body tissue is maintained around 7.4 in a healthy human. However, there exist several mechanisms to modulate pH inside the body. The gastro-intestinal tract changes the pH along the tube, which is ∼1–3 in the stomach and ∼7 in the intestine. Each mechanism has been used as a triggering signal for pH-responsive TDD. Basically, ionizable moieties, such as carboxylic acid, amine, azo, phenylboronic acid, imidazole, pyridine, sulfonamide, and thiol group functionalized IONPs can afford pH-sensitivity drug loaded carriers [319]. A thermosensitive polymer obtained by simple aliphatic modification of biocompatibility/biodegradable block copolymers exhibited a low critical solution temperature of ∼38 °C, thus the functionalized IONPs released the drugs in response to a variation in external temperature. For example, Zhang *et al* have successfully developed a novel magnetic drug-targeting carrier consisting of encapsulated magnetic IONPs with a smart thermosensitive polymer dextran-g-poly (N-isopropy-lacrylamide-co-N, N-dimethylacrylamide). The smart stimuli-responsive polymer enabled controllable drug release through small changes of temperature in the vicinity of a lower critical solution temperature (LCST) and pH. The system has a lower drug release at 20 °C (below the LCST), while at 40 °C (above the LCST) and at 37 °C (LCST) the drug release is high and rapid for the initial 5 h, followed by a sustained release at longer duration. The drug release is primarily influenced by a triggered drug release mechanism. The acidic medium favors drug release because of the acid-labile linker [320]. Additionally, targeted delivery of therapeutic agents to the brain has enormous potential for the treatment of several neurological disorders such as Alzheimer's disease and brain tumors. However, the blood–brain barrier (BBB) significantly impedes the entry of drug molecules into the brain from the bloodstream. IONP-based targeted delivery represents a promising alternative strategy in overcoming the BBB [321].

Presently, the development of multifunctional magnetic IONPs which were coated or functionalized with polymers, lipidic, or inorganic shells further boost the potential use in medicine. These multifunctional IONPs not only serve as a vehicle for TDD but also have applications in MRI [322], targeted thermosensitive chemotherapy [323], and fluores-cent/luminescence imaging [324]. For instance, Chourpa *et al* have developed novel biocompatible nanosystems, which are useful for cancer therapeutics and diagnostics (theranostics). These multifunctional NPs (SPION–DOX–PEG–FA) are not only for bimodal cancer cell imaging (by means of MRI and fluorescence) but also for bimodal cancer treatment (by targeted drug delivery and by the hyperthermia effect). Comparing the incubated cells with suspensions of SPION–DOX–PEG–FA and SPION–DOX–PEG shows they provide the same DOX fluorescence intensity. However, the uptake of the FA-functionalized NPs was twice that of SPION–DOX–PEG after 120 min of cell culture, while qualitatively the NP distribution remained similar and appeared as cytosolic staining, indicating that the quantity of FA grafted on the elaborated NPs appears sufficient to significantly increase their uptake by MCF-7 cancer cells [202]. Although

considerable achievements have been reached in magnetic TDD systems, to date, actual clinical trials are still problematic. IONPs may be considered to be biocompatible, but the immune response during the residence time of the carrier–drug conjugate, the toxicity of carrier materials and their possible decomposition products still warrant further investigation.

4.1.2. MRI. MRI is an imaging technique used primarily in medical settings to produce high quality images of the inside of the human body, which is based on the principles of nuclear magnetic resonance (NMR). Ultra small and related functionalized IONPs possess unique superparamagnetic properties, which generate significant susceptibility effects resulting in strong T_2 (spin–spin relaxation process) and T_2^* contrast, as well as T_1 effects (spin–lattice relaxation process) at very low concentrations for MRI, and are widely used for clinical oncology imaging as contrast agents [325–327]. A major barrier in the use of nanotechnology for practical applications is the difficulty in delivering NPs to intracranial positions. However, IONPs can deliver to the targeted site by external magnetic field. Additionally, a cellular magnetic-linked immunosorbent assay (C-MALISA) has been developed as an application of MRI for *in vitro* clinical diagnosis: first the different antibodies or fragments directed to several types of receptors can couple onto the surface of IONPs, then they can form a specific bind with the tumor for *in vivo* testing and magnetomotive optical molecular imaging [328]. Therefore, MRI is one of the most promising applications for magnetic IONPs [153].

Recently, Hadjipanayis *et al* reported IONPs (10 nm in core size) conjugated to a purified antibody that selectively binds to the epidermal growth factor receptor (EGFR) deletion mutant (EGFRvIII) present on human glioblastoma multiforme (GBM) cells and used for therapeutic targeting and MRI contrast enhancement of experimental glioblastoma, after convection-enhanced delivery. The MRI results revealed that a significant decrease in glioblastoma cell survival was observed after NP treatment and no toxicity was observed with treatment of human astrocytes ($P < 0.001$) [329]. Basly *et al* grafted small dendritic molecules through a phosphonate anchor by covalent attachment in order to stabilize iron oxide suspensions. The enhancement contrast ratio values are 15% to 75% higher than those obtained for Endorem™ (a commercial IONP contrast agent) on a MR T_{2w} image at 7 T. Such hybrid and biocompatible nanoscale objects may open a new route for the development of highly relaxing contrast agents displaying a quite satisfactory R_2/R_1 ratio even at high field [330].

In vivo cell tracking or labeling by MRI can provide the observation of biological processes and monitor cell therapy directly, which is another successful application of IONPs in MRI [331–333]. MRI allows for cell tracking with a resolution approaching the size of the cell when the cell loaded enough magnetic IONPs (for increasing the iron concentration). As shown in figure 22, Branca *et al* used cancer-binding ligand functionalized IONPs to target the cancer cells, then imaged by high-resolution hyperpolarized
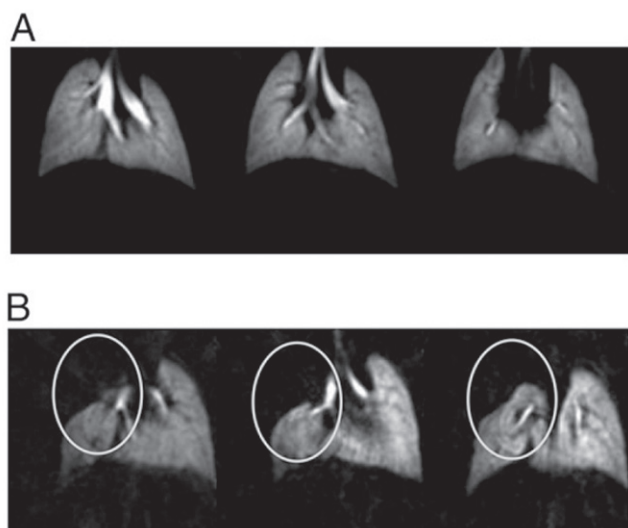
Figure 22. Detection of pulmonary metastases in a breast adenocarcinoma mouse model. (a) HP images (TE = 4 ms) from a control mouse, showing normal ventilation patterns. (b) Images from a human breast adenocarcinoma mouse model (TE = 4 ms) after injection of LHRH-SPIONs. A clear signal defect can be seen in the right lobe (yellow circles). All of the HP 3He lung MR images are formatted with 1 mm slice thickness. (Reprinted with permission from R T Branca *et al* 2010 *Proc. Natl Acad. Sci.* **107** 3693.)

[3]He MRI. *In vivo* detection of pulmonary micrometastates was demonstrated in mice injected with breast adenocarcinoma cells. This method not only holds promise for cancer imaging but more generally suggests a fundamentally unique approach to molecular imaging and cell tracking in the lungs [334]. Zhang *et al* investigated the feasibility of imaging green fluorescent protein (GFP)-expressing cells labeled with IONPs with the fast low-angle positive contrast steady-state free precession (FLAPS) method and to compare them with the traditional negative contrast technique. The GFP cell was incubated for 24 h using 20 μg Fe mL^{-1} concentration of SPIO and USPIO NPs. The labeled cells were imaged using positive contrast with FLAPS imaging, and FLAPS images were compared with negative contrast T_2*-weighted images. The results demonstrated that SPIO and USPIO labeling of GFP cells had no effect on cell function or GFP expression. Labeled cells were successfully imaged with both positive and negative contrast MRI. The labeled cells were observed as a narrow band of signal enhancement surrounding signal voids in FLAPS images and were visible as signal voids in T_2*-weighted images. Positive contrast and negative contrast imaging were both valuable for visualizing labeled GFP cells [335].

The use of these IONP colloids as specific contrast agents for MRI is now a well-established area of pharmaceutical development. Feridex®, Endorem™, GastroMARK®, Lumirem®, Sinerem®, Resovist® and more pending patents tell us that the last word in this area has not been said. There are three remarkable advantages of IONPs in MRI applications as follows: (1) a minimum delay of about 10 min between injection (or infusion) and MR imaging extends the examination time; (2) cross-section flow void in narrow

blood vessels may impede the differentiation from small liver lesions; and (3) aortic pulsation artifacts become more pronounced [336].

It is noteworthy that more functionalized IONPs have been utilized in MRI [337–339]. For example, Smolensky *et al* have demonstrated that the incorporation of a thin organic coating containing efficient iron oxide and gold chelators significantly increased the saturation magnetization of core–shell iron oxide@gold NPs. The resulting high relaxivity of the nanocomposites, together with the small, compact structure of the assemblies and their characteristic plasmonic behavior, renders Fe_3O_4@organic@gold an attractive alternative to current magnetoplasmonic agents for multimodal cell imaging [340]. Recently, Zhou *et al* have prepared nearly monodispersed yolk-type Au@Fe_3O_4@C nanospheres with hollow cores of 50 nm in diameter through coating Au@SiO_2 NPs with Fe_3O_4@C double layers, followed by dissolving SiO_2. The coexistence of Fe_3O_4 and Au also makes the nanospheres dual probes for MRI with a specific relaxivity (r_2*) of 384.38 mM^{-1} s^{-1} and optical fluorescence imaging using a near-infrared excitation [341].

4.1.3. Magnetic hyperthermia and thermoablation. The use of ferromagnetic NPs for magnetic hyperthermia and thermoablation therapies has attracted considerable attention as one of the promising treatments for cancer [342, 343]. Hyperthermia is the heating of cells in the range of 41–47 °C, which causes the preferential death of tumor cells [344]. When magnetic IONPs are subjected to an alternating magnetic field, heat generation is a result of a combination of internal Néel fluctuations of the particle magnetic moment, hysteresis, and the external Brownian fluctuations that all rely on the magnetic properties of IONPs. However, the temperature of the thermoablation method is often greater than 47 °C, which causes the rapid death of tumor cells due to the high temperature. Thus, some difficulties are faced when heating the tumor part to a sufficiently high temperature while simultaneously maintaining the normal tissues at a lower temperature. Modern techniques generally employ localized hyperthermia for cancer therapy [345]. Many techniques have been developed for the localized heating treatment of cancers, for example, radio-frequency waves (as shown in figure 23 [346]), microwaves and ultrasounds [347–349].

In general, the specific adsorption rate (SAR) is the main parameter determining how effectively NPs generate heat to the tissue during magnetic hyperthermia treatment. SAR is the rate at which electromagnetic energy (E_{em}) is absorbed by a unit mass of a biological material (*m*) when exposed to a radio frequency (R_F) electromagnetic field.

It can be expressed as follows:

$$\text{SAR} = \frac{d}{dt}\left(\frac{E_{em}}{dm}\right).$$

For a ferrofluid sample, the SAR is usually averaged either over the whole body, or over a small sample volume (typically 1 g or 10 g of tissue). It is also related to the electric field or the temperature rise at a given point [350], and hence
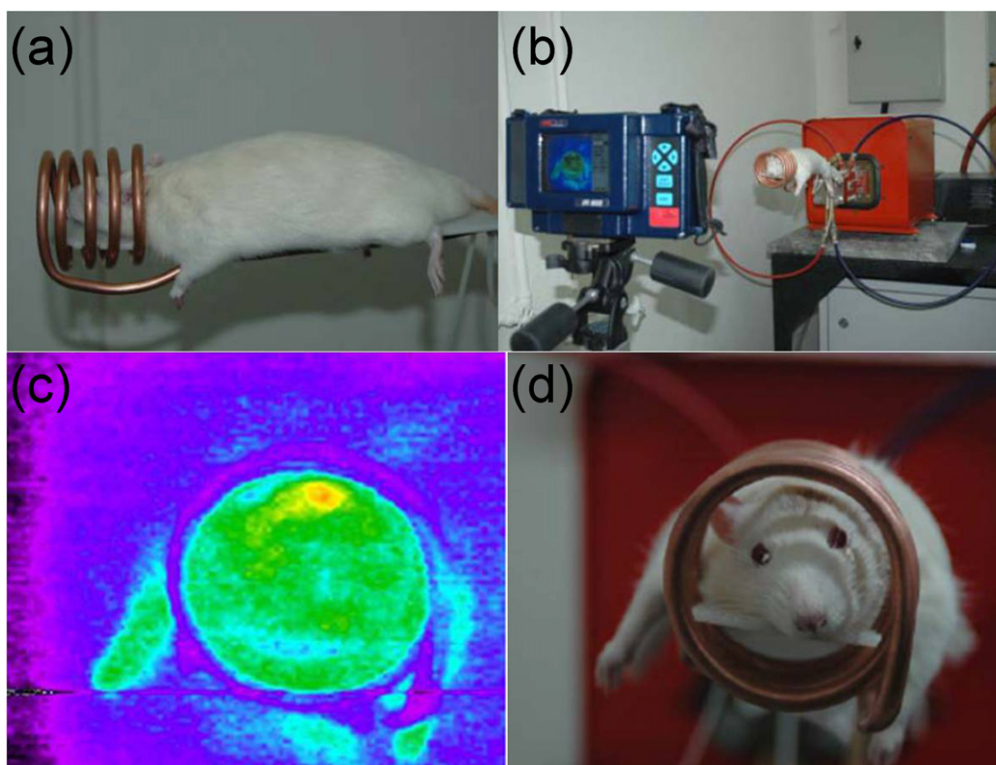
Figure 23. Ferrofluids containing IONPs are synthesized and characterized as possible agents for medical treatment and diagnosis. Specifically, novel iron-oxide-based NPs are investigated (i) as contrast agents for MRI, and (ii) for tumor treatment using the technique of magnetic hyperthermia where magnetic NPs are injected in the tumor and heated by applying a strong ac magnetic field. In the left picture the temperature increase of an extracranial tumor, after injecting a small quantity of ferrofluid and irradiating with low frequency radiofrequency waves (150 kHz).

it can be calculated from the electric field within the tissue as follows,

$$\mathrm{SAR} = \int_{\mathrm{sample}} \frac{\sigma(r)|E(\mathrm{r})|^2}{\rho(\mathrm{r})} \mathrm{d}r \approx 4.1868 \frac{P}{m_e} = C_e \frac{\Delta T}{\Delta t}$$

where σ is the sample's electrical conductivity, E is the RMS electric field, ρ is the sample density, P is the electromagnetic wave power absorbed by the sample, m_e is the mass of the sample, and C_e is the specific heat capacity of the sample. Therefore, SAR can expressed as being proportional to the rate of the temperature increase ($\Delta T/\Delta t$). Furthermore, according to the equation, for both the ferrofluid sample and the human body, the conductivity can be zero. Generally, SAR is commonly used to measure power absorbed from mobile phones and during MRI scans. The value will depend heavily on the geometry of the part of the body that is exposed to the RF energy (low-frequency magnetic wave of 100–400 KHz), and on the exact location and geometry of the RF source.

Hence, increased heating rates of magnetic IONPs are an important challenge in order to minimize dosages of magnetic IONPs needed to reach therapeutic temperatures in magnetic hyperthermia or thermoablation. Possible approaches to increase heating rates are increasing the anisotropy of the NPs (shape or magnetocrystalline) or increasing the field strength. An alternative approach to increase the heating rates would be to increase the monodispersity of a sample of magnetite NPs. Gonzales-Weimuller *et al* reported the size-dependant heating rates of IONPs for magnetic fluid hyperthermia. The results demonstrated that the SAR does indeed vary with particle size. The highest SAR measured was 447 W g^{-1} at 24.5 kA m^{-1} for 11.2 nm particles and models, indicating that higher heating rates were possible by increasing the size of the particles to 12.5 nm [351].

Some reports reveal that the surface functionalization improved the hyperthermic effect. As shown in figure 24, Liu *et al* reported that enhanced SAR with decreased surface coating thickness was observed and ascribed to the increased Brownian loss, improved thermal conductivity as well as improved dispersibility [352]. Moreover, the inorganic coating can also improve the SAR value. For example, Mohammad *et al* found that the hyperthermic effect of SPIONs is enhanced dramatically on coating with Au. The results indicated possibilities for utilization of very low frequency oscillating magnetic fields in hyperthermia treatment. The gold coating should retain the superparamagnetic fraction of the SPIONs much better than when compared to uncoated SPIONs alone; this leads to a higher energy of magnetic anisotropy of superparamagnetic NPs within the gold shell as compared to uncoated SPIONs. Excellent hyperthermia exhibited by SPION@Au NPs coupled with their lack of cytotoxicity was anticipated to make them into suitable candidates for thermolysis of cancer cells [353]. Recently, Balvata *et al* reported their magnetic hyperthermia
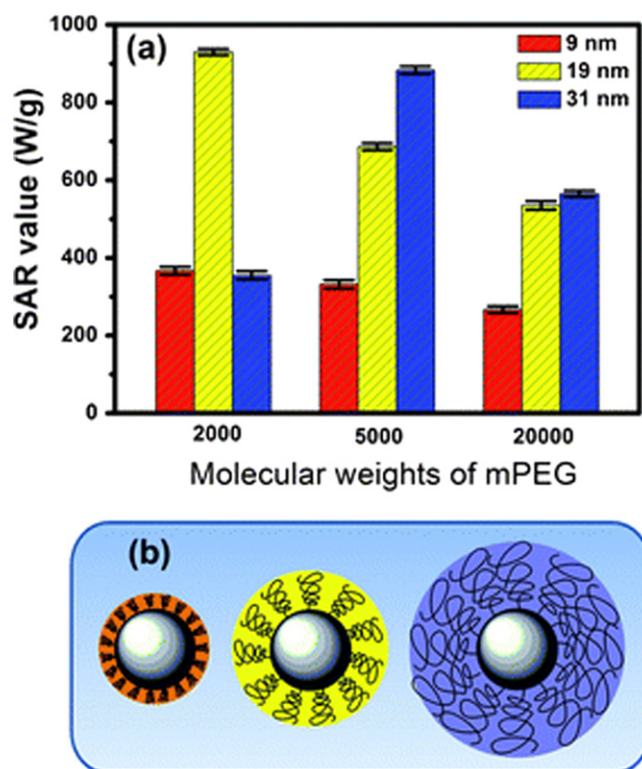
Figure 24. (a) The SAR values of the different sized Fe_3O_4 NPs for different mPEG: 9 nm (orange), 19 nm (yellow), 31 nm (blue). (b) A schematic diagram of nanoparticle based hyperthermia agents with iron oxide core and varied mPEG coating. (Reprinted with permission from X L Liu *et al* 2012 *J. Mater. Chem.* **22** 8235. Copyright 2012 Royal Society of Chemistry.)

results obtained after intratumoral injection, demonstrating that micromolar concentrations of iron given within the modified core–shell Fe/Fe_3O_4 NPs caused a significant anti-tumor effect on murine subcutaneous mouse melanoma with three short 10 min alternating magnetic field (AFM) exposures. These results indicated that intratumoral administration of surface modified MNPs attenuated mouse melanoma after AMF exposure, and these MNPs were capable of causing an anti-tumor effect in a mouse melanoma model after only a short AMF exposure time [354].

SPIONs can be considered as a very promising agent for hyperthermia therapy, but this new field of application requires an improvement of the reproducibility, size and shape controlling in the preparing process and its biocompatibility. Moreover, how to apply the cancer treatment of fine tissues (such as brain and kidney) is also an ongoing challenge.

4.2. In vitro applications

Another important kind of application of functionalized IONPs is *in vitro* application (such as biosensor, cell biose-paration), which promises increased sensitivity, speed, and cost-effectiveness. There are several promising nanocomposi-sites for *in vitro* application, such as Au NPs, and quantum dots (QDs). There are already *in vitro* diagnostic products on the market, based on magnetic IONPs.

4.2.1. Bioseparation. As a successful application of magnetic IONPs, bioseparation is also an important kind of application, especially for *in vitro* DNA, antibody, protein, gene, enzyme, cell, virus and bacteria separation [355–358]. Compared with the traditional separation procedures, magnetic separation has many advantages of being able to be quickly localized or retrieved with a common magnet (as shown in figure 25(a)) [18], which is faster and more cost-effective than traditional column affinity chromatography. Generally, surface functionalized magnetic IONPs with suitable intermediates are commonly used to enhance the separation efficiency with such modification of surfactants, polymers, and ligands for introducing functional end groups (such as –OH, –NH2, –SH, –COOH, etc) through the selective adsorption to the target biomolecules [359].

Recently, Chang *et al* reported a novel approach to efficiently separate proteins such as bovine serum albumin (BSA) by the modification of hydrophobic pockets on the surface of $Fe_3O_4@SiO_2$ NPs with various alkyl groups at various pH levels. The magnetic separation efficiency was strongly reflected and could be attained by controlling the size of the hydrophobic pocket and other factors such as the alkyl chain length, salt concentration, and pH levels [360]. Wang and Irudayaraj described the development of a facile route to the site-selective assembly of Fe_3O_4 NPs onto the ends, or ends and sides, of gold nanorods with different aspect ratios to create multifunctional nanorods incorporating optical and magnetic materials that provided tunable plasmonic and magnetic properties. As shown in figure 25(b), the Fe_3O_4–Au necklace-like hybrid NPs were functionalized with relevant antibodies to construct efficient platforms for simultaneous optical detection, magnetic separation, and thermal ablation of multiple pathogens from a single sample [361].

Additionally, IONP-based magnetic separation applica-tions involve strict requirements such as chemical composi-tion, particle size and size distribution, stability of magnetic properties, morphology, adsorption properties and low toxicity, and so on. For instance, Reza *et al* found that the BSA protein adhesions for magnetite–silica, magnetite–aminosilane and magnetite–silica–aminosilane arrays were 12.5%, 79.5% and 145.75% higher than for pure magnetite, respectively [362]. Arsianti *et al* systematically investigated the effect of IONP–PEI–DNA arrangement on transfection efficiency by varying the vector component mixing order. The aim was to elucidate the role of IONPs and PEI in gene delivery and to gain a fundamental understanding of the design of a suitable IONP-based vector for optimal plasmid DNA transfection. The highest magnetic vector cellular uptake was observed for the largest IONP vector (IONPs + PEI/DNA) due to enhanced gravitational and magnetic aided sedimentation onto the adherent cells. The highest gene expression was also observed for this MNP vector config-uration [363].

Magnetic IONPs with a core–shell structure may enable this development of bioseparation fields, especially silica coated IONPs [364–366]. For example, Shao *et al* have reported three-component microspheres containing a SiO_2-coated Fe_3O_4 magnetite core and a layered double hydroxide
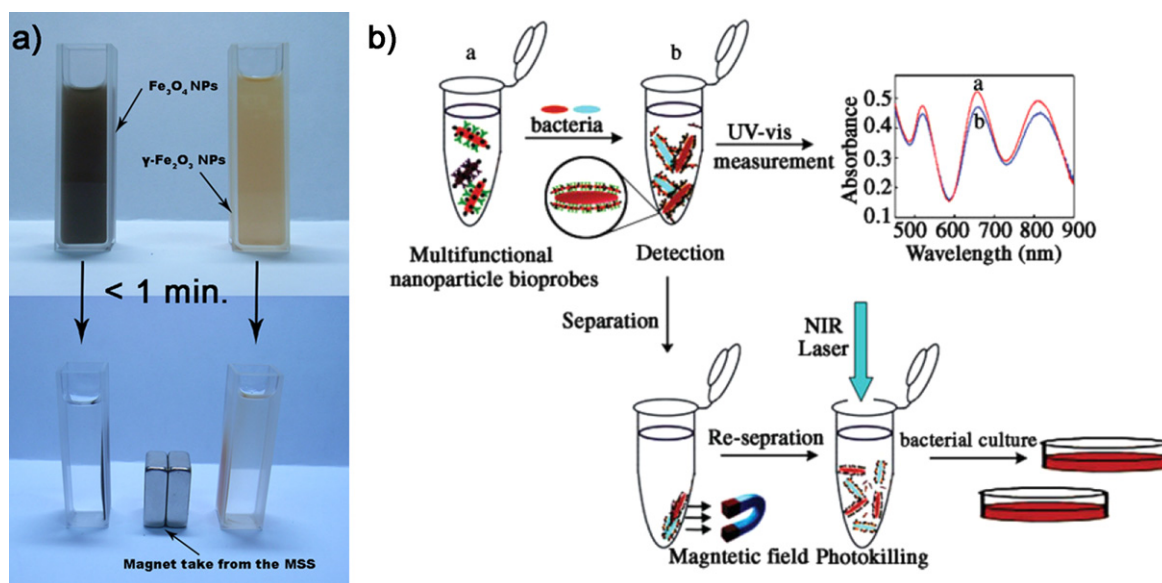
Figure 25. (a) The Fe_3O_4 and γ-Fe_2O_3 hollow NPs (dispersed in ethanol solution) before and after magnetic separation by an external magnet. (b) The detection, separation, and thermal ablation of multiple bacterial targets. (Reprinted with permission from C G Wang and J Irudayar 2010 *Small* **6** 283. Copyright 2010 John Wiley and Sons.)

(LDH) nanoplatelet shell via an *in situ* growth method. The microspheres possess superparamagnetism and high saturation magnetization (36.8 emu g^{-1}), which allows their easy separation from the solution, by means of an external magnetic field, and subsequent reuse. The microspheres show highly selective adsorption of the His-tagged protein from *Escherichia coli* lysate, demonstrating their utility [367]. The collection and separation rates for targets in a complex environment are crucial in bioscience.

4.2.2. Biosensor. Biosensing as an effective diagnostic platform has been developed to detect biomolecules and cells with high sensitivity that could enable early disease diagnosis [368]. Magnetic nanosensors exhibiting high specificity and biocompatibility have been synthesized for the *in vitro* and *in vivo* detection of molecular interactions. Upon target-induced nano-assembly formation, a sensitive and dose-dependent decrease in the spin–spin relaxation time (T_2, can be detected by magnetic resonance (NMR/MRI) techniques) of adjacent water [369]. Furthermore, the superparamagnetic IONP core of an individual nanoparticle becomes more efficient at dephasing the spins of surrounding water protons, enhancing T_2 relaxation times so that the NPs act as magnetic relaxation switches (MRS) in the cooperative assembly process. For example, Perez *et al* found that the MRS nanosensor can detect specific mRNA, proteins, enzymatic activity, and pathogens (e.g., a virus) with sensitivity in the low femtomole range (0.5–30 fmol) [370, 371]. In addition, the anisotropy of the magnetic shape was used to control the critical applied magnetic field required to switch the magnetization of the element between its two stable states, thus creating a binary barcode.

However, to date, magnetic biosensors for diagnosis have not only been based on the properties of IONPs, but also on

functionalized coated materials. The magnetic bead-based biosensors are functionalized IONPs by conjugating targeting ligands, which endow new specificity to the magnetic bead–based biosensors. Simultaneously, the IONPs, together with targeted receptors and functionalized layers/materials, act as the generator or detector of a signal, assigning the sensitivity of magnetic bead-based biosensors (figure 26). Generally, optical-magnetic bead-based biosensors exhibit excellent optical performance because of the unique interactions between light waves and the surface coating materials (such as Au, Ag, QDs and fluorescent molecules), which displayed excellent localized surface plasmon resonance (LSPR), surface-enhanced Raman scattering (SERS), and fluorescence [372, 373]. One-dimensional nanostructures (such as carbon nanotube, nanowires, and grapheme) have been applied as functional components for electrochemical magnetic bead-based biosensors [374, 375]. Those are usually based on a field-effect transistor (FET) where analyte molecules act as a gate, which controls the electrical resistance by causing depletion or accumulation of charge carriers. And the electrochemical–magnetic bead-based biosensors in clinical diagnosis are based on glucose, lactate, cholesterol, urea, creatine, and creatinine biosensors [376–378].

Many studies have been conducted on developing all kinds of magnetic bead-based biosensors with high-sensitivity and high-specificity, which have opened up an era of early disease diagnosis and better treatment [379, 380]. A composite electrode of glucose oxidase (GOD)–Fe_3O_4–Cs–Nafion was developed for glucose by combining the intrinsic peroxidase-like activity of Fe_3O_4 NPs and the anti-interference ability of the Nafion film. The novel glucose biosensor showed a relatively rapid response, high sensitivity (11.54 μAcm^{-2} mM^{-1}), low detection limit (6×10^{-6} M) and broad linear range (from 6×10^{-6} to 2.2×10^{-3} M). Furthermore, the wide detection range and high sensitivity may be
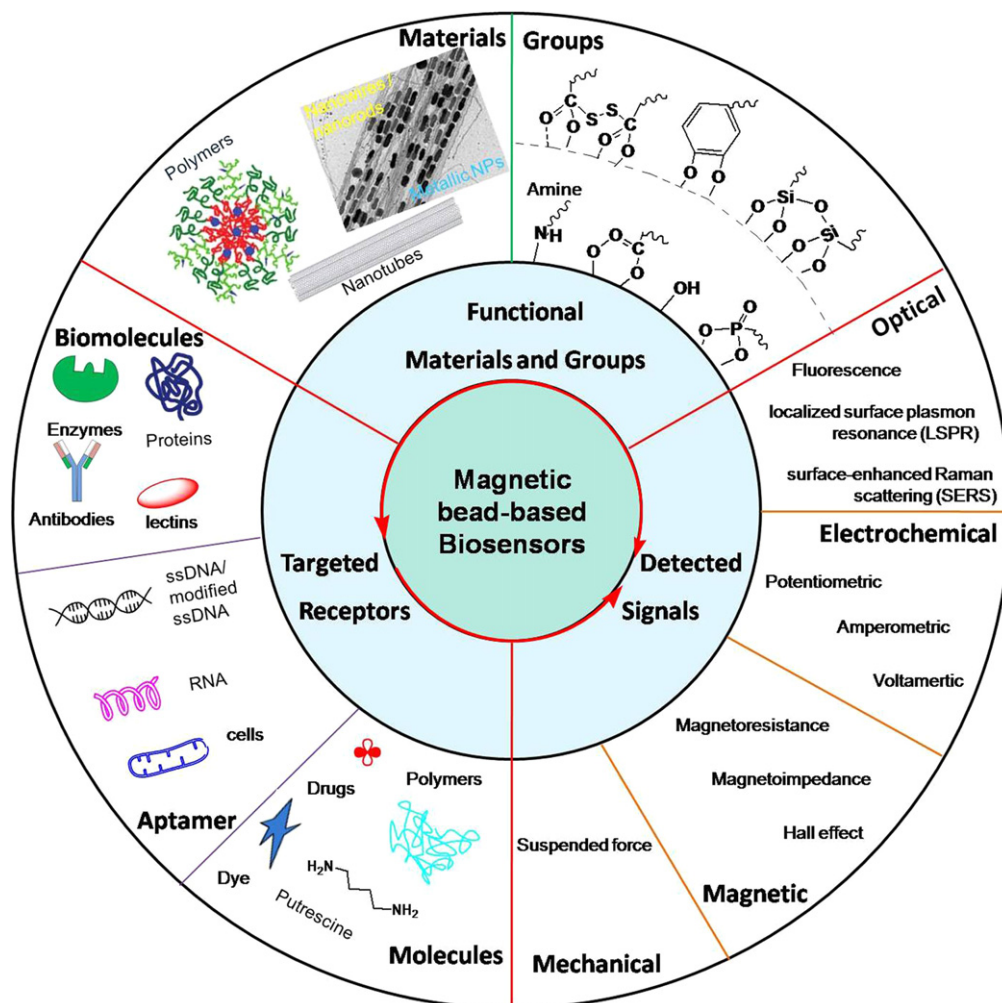
Figure 26. The components for magnetic biosensor and detail information.

assigned to the amplification of the magnitude of the current response for catalysis of H_2O_2 by Fe_3O_4 NPs [381]. Composite immunosensors based on gold NPs (GNPs), Fe_3O_4 NP–functionalized multiwalled carbon nanotube–chitosan (Fe_3O_4–FCNT–CS) and BSA composite film, were developed for the determination of carbofuran. The immunosensors exhibited good accuracy, high sensitivity, and stability for the detection of carbofuran. Under optimal conditions, the current detection limit was proportional to the concentration of carbofuran ranging from $1.0\ ng\ mL^{-1}$ to $100.0\ ng\ mL^{-1}$ and from $100.0\ ng\ mL^{-1}$ to $200\ lg\ mL^{-1}$ with the detection limit $0.032\ ng\ mL^{-1}$ [382].

Importantly, the sensitivity and specificity of magnetic biosensors are the crucial indicators to evaluate the newly developed magnetic biosensors for diagnosis. Furthermore, continuously improving the sensitivity and specificity of magnetic biosensors is a requirement of analysis testing [383, 384]. The routes for improvement of the sensitivity and specificity of magnetic biosensors were adopted by the measurement signal amplification via enzymatic amplification [385], signal amplification by applying NPs [386] polymers combination with functional groups [387]. For instance, IONPs and a grating-coupled surface plasmon resonance

(GC-SPR) sensor surface with metallic diffraction grating were modified with antibodies that specifically recognize different epitopes of the analyte of interest. Furthermore, the detection of β human chorionic gonadotropin (βhCG) was implemented to evaluate the sensitivity of the IONP-enhanced GC-SPR biosensor. The results revealed that the sensitivity of βhCG detection was improved by four orders of magnitude compared with the regular SPR sensor with direct detection format, and a limit of detection below pM was achieved [372].

Due to the complex components, and sensitivity and specificity requirements, the conventional routes for magnetic bead-based biosensors are a stepwise assembly process [388, 389], layer-by-layer assembly [390], and primary products that are solid-state platforms. Recently, however, research has demonstrated that solution-based platforms are beneficial over solid-state platforms because of the increasing probability of interaction between magnetic bead-based biosensors and analytes and allowing for biomolecule-based analytes to preserve their native form and function when in solution. For example, the lysine-modified diacetylene monomer with 10,12-pentacosadiynoic acid (Lys-PCDA)–SPION particles was prepared by the self-assembly of Lys-

PCDA onto OA-SPIONs in the solution phase, which acted as a platform for the capture and detection of serum proteins. This magnetic biosensor showed a colorimetric response that corresponded to an increasing concentration of anti-BSA antibodies, with a lower detection limit of 0.5 mg mL^{-1} [391].

The present trend for magnetic bead-based biosensors is not only to connect the sensitivity and specificity but also to develop multiplexed magnetic bead-based biosensors for multi-detection [392]. There has been huge progress in the development of magnetic bead-based biosensors in recent years, but their application in clinical diagnosis is not common, except for glucose magnetic bead-based biosensors, which represents the large global market. There are still challenges for magnetic bead-based biosensors in clinical diagnosis [393].

5. Summary and perspectives

The size, size distribution, and shape of IONPs are the important parameters influencing the pharmacokinetic and bio-distribution *in vivo* applications [394]. However, absolute control over the shape and size distribution of magnetic IONPs remains a challenge, and the different formation mechanisms of iron oxides under different conditions still need to be investigated. Furthermore, the ligands and functional layers are often comparable in size to the IONPs, and their coupling effect can significantly increase the hydrodynamic size. Concequently, the increasing hydrodynamic diameter contributes to the macrophage and systemic clearance of functionalized IONPs. Therefore, it is necessary to measure the hydrodynamic diameter and zeta potential of IONPs before and after functionalization. Moreover, biodistribution is also related to the IONP size and final colloid stability, which determines the fate of IONPs in *in vivo* and *in vitro* applications. Mitragotri and Lahann already concluded the size-dependent processes of NP transport in the human body [395], and the optimal hydrodynamic diameter range for *in vivo* application of intravenously injected NPs is 10–100 nm [396].

In addition, the surface properties IONPs such as surface charge play an important role in the physical stability and influence the interaction of IONPs with the biological system and their safety. In general, positively charged IONPs interacting strongly with blood components undergo relatively rapid clearance from systemic circulation, leading to non-specific tissue uptake. In contrast, negatively and neutrally charged IONPs show lower interaction with plasma proteins than positively charged IONPs, and tend to nonspecifically stick to the cells [397]. Furthermore, studies on the influence of the thickness of the functional layer, dispersant packing density, and dispersant conformation on the protein resistance of sterically stabilized IONPs have to be designed carefully to make sure that the right outcomes are arrived at.

The saturation magnetization (M_s) of uncoated and functionalized IONPs is one essential parameter that describes the magnetic response of IONPs. The M_s has been shown to decrease if the IONPs are satirically stabilized. However, M_s

is increased by agglomeration of IONPs. Furthermore, the anchor chemistry can also affect M_s via strong interactions with the ions in the surface layer of the magnetic core [397, 398].

Though magnetic IONPs exhibit many unique properties which endow various advantages and opportunities in biomedical applications, more toxicological research is needed on the as-synthesized IONPs, and the criteria to evaluate toxicity need to be clearly defined [399, 400]. For future studies, the use of better and faster methods to improve our understanding of nanoparticle toxicity mechanisms should greatly advance the field [401]. Additionally, the biocompatibility of IONPs is linked to both the intrinsic toxicity of functional layers and its biodegradation metabolites, and to the immune system response following its administration. Importantly, when associated with functional layers, the toxicity profile of the IONPs may be increased or decreased as a consequence of the modification of their cell/tissue biodistribution and clearance/metabolization. Accumulation may, indeed, occur in biological sanctuaries where IONPs cannot diffuse when administered alone.

It is desirable, especially for research and application purposes, to add multifunctional labels or (imaging modalities), such as fluorophores or radiotracers to IONP surfaces. The successful engineering of multifunctional NPs would be of particular interest for the development of theranostic nanomedicine. However, the challenge remains in the clinical translation of nanoparticle probes, and issues such as biocompatibility, toxicity, *in vivo* and *in vitro* targeting efficiency, and long-term stability of the functionalized IONPs need to be addressed [402].

Acknowledgments

References

[1] Wu W, He Q G and Jiang C Z 2008 Magnetic iron oxide nanoparticles: synthesis and surface functionalization strategies *Nanoscale Res. Lett.* **3** 397

[2] Gupta A K and Gupta M 2005 Synthesis and surface engineering of iron oxide nanoparticles for biomedical applications *Biomater.* **26** 3995

[3] Gilchrist R, Medal R, Shorey W D, Hanselman R C, Parrott J C and Taylor C B 1957 Selective inductive heating of lymph nodes *Ann. Surg.* **146** 596

[4] Yang L *et al* 2008 Development of receptor targeted magnetic iron oxide nanoparticles for efficient drug delivery and tumor imaging *J. Biomed. Nanotechnol.* **4** 439

[5] Lee N and Hyeon T 2012 Designed synthesis of uniformly sized iron oxide nanoparticles for efficient magnetic resonance imaging contrast agents *Chem. Soc. Rev.* **41** 2575

[6] Laurent S, Dutz S, Häfeli U O and Mahmoudi M 2011 Magnetic fluid hyperthermia: focus on superparamagnetic iron oxide nanoparticles *Adv. Colloid Interface Sci.* **166** 8

[7] Cao M, Li Z, Wang J, Ge W, Yue T, Li R, Colvin V L and Yu W W 2012 Food related applications of magnetic iron oxide nanoparticles: enzyme immobilization, protein purification, and food analysis *Trend. Food Sci. Technol.* **27** 47

[8] Lu A H, Salabas E L and Schuth F 2007 Magnetic nanoparticles: synthesis, protection, functionalization, and application *Angew. Chem. Int. Edn* **46** 1222

[9] Cornell R M and Schwertmann U 2003 *The Iron Oixdes: Structures, Properties, Reactions, Occurences and Used* (Weinheim: Wiley)

[10] Wu W, Xiao X H, Zhang S F, Zhou J A, Fan L X, Ren F and Jiang C Z 2010 Large-scale and controlled synthesis of iron oxide magnetic short nanotubes: shape evolution, growth mechanism, and magnetic properties *J. Phys. Chem. C* **114** 16092

[11] Zhang Z, Boxall C and Kelsall G H 1993 Photoelectrophoresis of colloidal iron oxides: 1. Hematite (α-Fe$_2$O$_3$) *Colloids Surf.* A **73** 145

[12] Boxall C, Kelsall G and Zhang Z 1996 Photoelectrophoresis of colloidal iron oxides. Part 2—magnetite (Fe$_3$O$_4$) *J. Chem. Soc. Faraday Trans.* **92** 791

[13] Wu W, Xiao X H, Zhang S F, Peng T C, Zhou J, Ren F and Jiang C Z 2010 Synthesis and magnetic properties of maghemite (γ-Fe$_2$O$_3$) short-nanotubes *Nanoscale Res. Lett.* **5** 1474

[14] Yamaura M, Camilo R L, Sampaio L C, Macedo M A, Nakamura M and Toma H E 2004 Preparation and characterization of (3-aminopropyl) triethoxysilane-coated magnetite nanoparticles *J. Magn. Magn. Mater.* **279** 210

[15] Levy M *et al* 2011 Correlating magneto-structural properties to hyperthermia performance of highly monodisperse iron oxide nanoparticles prepared by a seeded-growth route *Chem. Mater.* **23** 4170

[16] Guardia P, Labarta A and Batlle X 2010 Tuning the size, the shape, and the magnetic properties of iron oxide nanoparticles *J. Phys. Chem. C* **115** 390

[17] Wu W, Xiao X H, Ren F, Zhang S F and Jiang C Z 2012 A comparative study of the magnetic behavior of single and tubular clustered magnetite nanoparticles *J. Low Temp. Phys.* **168** 306

[18] Wu W, Xiao X H, Zhang S F, Li H, Zhou X D and Jiang C Z 2009 One-pot reaction and subsequent annealing to synthesis hollow spherical magnetite and maghemite nanocages *Nanoscale Res. Lett.* **4** 926

[19] Zhang L Y and Zhang Y F 2009 Fabrication and magnetic properties of Fe$_3$O$_4$ nanowire arrays in different diameters *J. Magn. Magn. Mater.* **321** L15

[20] Hou Y L, Gao S, Ohta T and Kondoh H 2004 Towards 3D spherical self-assembly by ternary surfactant combinations: the case of magnetite nanoparticles *Eur. J. Inorg. Chem.* **2004** 1169–73

[21] Massart R 1981 Preparation of aqueous magnetic liquids in alkaline and acidic media *IEEE Trans. Magn.* **17** 1247

[22] Wu W, He Q G, Hu R, Huang J K and Chen H 2007 Preparation and characterization of magnetite Fe$_3$O$_4$ nanopowders *Rare Met. Mater. Eng.* **36** 238

[23] Wu S, Sun A Z, Zhai F Q, Wang J, Xu W H, Zhang Q and Volinsky A A 2011 Fe$_3$O$_4$ magnetic nanoparticles synthesis from tailings by ultrasonic chemical co-precipitation *Mater. Lett.* **65** 1882

[24] Pereira C *et al* 2012 Superparamagnetic MFe$_2$O$_4$ (M = Fe, Co, Mn) nanoparticles: tuning the particle size and magnetic properties through a novel one-step coprecipitation route *Chem. Mater.* **24** 1496

[25] Salavati-Niasari M, Mahmoudi T and Amiri O 2012 Easy synthesis of magnetite nanocrystals via coprecipitation method *J. Cluster Sci.* **23** 597

[26] Liu Y, Jia S Y, Wu Q A, Ran J Y, Zhang W and Wu S H 2011 Studies of Fe$_3$O$_4$-chitosan nanoparticles prepared by co-precipitation under the magnetic field for lipase immobilization *Catal. Commun.* **12** 717

[27] Suh S K, Yuet K, Hwang D K, Bong K W, Doyle P S and Hatton T A 2012 Synthesis of nonspherical superparamagnetic particles: *in situ* coprecipitation of magnetic nanoparticles in microgels prepared by stop-flow lithography *J. Am. Chem. Soc.* **134** 7337

[28] Blanco-Andujar C, Ortega D, Pankhurst Q A and Thanh N T K 2012 Elucidating the morphological and structural evolution of iron oxide nanoparticles formed by sodium carbonate in aqueous medium *J. Mater. Chem.* **22** 12498

[29] Sun S and Zeng H 2002 Size-controlled synthesis of magnetite nanoparticles *J. Am. Chem. Soc.* **124** 8204

[30] Li Z, Tan B, Allix M, Cooper A I and Rosseinsky M J 2008 Direct coprecipitation route to monodisperse dual-functionalized magnetic iron oxide nanocrystals without size selection *Small* **4** 231

[31] Woo K, Hong J, Choi S, Lee H-W, Ahn J-P, Kim C S and Lee S W 2004 Easy synthesis and magnetic properties of iron oxide nanoparticles *Chem. Mater.* **16** 2814

[32] Wang Y, Zhu Z, Xu F and Wei X 2012 One-pot reaction to synthesize superparamagnetic iron oxide nanoparticles by adding phenol as reducing agent and stabilizer *J. Nanopart. Res.* **14** 1

[33] Bronstein L M, Huang X, Retrum J, Schmucker A, Pink M, Stein B D and Dragnea B 2007 Influence of iron oleate complex structure on iron oxide nanoparticle formation *Chem. Mater.* **19** 3624

[34] Rockenberger J, Scher E C and Alivisatos A P 1999 A new nonhydrolytic single-precursor approach to surfactant-capped nanocrystals of transition metal oxides *J. Am. Chem. Soc.* **121** 11595

[35] Liang X, Wang X, Zhuang J, Chen Y, Wang D and Li Y 2006 Synthesis of nearly monodisperse iron oxide and oxyhydroxide nanocrystals *Adv. Funct. Mater.* **16** 1805

[36] Hu M, Jiang J-S, Bu F-X, Cheng X-L, Lin C-C and Zeng Y 2012 Hierarchical magnetic iron (III) oxides prepared by solid-state thermal decomposition of coordination polymers *RSC Adv.* **2** 4782

[37] Hu M, Jiang J-S and Zeng Y 2010 Prussian blue microcrystals prepared by selective etching and their conversion to mesoporous magnetic iron(III) oxides *Chem. Commun.* **46** 1133

[38] Asuha S, Zhao S, Wu H Y, Song L and Tegus O 2009 One step synthesis of maghemite nanoparticles by direct thermal decomposition of Fe-urea complex and their properties *J. Alloys Compd.* **472** L23

[39] Amara D and Margel S 2011 Solventless thermal decomposition of ferrocene as a new approach for the synthesis of porous superparamagnetic and ferromagnetic composite microspheres of narrow size distribution *J. Mater. Chem.* **21** 15764

[40] Maity D, Choo S G, Yi J B, Ding J and Xue J M 2009 Synthesis of magnetite nanoparticles via a solvent-free thermal decomposition route *J. Magn. Magn. Mater.* **321** 1256

[41] Park J, An K, Hwang Y, Park J G, Noh H J, Kim J Y, Park J H, Hwang N M and Hyeon T 2004 Ultra-large-scale syntheses of monodisperse nanocrystals *Nat. Mater.* **3** 891

[42] Amara D, Grinblat J and Margel S 2012 Solventless thermal decomposition of ferrocene as a new approach for one-step synthesis of magnetite nanocubes and nanospheres *J. Mater. Chem.* **22** 2188

[43] Chalasani R and Vasudevan S 2011 Form, content, and magnetism in iron oxide nanocrystals *J. Phys. Chem.* C **115** 18088

[44] Gao G, Liu X, Shi R, Zhou K, Shi Y, Ma R, Takayama-Muromachi E and Qiu G 2010 Shape-controlled synthesis and magnetic properties of monodisperse Fe_3O_4 nanocubes *Cryst. Growth Des.* **10** 2888

[45] Ho C-H, Tsai C-P, Chung C-C, Tsai C-Y, Chen F-R, Lin H-J and Lai C-H 2011 Shape-controlled growth and shape-dependent cation site occupancy of monodisperse Fe_3O_4 nanoparticles *Chem. Mater.* **23** 1753

[46] Shavel A and Liz-Marzan L M 2009 Shape control of iron oxide nanoparticles *Phys. Chem. Chem. Phys.* **11** 3762

[47] Demortiere A, Panissod P, Pichon B P, Pourroy G, Guillon D, Donnio B and Begin-Colin S 2011 Size-dependent properties of magnetic iron oxide nanocrystals *Nanoscale* **3** 225

[48] Park J *et al* 2005 One-nanometer-scale size-controlled synthesis of monodisperse magnetic iron oxide nanoparticles *Angew. Chem. Int. Edn* **44** 2872

[49] Lynch J, Zhuang J, Wang T, LaMontagne D, Wu H and Cao Y C 2011 Gas-bubble effects on the formation of colloidal iron oxide nanocrystals *J. Am. Chem. Soc.* **133** 12664

[50] Laudise R A 2004 Hydrothermal synthesis of crystals *50 Years Progress in Crystal Growth: A Reprint Collection* (Amsterdam: Elsevier) p 185

[51] Walton R I 2002 Subcritical solvothermal synthesis of condensed inorganic materials *Chem. Soc. Rev.* **31** 230

[52] Hu P, Yu L, Zuo A, Guo C and Yuan F 2008 Fabrication of monodisperse magnetite hollow spheres *J. Phys. Chem.* C **113** 900

[53] Ji G, Lin X, Liu Y, Huang Q, Yang Z and du Y 2012 Formation mechanism and magnetic properties of hollow Fe_3O_4 nano-spheres synthsized without any surfactant *Crystengcomm* **14** 8658

[54] You L-J, Xu S, Ma W-F, Li D, Zhang Y-T, Guo J, Hu J J and Wang C-C 2012 Ultrafast hydrothermal synthesis of high quality magnetic core phenol-formaldehyde shell composite microspheres using the microwave method *Langmuir* **28** 10565

[55] Chen Y, Xia H, Lu L and Xue J M 2012 Synthesis of porous hollow Fe_3O_4 beads and their applications in lithium ion batteries *J. Mater. Chem.* **22** 5006

[56] Sun X H, Zheng C M, Zhang F X, Yang Y L, Wu G J, Yu A M and Guan N J 2009 Size-controlled synthesis of magnetite (Fe_3O_4) nanoparticles coated with glucose and gluconic acid from a single Fe(III) precursor by a sucrose bifunctional hydrothermal method *J. Phys. Chem.* C **113** 16002

[57] Gao G, Shi R, Qin W, Shi Y, Xu G, Qiu G and Liu X 2010 Solvothermal synthesis and characterization of size-controlled monodisperse Fe_3O_4 nanoparticles *J. Mater. Sci.* **45** 3483

[58] Xu J-S and Zhu Y-J 2011 α-Fe_2O_3 hierarchically hollow microspheres self-assembled with nanosheets: surfactant-free solvothermal synthesis, magnetic and photocatalytic properties *Cryst. Eng. comm.* **13** 5162

[59] Cheng X-L, Jiang J-S, Hu M, Mao G-Y, Liu Z-W, Zeng Y and Zhang Q-H 2012 Liquid-liquid interface-assisted solvothermal synthesis of durian-like α-Fe_2O_3 hollow spheres constructed by nano-polyhedrons *Crystengcomm* **14** 3056

[60] Ma J, Lian J, Duan X, Liu X and Zheng W 2010 α-Fe_2O_3: Hydrothermal synthesis, magnetic and electrochemical properties *J. Phys. Chem.* C **114** 10671

[61] Tian Y, Yu B, Li X and Li K 2011 Facile solvothermal synthesis of monodisperse Fe_3O_4 nanocrystals with precise size control of one nanometre as potential MRI contrast agents *J. Mater. Chem.* **21** 2476

[62] Pandey S and Mishra S 2011 Sol–gel derived organic–inorganic hybrid materials: synthesis, characterizations and applications *J. Sol-Gel Sci. Technol.* **59** 73

[63] Dong W T and Zhu C S 2002 Use of ethylene oxide in the sol-gel synthesis of α-Fe_2O_3 nanoparticles from Fe(III) salts *J. Mater. Chem.* **12** 1676

[64] Lemine O M, Omri K, Zhang B, El Mir L, Sajieddine M, Alyamani A and Bououdina M 2012 Sol–gel synthesis of 8 nm magnetite (Fe_3O_4) nanoparticles and their magnetic properties *Superlattices Microstruct.* **52** 793

[65] Qi H, Yan B, Lu W, Li C and Yang Y 2011 A non-alkoxide sol-gel method for the preparation of magnetite (Fe_3O_4) nanoparticles *Curr. Nanosci.* **7** 381

[66] Woo K, Lee H J, Ahn J P and Park Y S 2003 Sol–gel mediated synthesis of Fe_2O_3 nanorods *Adv. Mater.* **15** 1761

[67] Qi H Z, Yan B, Li C K and Lu W 2011 Synthesis and characterization of water-soluble magnetite nanocrystals via one-step sol-gel pathway *Sci. Chin. Phys., Mech.* **54** 1239

[68] Laurent S, Forge D, Port M, Roch A, Robic C, Elst L V and Muller R N 2008 Magnetic iron oxide nanoparticles: synthesis, stabilization, vectorization, physicochemical characterizations, and biological applications *Chem. Rev.* **108** 2064

[69] Cai W and Wan J 2007 Facile synthesis of superparamagnetic magnetite nanoparticles in liquid polyols *J. Colloid Interface Sci.* **305** 366

[70] Caruntu D, Caruntu G and O'Connor C J 2007 Magnetic properties of variable-sized Fe_3O_4 nanoparticles synthesized from non-aqueous homogeneous solutions of polyols *J. Phys. D: Appl. Phys.* **40** 5801

[71] Shen Y F, Tang J, Nie Z H, Wang Y D, Ren Y and Zuo L 2009 Preparation and application of magnetic Fe_3O_4 nanoparticles for wastewater purification *Sep. Purif. Technol.* **68** 312

[72] Wongwailikhit K and Horwongsakul S 2011 The preparation of iron (III) oxide nanoparticles using w/o microemulsion *Mater. Lett.* **65** 2820

[73] Han L-H, Liu H and Wei Y 2011 *In situ* synthesis of hematite nanoparticles using a low-temperature microemulsion method *Powder Technol.* **207** 42

[74] Ladj R, Bitar A, Eissa M, Mugnier Y, Le Dantec R, Fessi H and Elaissari A 2013 Individual inorganic nanoparticles: preparation, functionalization and *in vitro* biomedical diagnostic applications *J. Mater. Chem.* B **1** 1381

[75] Darbandi M, Stromberg F, Landers J, Reckers N, Sanyal B, Keune W and Wende H 2012 Nanoscale size effect on surface spin canting in iron oxide nanoparticles synthesized by the microemulsion method *J. Phys. D: Appl. Phys.* **45** 195001

[76] Okoli C, Boutonnet M, Mariey L, Järås S and Rajarao G 2011 Application of magnetic iron oxide nanoparticles prepared from microemulsions for protein purification *J. Chem. Technol. Biot.* **86** 1386

[77] Okoli C, Sanchez-Dominguez M, Boutonnet M, Järås S, Civera C, Solans C and Kuttuva G R 2012 Comparison and functionalization study of microemulsion-prepared magnetic iron oxide nanoparticles *Langmuir* **28** 8479

[78] Xu H, Zeiger B W and Suslick K S 2013 Sonochemical synthesis of nanomaterials *Chem. Soc. Rev.* **42** 2555

[79] Suslick K S 1990 Sonochemistry *Science* **247** 1439

[80] Bang J H and Suslick K S 2010 Applications of ultrasound to the synthesis of nanostructured materials *Adv. Mater.* **22** 1039

[81] Mukh-Qasem R A and Gedanken A 2005 Sonochemical synthesis of stable hydrosol of Fe_3O_4 nanoparticles *J. Colloid Interface Sci.* **284** 489

[82] Abu-Much R and Gedanken A 2008 Sonochemical synthesis under a magnetic field: structuring magnetite nanoparticles and the destabilization of a colloidal magnetic aqueous solution under a magnetic field *J. Phys. Chem.* C **112** 35

[83] Morel A L *et al* 2008 Sonochemical approach to the synthesis of Fe$_3$O$_4$@SiO$_2$ core–shell nanoparticles with tunable properties *Acs Nano* **2** 847

[84] Wu W, He Q G, Chen H, Tang J X and Nie L B 2007 Sonochemical synthesis, structure and magnetic properties of air-stable Fe$_3$O$_4$/Au nanoparticles *Nanotechnology* **18** 145609

[85] Zhang S G, Zhang Y, Wang Y, Liu S M and Deng Y Q 2012 Sonochemical formation of iron oxide nanoparticles in ionic liquids for magnetic liquid marble *Phys. Chem. Chem. Phys.* **14** 5132

[86] Theerdhala S, Bahadur D, Vitta S, Perkas N, Zhong Z Y and Gedanken A 2010 Sonochemical stabilization of ultrafine colloidal biocompatible magnetite nanoparticles using amino acid, L-arginine, for possible bio applications *Ultrason. Sonochem.* **17** 730

[87] Zhu S, Guo J, Dong J, Cui Z, Lu T, Zhu C, Zhang D and Ma J 2013 Sonochemical fabrication of Fe$_3$O$_4$ nanoparticles on reduced graphene oxide for biosensors *Ultrason. Sonochem.* **20** 872

[88] Teo B M, Chen F, Hatton T A, Grieser F and Ashokkumar M 2009 Novel one-pot synthesis of magnetite latex nanoparticles by ultrasound irradiation *Langmuir* **25** 2593

[89] Hu X, Yu J C, Gong J, Li Q and Li G 2007 α-Fe$_2$O$_3$ nanorings prepared by a microwave-assisted hydrothermal process and their sensing properties *Adv. Mater.* **19** 2324

[90] Wu L H, Yao H B, Hu B and Yu S H 2011 Unique lamellar sodium/potassium iron oxide nanosheets: facile microwave-assisted synthesis and magnetic and electrochemical properties *Chem. Mater.* **23** 3946

[91] Ai Z, Deng K, Wan Q, Zhang L and Lee S 2010 Facile microwave-assisted synthesis and magnetic and gas sensing properties of Fe$_3$O$_4$ nanoroses *J. Phys. Chem.* C **114** 6237

[92] Qiu G, Huang H, Genuino H, Opembe N, Stafford L, Dharmarathna S and Suib S L 2011 Microwave-assisted hydrothermal synthesis of nanosized α-Fe$_2$O$_3$ for catalysts and adsorbents *J. Phys. Chem.* C **115** 19626

[93] Sreeja V and Joy P A 2007 Microwave–hydrothermal synthesis of γ-Fe$_2$O$_3$ nanoparticles and their magnetic properties *Mater. Res. Bull.* **42** 1570

[94] Jiang F Y, Wang C M, Fu Y and Liu R C 2010 Synthesis of iron oxide nanocubes via microwave-assisted solvolthermal method *J. Alloys Compd.* **503** L31

[95] Hu L, Percheron A, Chaumont D and Brachais C H 2011 Microwave-assisted one-step hydrothermal synthesis of pure iron oxide nanoparticles: magnetite, maghemite and hematite *J. Sol-Gel Sci. Technol.* **60** 198

[96] Osborne E A, Atkins T M, Gilbert D A, Kauzlarich S M, Liu K and Louie A Y 2012 Rapid microwave-assisted synthesis of dextran-coated iron oxide nanoparticles for magnetic resonance imaging *Nanotechnology* **23** 215602

[97] Liu S, Lu F, Jia X, Cheng F, Jiang L-P and Zhu J-J 2011 Microwave-assisted synthesis of a biocompatible polyacid-conjugated Fe$_3$O$_4$ superparamagnetic hybrid *CrystEngComm* **13** 2425

[98] Pascu O, Carenza E, Gich M, Estrade S, Peiro F, Herranz G and Roig A 2012 Surface reactivity of iron oxide nanoparticles by microwave-assisted synthesis; comparison with the thermal decomposition route *J. Phys. Chem.* C **116** 15108

[99] TC P, Mathew L, Chandrasekaran N, Raichur A M and Mukherjee A 2010 *Biomimetics Learning from Nature* ed A Mukherjee (Rijeka: InTech)

[100] Vali H, Weiss B, Li Y L, Sears S K, Kim S S, Kirschvink J L and Zhang L 2004 Formation of tabular single-domain magnetite induced by Geobacter metallireducens GS-15 *Proc. Natl Acad. Sci.* **101** 16121

[101] Scheffel A, Gruska M, Faivre D, Linaroudis A, Plitzko J M and Schuler D 2006 An acidic protein aligns magnetosomes along a filamentous structure in magnetotactic bacteria *Nature* **440** 110

[102] Bazylinski D A and Frankel R B 2004 Magnetosome formation in prokaryotes *Nat. Rev. Microbiol.* **2** 217

[103] Bharde A A, Parikh R Y, Baidakova M, Jouen S, Hannoyer B, Enoki T, Prasad B L V, Shouche Y S, Ogale S and Sastry M 2008 Bacteria-mediated precursor-dependent biosynthesis of superparamagnetic iron oxide and iron sulfide nanoparticles *Langmuir* **24** 5787

[104] Sundaram P A, Augustine R and Kannan M 2012 Extracellular biosynthesis of iron oxide nanoparticles by Bacillus subtilis strains isolated from rhizosphere soil *Biotechnol. Bioprocess Eng.* **17** 835

[105] Pascal C, Pascal J L, Favier F, Elidrissi Moubtassim M L and Payen C 1998 Electrochemical synthesis for the control of γ-Fe$_2$O$_3$ nanoparticle size: morphology, microstructure, and magnetic behavior *Chem. Mater.* **11** 141

[106] Starowicz M, Starowicz P, Żukrowski J, Przewoźnik J, Lemański A, Kapusta C and Banaś J 2011 Electrochemical synthesis of magnetic iron oxide nanoparticles with controlled size *J. Nanopart. Res.* **13** 7167

[107] Wang G, Ling Y, Wheeler D A, George K E N, Horsley K, Heske C, Zhang J Z and Li Y 2011 Facile synthesis of highly photoactive α-Fe$_2$O$_3$-based films for water oxidation *Nano Lett.* **11** 3503

[108] Salazar-Alvarez G, Muhammed M and Zagorodni A A 2006 Novel flow injection synthesis of iron oxide nanoparticles with narrow size distribution *Chem. Eng. Sci.* **61** 4625

[109] Huang H Y, Shieh Y T, Shih C M and Twu Y K 2010 Magnetic chitosan/iron (II, III) oxide nanoparticles prepared by spray-drying *Carbohydr. Polym.* **81** 906

[110] Morjan I *et al* 2010 Iron oxide-based nanoparticles with different mean sizes obtained by the laser pyrolysis: structural and magnetic properties *J. Nanosci. Nanotechnol.* **10** 1223

[111] Martínez G, Malumbres A, Mallada R, Hueso J, Irusta S, Bomatí-Miguel O and Santamaría J 2012 Use of a polyol liquid collection medium to obtain ultrasmall magnetic nanoparticles by laser pyrolysis *Nanotechnology* **23** 425605

[112] Cabrera L, Gutierrez S, Menendez N, Morales M P and Herrasti P 2008 Magnetite nanoparticles: electrochemical synthesis and characterization *Electrochim. Acta* **53** 3436

[113] Rodríguez-López A, Paredes-Arroyo A, Mojica-Gomez J, Estrada-Arteaga C, Cruz-Rivera J J, Elías Alfaro C G and Antaño-López R 2012 Electrochemical synthesis of magnetite and maghemite nanoparticles using dissymmetric potential pulses *J. Nanopart. Res.* **14** 993

[114] Abid A D, Kanematsu M, Young T M and Kennedy I M 2013 Arsenic removal from water using flame-synthesized iron oxide nanoparticles with variable oxidation states *Aerosol Sci. Technol.* **47** 169

[115] Costo R, Bello V, Robic C, Port M, Marco J F, Puerto Morales M and Veintemillas-Verdaguer S 2011 Ultrasmall iron oxide nanoparticles for biomedical applications: improving the colloidal and magnetic properties *Langmuir* **28** 178

[116] Hu Q, Lee S C, Baek Y-J, Lee H H, Kang C J, Kim H-M, Kim K-B and Yoon T-S 2013 Non-volatile nano-floating gate memory with Pt-Fe$_2$O$_3$ composite nanoparticles and indium gallium zinc oxide channel *J. Nanopart. Res.* **15** 1435

[117] Luo Y *et al* 2012 Seed-assisted synthesis of highly ordered TiO$_2$@α-Fe$_2$O$_3$ core/shell arrays on carbon textiles for lithium-ion battery applications *Energy Environ. Sci.* **5** 6559

[118] Wei Z, Zhou Z, Yang M, Lin C, Zhao Z, Huang D, Chen Z and Gao J 2011 Multifunctional Ag@Fe$_2$O$_3$ yolk-shell nanoparticles for simultaneous capture, kill, and removal of pathogen *J. Mater. Chem.* **21** 16344

[119] Zhan F and Zhang C-Y 2011 Bifunctional nanoparticles with superparamagnetic and luminescence properties *J. Mater. Chem.* **21** 4765

[120] Behrens S 2011 Preparation of functional magnetic nanocomposites and hybrid materials: recent progress and future directions *Nanoscale* **3** 877

[121] Yu H, Chen M, Rice P M, Wang S X, White R L and Sun S H 2005 Dumbbell-like bifunctional Au-Fe$_3$O$_4$ nanoparticles *Nano Lett.* **5** 379

[122] Wang C, Daimon H and Sun S H 2009 Dumbbell-like Pt-Fe$_3$O$_4$ nanoparticles and their enhanced catalysis for oxygen reduction reaction *Nano Lett.* **9** 1493

[123] Xu C J, Wang B D and Sun S H 2009 Dumbbell-like Au-Fe$_3$O$_4$ nanoparticles for target-specific platin delivery *J. Am. Chem. Soc.* **131** 4216

[124] Zhao N and Gao M Y 2009 Magnetic janus particles prepared by a flame synthetic approach: synthesis, characterizations and properties *Adv. Mater.* **21** 184

[125] Sperling R A and Parak W J 2010 Surface modification, functionalization and bioconjugation of colloidal inorganic nanoparticles *Phil. Trans. R. Soc.* A **368** 1333

[126] Tsai Z-T, Wang J-F, Kuo H-Y, Shen C-R, Wang J-J and Yen T-C 2010 *In situ* preparation of high relaxivity iron oxide nanoparticles by coating with chitosan: a potential MRI contrast agent useful for cell tracking *J. Magn. Magn. Mater.* **322** 208

[127] Kloust H *et al* 2013 *In situ* functionalization and PEO coating of iron oxide nanocrystals using seeded emulsion polymerization *Langmuir* **29** 4915

[128] Li L, Jiang W, Luo K, Song H, Lan F, Wu Y and Gu Z 2013 Superparamagnetic iron oxide nanoparticles as MRI contrast agents for non-invasive stem cell labeling and tracking *Theranostics* **3** 595

[129] Shen M, Cai H, Wang X, Cao X, Li K, Wang S, Guo R, Zheng L, Zhang G and Shi X 2012 Facile one-pot preparation, surface functionalization, and toxicity assay of APTS-coated iron oxide nanoparticles *Nanotechnology* **23** 105601

[130] Wei W, Quanguo H and Hong C 2007 *ICBBE 2007: The 1st Int. Conf. on Bioinformatics and Biomedical Engineering 2007* p 76

[131] Li D, Jiang D, Chen M, Xie J, Wu Y, Dang S and Zhang J 2010 An easy fabrication of monodisperse oleic acid-coated Fe$_3$O$_4$ nanoparticles *Mater. Lett.* **64** 2462

[132] Smolensky E D, Park H-Y E, Zhou Y, Rolla G A, Marjanska M, Botta M and Pierre V C 2013 Scaling laws at the nanosize: the effect of particle size and shape on the magnetism and relaxivity of iron oxide nanoparticle contrast agents *J. Mater. Chem.* B **1** 2818

[133] Bae J, Lawrence J, Miesch C, Ribbe A, Li W, Emrick T, Zhu J and Hayward R C 2012 Multifunctional nanoparticle-loaded spherical and wormlike micelles formed by interfacial instabilities *Adv. Mater.* **24** 2735

[134] Salas G, Casado C, Teran F J, Miranda R, Serna C J and Morales M P 2012 Controlled synthesis of uniform magnetite nanocrystals with high-quality properties for biomedical applications *J. Mater. Chem.* **22** 21065

[135] Barbeta V B, Jardim R F, Kiyohara P K, Effenberger F B and Rossi L M 2010 Magnetic properties of Fe$_3$O$_4$ nanoparticles coated with oleic and dodecanoic acids *J. Appl. Phys.* **107** 073913

[136] Lartigue L *et al* 2009 Water-soluble rhamnose-coated Fe$_3$O$_4$ nanoparticles *Org. Lett.* **11** 2992

[137] Chalasani R and Vasudevan S 2012 Cyclodextrin functionalized magnetic iron oxide nanocrystals: a host-carrier for magnetic separation of non-polar molecules and arsenic from aqueous media *J. Mater. Chem.* **22** 14925

[138] Xiao L *et al* 2011 Water-soluble superparamagnetic magnetite nanoparticles with biocompatible coating for enhanced magnetic resonance imaging *ACS Nano* **5** 6315

[139] Gao J, Ran X, Shi C, Cheng H, Cheng T and Su Y 2013 One-step solvothermal synthesis of highly water-soluble, negatively charged superparamagnetic Fe$_3$O$_4$ colloidal nanocrystal clusters *Nanoscale* **5** 7026–33

[140] Majeed M I, Lu Q, Yan W, Li Z, Hussain I, Tahir M N, Tremel W and Tan B 2013 Highly water-soluble magnetic iron oxide (Fe$_3$O$_4$) nanoparticles for drug delivery: enhanced *in vitro* therapeutic efficacy of doxorubicin and MION conjugates *J. Mater. Chem.* B **1** 2874

[141] Wang L, Neoh K, Kang E, Shuter B and Wang S C 2009 Superparamagnetic hyperbranched polyglycerol-grafted Fe$_3$O$_4$ nanoparticles as a novel magnetic resonance imaging contrast agent: an *in vitro* assessment *Adv. Funct. Mater.* **19** 2615

[142] Yang D, Ma J-Z, Gao M, Peng M, Luo Y, Hui W, Chen C, Wang Z and Cui Y 2013 Suppression of composite nanoparticle aggregation through steric stabilization and ligand exchange for colorimetric protein detection *RSC Adv.* **3** 9681

[143] Song M, Zhang Y, Hu S, Song L, Dong J, Chen Z and Gu N 2012 Influence of morphology and surface exchange reaction on magnetic properties of monodisperse magnetite nanoparticles *Colloids Surf.* A **408** 114

[144] Dong A, Ye X, Chen J, Kang Y, Gordon T, Kikkawa J M and Murray C B 2010 A generalized ligand-exchange strategy enabling sequential surface functionalization of colloidal nanocrystals *J. Am. Chem. Soc.* **133** 998

[145] Ninjbadgar T and Brougham D F 2011 Epoxy ring opening phase transfer as a general route to water dispersible superparamagnetic Fe$_3$O$_4$ nanoparticles and their application as positive MRI contrast agents *Adv. Funct. Mater.* **21** 4769

[146] Yang X Q, Grailer J J, Rowland I J, Javadi A, Hurley S A, Steeber D A and Gong S Q 2010 Multifunctional SPIO/DOX-loaded wormlike polymer vesicles for cancer therapy and MR imaging *Biomater.* **31** 9065

[147] Ray J R, Lee B, Baltrusaitis J and Jun Y-S 2012 Formation of iron (III)(hydr) oxides on polyaspartate-and alginate-coated substrates: effects of coating hydrophilicity and functional group *Environ. Sci. Technol.* **46** 13167

[148] Chen H, Deng C, Li Y, Dai Y, Yang P and Zhang X 2009 A facile synthesis approach to C8-functionalized magnetic carbonaceous polysaccharide microspheres for the highly efficient and rapid enrichment of peptides and direct MALDI-TOF-MS analysis *Adv. Mater.* **21** 2200

[149] Chang P R, Yu J, Ma X and Anderson D P 2011 Polysaccharides as stabilizers for the synthesis of magnetic nanoparticles *Carbohydr. Polym.* **83** 640

[150] Dias A, Hussain A, Marcos A and Roque A 2011 A biotechnological perspective on the application of iron oxide magnetic colloids modified with polysaccharides *Biotechnol. Adv.* **29** 142

[151] Gaihre B, Aryal S, Khil M S and Kim H Y 2008 Encapsulation of Fe$_3$O$_4$ in gelatin nanoparticles: effect of different parameters on size and stability of the colloidal dispersion *J. Microencapsulation* **25** 21

[152] Gaihre B, Khil M S, Lee D R and Kim H Y 2009 Gelatin-coated magnetic iron oxide nanoparticles as carrier system: drug loading and *in vitro* drug release study *Int. J. Pharm.* **365** 180

[153] Mahmoudi M, Sant S, Wang B, Laurent S and Sen T 2011 Superparamagnetic iron oxide nanoparticles (SPIONs): development, surface modification and applications in chemotherapy *Adv. Drug Delivery Rev.* **63** 24

[154] Dung T, Danh T, Hoa L, Chien D and Duc N 2009 Structural and magnetic properties of starch-coated magnetite nanoparticles *J. Exp. Nanosci.* **4** 259

[155] Alidokht L, Khataee A, Reyhanitabar A and Oustan S 2011 Reductive removal of Cr (VI) by starch-stabilized Fe^0 nanoparticles in aqueous solution *Desalination* **270** 105

[156] Lu W, Shen Y, Xie A and Zhang W 2013 Preparation and protein immobilization of magnetic dialdehyde starch nanoparticles *J. Phys. Chem.* B **117** 3720

[157] Hernández R and Mijangos C 2009 *In situ* synthesis of magnetic iron oxide nanoparticles in thermally responsive alginate-poly (N-isopropylacrylamide) semi-interpenetrating polymer networks *Macromol. Rapid Commun.* **30** 176

[158] Wu D, Zhao J, Zhang L, Wu Q and Yang Y 2010 Lanthanum adsorption using iron oxide loaded calcium alginate beads *Hydrometallurgy* **101** 76

[159] Kim J, Arifin D R, Muja N, Kim T, Gilad A A, Kim H, Arepally A, Hyeon T and Bulte J W 2011 Multifunctional capsule-in-capsules for immunoprotection and trimodal imaging *Angew. Chem.* **123** 2365

[160] Sondjaja R, Alan Hatton T and Tam M K 2009 Clustering of magnetic nanoparticles using a double hydrophilic block copolymer, poly (ethylene oxide)-b-poly (acrylic acid) *J. Magn. Magn. Mater.* **321** 2393

[161] Moscoso-Londoño O, Gonzalez J, Muraca D, Hoppe C, Alvarez V, López-Quintela A, Socolovsky L M and Pirota K R 2012 Structural and magnetic behavior of ferrogels obtained by freezing thawing of polyvinyl alcohol/poly (acrylic acid)(PAA)-coated iron oxide nanoparticles *Eur. Polym. J.* **49** 279–89

[162] Kang X J, Dai Y L, Ma P A, Yang D M, Li C X, Hou Z Y, Cheng Z Y and Lin J 2012 Poly (acrylic acid)-Modified Fe_3O_4 microspheres for magnetic-targeted and pH-triggered anticancer drug delivery *Chem.-Eur. J.* **18** 15676

[163] Mukhopadhyay A, Joshi N, Chattopadhyay K and De G 2011 A facile synthesis of PEG-coated magnetite (Fe_3O_4) nanoparticles and their prevention of the reduction of cytochrome C *ACS Appl. Mater. Interfaces* **4** 142

[164] Cole A J, David A E, Wang J, Galbán C J and Yang V C 2011 Magnetic brain tumor targeting and biodistribution of long-circulating PEG-modified, cross-linked starch-coated iron oxide nanoparticles *Biomater.* **32** 6291

[165] Prashant C, Dipak M, Yang C-T, Chuang K-H, Jun D and Feng S-S 2010 Superparamagnetic iron oxide-loaded poly (lactic acid)-d-α-tocopherol polyethylene glycol 1000 succinate copolymer nanoparticles as MRI contrast agent *Biomater.* **31** 5588

[166] Tan Y F, Chandrasekharan P, Maity D, Yong C X, Chuang K-H, Zhao Y, Wang S, Ding J and Feng S-S 2011 Multimodal tumor imaging by iron oxides and quantum dots formulated in poly (lactic acid)-d-alpha-tocopheryl polyethylene glycol 1000 succinate nanoparticles *Biomater.* **32** 2969

[167] Zheng X, Zhou S, Xiao Y, Yu X, Li X and Wu P 2009 Shape memory effect of poly (d, l-lactide)/Fe_3O_4 nanocomposites by inductive heating of magnetite particles *Colloids Surf.* B **71** 67

[168] Wang Q, Zhang J and Wang A 2013 Spray-dried magnetic chitosan/Fe_3O_4/halloysite nanotubes/ofloxacin microspheres for sustained release of ofloxacin *RSC Adv.* **3** 23423

[169] Bhattacharya D, Das M, Mishra D, Banerjee I, Sahu S K, Maiti T K and Pramanik P 2011 Folate receptor targeted, carboxymethyl chitosan functionalized iron oxide nanoparticles: a novel ultradispersed nanoconjugates for bimodal imaging *Nanoscale* **3** 1653

[170] Rovers S A, Dietz C H, vd Poel L A, Hoogenboom R, Kemmere M F and Keurentjes J T 2010 Influence of distribution on the heating of superparamagnetic iron oxide nanoparticles in poly (methyl methacrylate) in an alternating magnetic field *J. Phys. Chem.* C **114** 8144

[171] Pimpha N, Chaleawlert-umpon S and Sunintaboon P 2012 Core/shell polymethyl methacrylate/polyethyleneimine particles incorporating large amounts of iron oxide nanoparticles prepared by emulsifier-free emulsion polymerization *Polymer* **53** 2015

[172] Lan F, Liu K-X, Jiang W, Zeng X-B, Wu Y and Gu Z-W 2011 Facile synthesis of monodisperse superparamagnetic Fe_3O_4/PMMA composite nanospheres with high magnetization *Nanotechnology* **22** 225604

[173] Oh J K and Park J M 2011 Iron oxide-based superparamagnetic polymeric nanomaterials: design, preparation, and biomedical application *Prog. Polym. Sci.* **36** 168

[174] Zhou L, He B and Zhang F 2012 Facile one-pot synthesis of iron oxide nanoparticles cross-linked magnetic poly(vinyl alcohol) gel beads for drug delivery *ACS Appl. Mater. Interfaces* **4** 192

[175] El-Sherif H, El-Masry M and Emira H S 2010 Magnetic polymer composite particles via *in situ* inverse miniemulsion polymerization process *J. Macromol. Sci.* A **47** 1096

[176] Shkilnyy A, Munnier E, Hervé K, Soucé M, Benoit R, Cohen-Jonathan S, Limelette P, Saboungi M-L, Dubois P and Chourpa I 2010 Synthesis and evaluation of novel biocompatible super-paramagnetic iron oxide nanoparticles as magnetic anticancer drug carrier and fluorescence active label *J. Phys. Chem.* C **114** 5850

[177] Lu C C, Quan Z S, Sur J C, Kim S H, Lee C H and Chai K Y 2010 One-pot fabrication of carboxyl-functionalized biocompatible magnetic nanocrystals for conjugation with targeting agents *New J. Chem.* **34** 2040

[178] Amara D and Margel S 2012 Synthesis and characterization of superparamagnetic core–shell micrometresized particles of narrow size distribution by a swelling process *J. Mater. Chem.* **22** 9268

[179] Douadi-Masrouki S, Frka-Petesic B, Save M, Charleux B, Cabuil V and Sandre O 2010 Incorporation of magnetic nanoparticles into lamellar polystyrene-b-poly(n-butyl methacrylate) diblock copolymer films: influence of the chain end-groups on nanostructuration *Polymer* **51** 4673

[180] Jarzyna P A, Skajaa T, Gianella A, Cormode D P, Samber D D, Dickson S D, Chen W, Griffioen A W, Fayad Z A and Mulder W J 2009 Iron oxide core oil-in-water emulsions as a multifunctional nanoparticle platform for tumor targeting and imaging *Biomater.* **30** 6947

[181] Howes P, Green M, Bowers A, Parker D, Varma G, Kallumadil M, Hughes M, Warley A, Brain A and Botnar R 2010 Magnetic conjugated polymer nanoparticles as bimodal imaging agents *J. Am. Chem. Soc.* **132** 9833

[182] Zhu C L, Liu L B, Yang Q, Lv F T and Wang S 2012 Water-soluble conjugated polymers for imaging, diagnosis, and therapy *Chem. Rev.* **112** 4687

[183] Sun B, Sun M J, Gu Z, Shen Q D, Jiang S J, Xu Y and Wang Y 2010 Conjugated polymer fluorescence probe for intracellular imaging of magnetic nanoparticles *Macromolecules* **43** 10348

[184] Fan X, Jiao G, Zhao W, Jin P and Li X 2013 Magnetic Fe_3O_4-graphene composites as targeted drug nanocarriers for pH-activated release *Nanoscale* **5** 1143

[185] Zhang S M, Zhang L N, He B F and Wu Z S 2008 Preparation and characterization of thermosensitive PNIPAA-coated iron oxide nanoparticles *Nanotechnology* **19** 325608

[186] Leal M P, Torti A, Riedinger A, La Fleur R, Petti D, Cingolani R, Bertacco R and Pellegrino T 2012 Controlled release of doxorubicin loaded within magnetic thermo-responsive nanocarriers under magnetic and thermal actuation in a microfluidic channel *ACS Nano* **6** 10535

[187] Santra S, Kaittanis C, Grimm J and Perez J M 2009 Drug/dye-loaded, multifunctional iron oxide nanoparticles for combined targeted cancer therapy and dual optical/magnetic resonance imaging *Small* **5** 1862

[188] Chan T and Gu F 2013 Development of acolorimetric, superparamagnetic biosensor for the capture and detection of biomolecules *Biosens. Bioelectron.* **42** 12

[189] Zhu J and Hayward R C 2008 Spontaneous generation of amphiphilic block copolymer micelles with multiple morphologies through interfacial Instabilities *J. Am. Chem. Soc.* **130** 7496

[190] Truby R L, Emelianov S and Homan K A 2013 Ligand-mediated self-assembly of hybrid plasmonic and superparamagnetic nanostructures *Langmuir* **29** 2465

[191] Yang S, Chen D Y, Li N J, Mei X, Qi X X, Li H, Xu Q F and Lu J M 2012 A facile preparation of targetable pH-sensitive polymeric nanocarriers with encapsulated magnetic nanoparticles for controlled drug release *J. Mater. Chem.* **22** 25354

[192] Liu H B, Guo J, Jin L, Yang W L and Wang C C 2008 Fabrication and functionalization of dendritic poly (amidoamine)-immobilized magnetic polymer composite microspheres *J. Phys. Chem.* B **112** 3315

[193] Jain N, Wang Y J, Jones S K, Hawkett B S and Warr G G 2010 Optimized steric stabilization of aqueous ferrofluids and magnetic nanoparticles *Langmuir* **26** 4465

[194] Bahadur R, Lee S M, Yoo E S, Choi J H and Do Ghim H 2009 Glycoconjugated chitosan stabilized iron oxide nanoparticles as a multifunctional nanoprobe *Mat. Sci. Eng.* C **29** 1668

[195] Wang D, Su H Y, Liu Y, Wu C, Xia C, Sun J, Gao F, Gong Q, Song B and Ai H 2012 Near-infrared fluorescent amphiphilic polycation wrapped magnetite nanoparticles as multimodality probes *Chinese Sci. Bull.* **57** 4012

[196] Wang Z Y, Liu G, Sun J, Wu B Y, Gong Q Y, Song B, Ai H and Gu Z W 2009 Self-assembly of magnetite nanocrystals with amphiphilic polyethylenimine: structures and applications in magnetic resonance imaging *J. Nanosci. Nanotechnol.* **9** 378

[197] Riedinger A, Leal M P, Deka S R, George C, Franchini I R, Falqui A, Cingolani R and Pellegrino T 2011 'Nanohybrids' based on pH-responsive hydrogels and inorganic nanoparticles for drug delivery and sensor applications *Nano Lett.* **11** 3136

[198] Mohammadi Z, Cole A and Berkland C J 2009 *In situ* synthesis of iron oxide within polyvinylamine nanoparticle reactors *J. Phys. Chem.* C **113** 7652

[199] Jaiswal M K, Banerjee R, Pradhan P and Bahadur D 2010 Thermal behavior of magnetically modalized poly(N-isopropylacrylamide)-chitosan based nanohydrogel *Colloid Surf.* B **81** 185

[200] Lin J J, Chen J S, Huang S J, Ko J H, Wang Y M, Chen T L and Wang L F 2009 Folic acid-Pluronic F127 magnetic nanoparticle clusters for combined targeting, diagnosis, and therapy applications *Biomater.* **30** 5114

[201] Jia Y H *et al* 2012 Co-encapsulation of magnetic Fe_3O_4 nanoparticles and doxorubicin into biodegradable PLGA nanocarriers for intratumoral drug delivery *Int. J. Nanomed.* **7** 1697

[202] Kaaki K, Hervé-Aubert K, Chiper M, Shkilnyy A, Soucé M, Benoit R, Paillard A, Dubois P, Saboungi M-L and Chourpa I 2012 Magnetic nanocarriers of doxorubicin coated with poly(ethylene glycol) and folic acid: relation between coating structure, surface properties, colloidal stability, and cancer cell targeting *Langmuir* **28** 1496

[203] Nuytten N, Hakimhashemi M, Ysenbaert T, Defour L, Trekker J, Soenen S J H, Van der Meeren P and De Cuyper M 2010 PEGylated lipids impede the lateral diffusion of adsorbed proteins at the surface of (magneto) liposomes *Colloid Surf.* B **80** 227

[204] Tan Y F, Chandrasekharan P, Maity D, Yong C X, Chuang K H, Zhao Y, Wang S, Ding J and Feng S S 2011 Multimodal tumor imaging by iron oxides and quantum dots formulated in poly (lactic acid)-d-alpha-tocopheryl polyethylene glycol 1000 succinate nanoparticles *Biomater.* **32** 2969

[205] Samanta B, Yan H, Fischer N O, Shi J, Jerry D J and Rotello V M 2008 Protein-passivated Fe_3O_4 nanoparticles: low toxicity and rapid heating for thermal therapy *J. Mater. Chem.* **18** 1204

[206] Iwaki Y, Kawasaki H and Arakawa R 2012 Human serum albumin-modified Fe_3O_4 magnetic nanoparticles for affinity-SALDI-MS of small-molecule drugs in biological liquids *Anal. Sci.* **28** 893

[207] Okuda M, Eloi J-C, Jones S E W, Sarua A, Richardson R M and Schwarzacher W 2012 Fe_3O_4 nanoparticles: protein-mediated crystalline magnetic superstructures *Nanotechnology* **23** 415601

[208] Marcelo G, Muñoz-Bonilla A, Rodríguez-Hernández J and Fernández-García M 2013 Hybrid materials achieved by polypeptide grafted magnetite nanoparticles through a dopamine biomimetic surface anchored initiator *Polym. Chem.* **4** 558

[209] Xie J, Wang J, Niu G, Huang J, Chen K, Li X and Chen X 2010 Human serum albumin coated iron oxide nanoparticles for efficient cell labeling *Chem. Commun.* **46** 433

[210] Magro M, Faralli A, Baratella D, Bertipaglia I, Giannetti S, Salviulo G, Zboril R and Vianello F 2012 Avidin functionalized maghemite nanoparticles and their application for recombinant human biotinyl-SERCA purification *Langmuir* **28** 15392

[211] Bhattacharya D, Chakraborty S P, Pramanik A, Baksi A, Roy S, Maiti T K, Ghosh S K and Pramanik P 2011 Detection of total count of *Staphylococcus aureus* using anti-toxin antibody labelled gold magnetite nanocomposites: a novel tool for capture, detection and bacterial separation *J. Mater. Chem.* **21** 17273

[212] Zedan A F, Abdelsayed V, Mohamed M B and El-Shall M S 2013 Rapid synthesis of magnetic/luminescent (Fe_3O_4/CdSe) nanocomposites by microwave irradiation *J. Nanopart. Res.* **15** 1312

[213] Wang G, Jin L, Dong Y, Niu L, Liu Y, Ren F and Su X 2013 Multifunctional Fe_3O_4-CdTe@SiO_2@carboxymethyl chitosan drug nanocarriers: synergistic effect towards magnetic targeted drug delivery and cell imaging *New J. Chem.* **38** 700–8

[214] Gowd G S, Patra M K, Mathew M, Shukla A, Songara S, Vadera S R and Kumar N 2013 Synthesis of Fe_3O_4@Y_2O_3: Eu^{3+} core–shell multifunctional nanoparticles and their magnetic and luminescence properties *Opt. Mater.* **35** 1685

[215] Ye Y, Kuai L and Geng B 2012 A template-free route to a Fe_3O_4-Co_3O_4 yolk-shell nanostructure as a noble-metal free electrocatalyst for ORR in alkaline media *J. Mater. Chem.* **22** 19132

[216] Zhao Y, Zhang W, Lin Y and Du D 2013 The vital function of Fe_3O_4@Au nanocomposites for hydrolase biosensor design and its application in detection of methyl parathion *Nanoscale* **5** 1121

[217] He X, Tan L, Chen D, Wu X, Ren X, Zhang Y, Meng X and Tang F 2013 Fe_3O_4-Au@mesoporous SiO_2 microsphere: an ideal artificial enzymatic cascade system *Chem. Commun.* **49** 4643

[218] Wang D-W *et al* 2013 Folate-conjugated Fe_3O_4@SiO_2@gold nanorods@ mesoporous SiO_2 hybrid nanomaterial: a theranostic agent for magnetic resonance imaging and photothermal therapy *J. Mater. Chem.* B **1** 2934

[219] Stöber W, Fink A and Bohn E 1968 Controlled growth of monodisperse silica spheres in the micron size range *J. Colloid Interface Sci.* **26** 62

[220] Zhu Y, Ikoma T, Hanagata N and Kaskel S 2010 Rattle-type Fe_3O_4@SiO_2 hollow mesoporous spheres as carriers for drug delivery *Small* **6** 471

[221] Shao J, Xie X, Xi Y, Liu X and Yang Y 2013 Characterization of Fe_3O_4/SiO_2 composite core–shell nanoparticles synthesized in isopropanol medium *Glass Phys. Chem.* **39** 329

[222] Cao Z, Yang L, Ye Q, Cui Q, Qi D and Ziener U 2013 Transition-metal salt-containing silica nanocapsules elaborated via salt-induced interfacial deposition in inverse miniemulsions as precursor to functional hollow silica particles *Langmuir* **29** 6509

[223] Xuan S H *et al* 2012 Photocytotoxicity and magnetic relaxivity responses of dual-porous γ-Fe_2O_3@meso-SiO_2 microspheres *ACS Appl. Mater. Interfaces* **4** 2033

[224] Wu W, Xiao X H, Zhang S F, Fan L X, Peng T C, Ren F and Jiang C Z 2010 Facile fabrication of ultrafine hollow silica and magnetic hollow silica nanoparticles by a dual-templating approach *Nanoscale Res. Lett.* **5** 116

[225] Pinho S L C, Laurent S, Rocha J, Roch A, Delville M-H, Mornet S, Carlos L D, Elst L V, Muller R N and Geraldes. C F G C 2012 Relaxometric studies of γ-Fe_2O_3@SiO_2 core–shell nanoparticles: when the coating matters *J. Phys. Chem.* C **116** 2285

[226] Pinho S L C *et al* 2010 Fine tuning of the relaxometry of γ-Fe_2O_3@SiO_2 nanoparticles by tweaking the silica coating thickness *ACS Nano* **4** 5339

[227] Park J-N, Zhang P, Hu Y-S and McFarland E W 2010 Synthesis and characterization of sintering-resistant silica-encapsulated Fe_3O_4 magnetic nanoparticles active for oxidation and chemical looping combustion *Nanotechnology* **21** 225708

[228] Ding H L, Zhang Y X, Wang S, Xu J M, Xu S C and Li G H 2012 Fe_3O_4@SiO_2 core/shell nanoparticles: the silica coating regulations with a single core for different core sizes and shell thicknesses *Chem. Mater.* **24** 4572

[229] Li Y, Hu Y, Jiang H and Li C 2013 Double-faced γ-Fe_2O_3∥SiO_2 nanohybrids: flame synthesis, *in situ* selective modification and highly interfacial activity *Nanoscale* **5** 5360

[230] Basak S, Tiwari V, Fan J, Achilefu S, Sethi V and Biswas P 2011 Single step aerosol synthesis of nanocomposites by aerosol routes: γ-Fe_2O_3/SiO_2 and their functionalization *J. Mater. Res.* **26** 1225

[231] Bae H, Ahmad T, Rhee I, Chang Y, Jin S-U and Hong S 2012 Carbon-coated iron oxide nanoparticles as contrast agents in magnetic resonance imaging *Nanoscale Res. Lett.* **7** 44

[232] Lei C, Han F, Li D, Li W C, Sun Q, Zhang X Q and Lu A H 2013 Dopamine as the coating agent and carbon precursor for the fabrication of N-doped carbon coated Fe_3O_4 composites as superior lithium ion anodes *Nanoscale* **5** 1168

[233] Li L, Wang T T, Zhang L Y, Su Z M, Wang C G and Wang R S 2012 Selected-control synthesis of monodisperse Fe_3O_4@C core–shell spheres, chains, and rings as high-performance anode materials for lithium-ion batteries *Chem. Eur. J.* **18** 11417

[234] Chen D Y, Ji G, Ma Y, Lee J Y and Lu J M 2011 Graphene-encapsulated hollow Fe_3O_4 nanoparticle aggregates as a high-performance anode material for lithium ion batteries *ACS Appl. Mater. Interfaces* **3** 3078

[235] Chandra V, Park J, Chun Y, Lee J W, Hwang I-C and Kim K S 2010 Water-dispersible magnetite-reduced graphene oxide composites for arsenic removal *ACS Nano* **4** 3979

[236] Li J, Zhang S W, Chen C L, Zhao G X, Yang X, Li J X and Wang X K 2012 Removal of Cu(II) and fulvic acid by graphene oxide nanosheets decorated with Fe_3O_4 nanoparticles *ACS Appl. Mater. Interfaces* **4** 4991

[237] Liang J J, Huang Y, Oh J Y, Kozlov M, Sui D, Fang S L, Baughman R H, Ma Y F and Chen Y S 2011 Electromechanical actuators based on graphene and graphene/Fe_3O_4 hybrid paper *Adv. Funct. Mater.* **21** 3778

[238] Li X Y, Wang X, Song S Y, Liu D P and Zhang H J 2012 Selectively deposited noble metal nanoparticles on Fe_3O_4/graphene composites: stable, recyclable, and magnetically separable catalysts *Chem. Eur. J.* **18** 7601

[239] Liu Y W, Guan M X, Feng L, Deng S L, Bao J F, Xie S Y, Chen Z, Huang R B and Zheng L S 2013 Facile and straightforward synthesis of superparamagnetic reduced graphene oxide-Fe_3O_4 hybrid composite by a solvothermal reaction *Nanotechnology* **24** 025604

[240] Zhang Y, Chen B A, Zhang L M, Huang J, Chen F H, Yang Z P, Yao J L and Zhang Z J 2011 Controlled assembly of Fe_3O_4 magnetic nanoparticles on graphene oxide *Nanoscale* **3** 1446

[241] Fan X J, Jiao G Z, Zhao W, Jin P F and Li X 2013 Magnetic Fe_3O_4-graphene composites as targeted drug nanocarriers for pH-activated release *Nanoscale* **5** 1143

[242] Li X Y, Huang X L, Liu D P, Wang X, Song S Y, Zhou L and Zhang H J 2011 Synthesis of 3D hierarchical Fe_3O_4/graphene composites with high lithium storage capacity and for controlled drug delivery *J. Phys. Chem.* C **115** 21567

[243] Cong H-P, He J-J, Lu Y and Yu S-H 2010 Water-soluble magnetic-functionalized reduced graphene oxide sheets: *in situ* synthesis and magnetic resonance imaging applications *Small* **6** 169

[244] Chen W H, Yi P W, Zhang Y, Zhang L M, Deng Z W and Zhang Z J 2011 Composites of aminodextran-coated Fe_3O_4 nanoparticles and graphene oxide for cellular magnetic resonance imaging *ACS Appl. Mater. Interfaces* **3** 4085

[245] Henry A I, Bingham J M, Ringe E, Marks L D, Schatz G C and Van Duyne R P 2011 Correlated structure and optical property studies of plasmonic nanoparticles *J. Phys. Chem.* C **115** 9291

[246] Yen C W, Mahmoud M A and El-Sayed M A 2009 Photocatalysis in gold nanocage nanoreactors *J. Phys. Chem.* A **113** 4340

[247] Murphy C J, Gole A M, Hunyadi S E, Stone J W, Sisco P N, Alkilany A, Kinard B E and Hankins P 2008 Chemical sensing and imaging with metallic nanorods *Chem. Commun.* **544**

[248] Dreaden E C, Alkilany A M, Huang X, Murphy C J and El-Sayed M A 2011 The golden age: gold nanoparticles for biomedicine *Chem. Soc. Rev.* **41** 2740

[249] Zhang J H, Thurber A, Hanna C and Punnoose A 2010 Highly shape-selective synthesis, silica coating, self-assembly, and magnetic hydrogen sensing of hematite nanoparticles *Langmuir* **26** 5273

[250] Qiao B T, Wang A Q, Yang X F, Allard L F, Jiang Z, Cui Y T, Liu J Y, Li J and Zhang T 2011 Single-atom catalysis of CO oxidation using Pt-1/FeO_x *Nat. Chem.* **3** 634

[251] Thandavan K, Gandhi S, Sethuraman S, Rayappan J B and Krishnan U M 2011 A novel nanostructured iron oxide-gold bioelectrode for hydrogen peroxide sensing *Nanotechnology* **22** 265505

[252] Barnett C M, Gueorguieva M, Lees M R, McGarvey D J, Darton R J and Hoskins C 2012 Effect of the hybrid composition on the physicochemical properties and morphology of iron oxide-gold nanoparticles *J. Nanopart. Res.* **14** 1170

[253] Mahmoudi M, Serpooshan V and Laurent S 2011 Engineered nanoparticles for biomolecular imaging *Nanoscale* **3** 3007

[254] Arsianti M, Lim M, Lou S N, Goon I Y, Marquis C P and Amal R 2011 Bi-functional gold-coated magnetite

composites with improved biocompatibility *J. Colloid Interface Sci.* **354** 536

[255] Yallapu M M, Othman S F, Curtis E T, Gupta B K, Jaggi M and Chauhan S C 2011 Multi-functional magnetic nanoparticles for magnetic resonance imaging and cancer therapy *Biomater.* **32** 1890

[256] Guo S, Dong S and Wang E 2009 A general route to construct diverse multifunctional Fe_3O_4/metal hybrid nanostructures *Chem. Eur. J.* **15** 2416

[257] Kirui D K, Rey D A and Batt C A 2010 Gold hybrid nanoparticles for targeted phototherapy and cancer imaging *Nanotechnology* **21** 105105

[258] Chiang I C and Chen D H 2009 Structural characterization and self-assembly into superlattices of iron oxide-gold core–shell nanoparticles synthesized via a high-temperature organometallic route *Nanotechnology* **20** 015602

[259] Gu H W, Zheng R K, Zhang X X and Xu B 2004 Facile one-pot synthesis of bifunctional heterodimers of nanoparticles: a conjugate of quantum dot and magnetic nanoparticles *J. Am. Chem. Soc.* **126** 5664

[260] Kim D, Yu M K, Lee T S, Park J J, Jeong Y Y and Jon S 2011 Amphiphilic polymer-coated hybrid nanoparticles as CT/MRI dual contrast agents *Nanotechnology* **22** 155101

[261] Xu Y H Z and Sun S 2007 Magnetic core/shell Fe_3O_4/Au and Fe_3O_4/Au/Ag nanoparticles with tunable plasmonic properties *J. Am. Chem. Soc.* **129** 8698

[262] Wang L Y, Luo J, Maye M M, Fan Q, Qiang R D, Engelhard M H, Wang C M, Lin Y H and Zhong C J 2005 Iron oxide-gold core–shell nanoparticles and thin film assembly *J. Mater. Chem.* **15** 1821

[263] Zhai Y M, Zhai J F, Wang Y L, Guo S J, Ren W and Dong S J 2009 Fabrication of iron oxide core/gold shell submicrometer spheres with nanoscale surface roughness for efficient surface-enhanced raman scattering *J. Phys. Chem.* C **113** 7009

[264] Grzelczak M, Vermant J, Furst E M and Liz-Marzan L M 2010 Directed self-assembly of nanoparticles *ACS Nano* **4** 3591

[265] Ma L L *et al* 2009 Small multifunctional nanoclusters (nanoroses) for targeted cellular imaging and therapy *ACS Nano* **3** 2686

[266] Ou G F, Zhu H L, Zhu E Z, Gao L H and Chen J J 2010 Fe_3O_4-Au and Fe_2O_3-Au hybrid nanorods: layer-by-layer assembly synthesis and their magnetic and optical properties *Nanoscale Res. Lett.* **5** 1755

[267] Wang C, Xu C J, Zeng H and Sun S H 2009 Recent progress in syntheses and applications of dumbbell-like nanoparticles *Adv. Mater.* **21** 3045

[268] Wang C, Xu C, Zeng H and Sun S 2009 Recent progress in syntheses and applications of dumbbell-like nanoparticles *Adv. Mater.* **21** 3045

[269] Sun X, Guo S, Liu Y and Sun S 2012 Dumbbell-like PtPd–Fe_3O_4 nanoparticles for enhanced electrochemical detection of H_2O_2 *Nano Lett.* **12** 4859

[270] Wang C, Wei Y J, Jiang H Y and Sun S H 2009 Tug-of-war in nanoparticles: competitive growth of Au on Au-Fe_3O_4 nanoparticles *Nano Lett.* **9** 4544

[271] Sun X L, Guo S J, Liu Y and Sun S H 2012 Dumbbell-like PtPd-Fe_3O_4 nanoparticles for enhanced electrochemical detection of H_2O_2 *Nano Lett.* **12** 4859

[272] Buck M R, Bondi J F and Schaak R E 2011 A total-synthesis framework for the construction of high-order colloidal hybrid nanoparticles *Nat. Chem.* **4** 37

[273] Goon I Y, Lai L M H, Lim M, Munroe P, Gooding J J and Amal R 2009 Fabrication and dispersion of gold-shell-protected magnetite nanoparticles: systematic control using polyethyleneimine *Chem. Mater.* **21** 673

[274] Lim J K, Majetich S A and Tilton R D 2009 Stabilization of superparamagnetic iron oxide core-gold shell nanoparticles in high ionic strength media *Langmuir* **25** 13384

[275] Hsiao S C, Ou J L, Sung Y, Chang C P and Ger M D 2010 Preparation of sulfate- and carboxyl-functionalized magnetite/polystyrene spheres for further deposition of gold nanoparticles *Colloid Polym. Sci.* **288** 787

[276] Yeap S P, Toh P Y, Ahmad A L, Low S C, Majetich S A and Lim J 2012 Colloidal stability and magnetophoresis of gold-coated iron oxide nanorods in biological media *J. Phys. Chem.* C **116** 22561

[277] Zhou L, Gao C and Xu W J 2010 Robust Fe_3O_4/SiO_2-Pt/Au/Pd magnetic nanocatalysts with multifunctional hyperbranched polyglycerol amplifiers *Langmuir* **26** 11217

[278] Kyung Min Yeo J S A I S L 2010 Reductive dissolution of Fe_3O_4 facilitated by the Au domain of an Fe_3O_4/Au hybrid nanocrystal: formation of a nanorattle structure composed of a hollow porous silica nanoshell and entrapped Au nanocrystal *Chem. Commun.* **46** 64

[279] Sun L L, Wu W, Zhang S F, Liu Y C, Xiao X H, Ren F, Cai G X and Jiang C Z 2013 Spindle-like alpha-Fe_2O_3 embedded with TiO_2 nanocrystalline: ion implantation preparation and enhanced magnetic properties *J. Nanosci. Nanotechnol.* **13** 5428

[280] Sun L L, Wu W, Zhang S F, Zhou J, Cai G X, Ren F, Xiao X H, Dai Z G and Jiang C Z 2012 Novel doping for synthesis monodispersed TiO_2 grains filled into spindle-like hematite bi-component nanoparticles by ion implantation *AIP Adv.* **2** 032179

[281] Wu W, Xiao X H, Zhang S F, Ren F and Jiang C Z 2011 Facile method to synthesize magnetic iron oxides/TiO_2 hybrid nanoparticles and their photodegradation application of methylene blue *Nanoscale Res. Lett.* **6** 533

[282] Wu W, Zhang S F, Xiao X H, Zhou J, Ren F, Sun L L and Jiang C Z 2012 Controllable synthesis, magnetic properties, and enhanced photocatalytic activity of spindlelike mesoporous α-Fe_2O_3/ZnO core–shell heterostructures *ACS Appl. Mater. Interfaces* **4** 3602

[283] Wu W, Zhang S F, Ren F, Xiao X H, Zhou J and Jiang C Z 2011 Controlled synthesis of magnetic iron oxides@SnO_2 quasi-hollow core–shell heterostructures: formation mechanism, and enhanced photocatalytic activity *Nanoscale* **3** 4676

[284] Zhang S F, Ren F, Wu W, Zhou J, Xiao X H, Sun L L, Liu Y and Jiang C Z 2013 Controllable synthesis of recyclable core–shell γ-Fe_2O_3@SnO_2 hollow nanoparticles with enhanced photocatalytic and gas sensing properties *Phys. Chem. Chem. Phys.* **15** 8228

[285] Xi G C, Yue B, Cao J Y and Ye J H 2011 Fe_3O_4/WO_3 Hierarchical core–shell structure: high-performance and recyclable visible-light photocatalysis *Chem. Eur. J.* **17** 5145

[286] Li S K, Huang F Z, Wang Y, Shen Y H, Qiu L G, Xie A J and Xu S J 2011 Magnetic Fe_3O_4@C@Cu_2O composites with bean-like core/shell nanostructures: synthesis, properties and application in recyclable photocatalytic degradation of dye pollutants *J. Mater. Chem.* **21** 7459

[287] Joseph J, Nishad K K, Sharma M, Gupta D K, Singh R R and Pandey R K 2012 Fe_3O_4 and CdS based bifunctional core–shell nanostructure *Mater. Res. Bull.* **47** 1471

[288] Zhou S, Chen Q W, Hu X Y and Zhao T Y 2012 Bifunctional luminescent superparamagnetic nanocomposites of CdSe/CdS-Fe_3O_4 synthesized via a facile method *J. Mater. Chem.* **22** 8263

[289] Shi Y, Li H Y, Wang L, Shen W and Chen H Z 2012 Novel α-Fe_2O_3/CdS cornlike nanorods with enhanced photocatalytic performance *ACS Appl. Mater. Interfaces* **4** 4800

[290] Yu X, Wan J, Shan Y, Chen K and Han X 2009 A facile approach to fabrication of bifunctional magnetic-optical Fe$_3$O$_4$@ ZnS microspheres *Chem. Mater.* **21** 4892

[291] Liu L, Xiao L, Zhu H-Y and Shi X-W 2013 Studies on interaction and illumination damage of CS-Fe$_3$O$_4$@ZnS: Mn to bovine serum albumin *J. Nanopart. Res.* **15** 1394

[292] Zhou W, Chen Y, Wang X, Guo Z and Hu Y 2011 Synthesis of Fe$_3$O$_4$@PbS hybrid nanoparticles through the combination of surface-initiated atom transfer radical polymerization and acidolysis by H$_2$S *J. Nanosci. Nanotechnol.* **11** 98

[293] Luo S R, Chai F, Zhang L Y, Wang C G, Li L, Liu X C and Su Z M 2012 Facile and fast synthesis of urchin-shaped Fe$_3$O$_4$@Bi$_2$S$_3$ core–shell hierarchical structures and their magnetically recyclable photocatalytic activity *J. Mater. Chem.* **22** 4832

[294] Lee N *et al* 2012 Multifunctional Fe$_3$O$_4$/TaO$_x$ core/shell nanoparticles for simultaneous magnetic resonance imaging and x-ray computed tomography *J. Am. Chem. Soc.* **134** 10309

[295] Wang Z, Wu L, Chen M and Zhou S 2009 Facile synthesis of superparamagnetic fluorescent Fe$_3$O$_4$/ZnS hollow nanospheres *J. Am. Chem. Soc.* **131** 11276

[296] Tian Y, Wu D, Jia X, Yu B and Zhan S 2011 Core–shell nanostructure of α-Fe$_2$O$_3$/Fe$_3$O$_4$: synthesis and photocatalysis for methyl orange *J. Nanomater.* **2011** 29

[297] Wang X, Zhong Y, Zhai T, Guo Y, Chen S, Ma Y, Yao J, Bando Y and Golberg D 2011 Multishelled Co$_3$O$_4$-Fe$_3$O$_4$ hollow spheres with even magnetic phase distribution: synthesis, magnetic properties and their application in water treatment *J. Mater. Chem.* **21** 17680

[298] Kumari S and Singh R P 2013 Glycolic acid-functionalized chitosan-Co$_3$O$_4$-Fe$_3$O$_4$ hybrid magnetic nanoparticles-based nanohybrid scaffolds for drug-delivery and tissue engineering *J. Mater. Sci.* **48** 1524

[299] Zhang S, Li J, Wen T, Xu J and Wang X 2013 Magnetic Fe$_3$O$_4$@NiO hierarchical structures: preparation and their excellent As(V) and Cr(VI) removal capabilities *RSC Adv.* **3** 2754

[300] Estrade S, Yedra L, Lopez-Ortega A, Estrader M, Salazar-Alvarez G, Baro M, Nogues J and Peiro F 2012 Distinguishing the core from the shell in MnO$_x$/MnO$_y$ and FeO$_x$/MnO$_x$ core/shell nanoparticles through quantitative electron energy loss spectroscopy (EELS) analysis *Micron* **43** 30

[301] Krycka K L *et al* 2013 Resolving material-specific structures within Fe$_3$O$_4$|γ-Mn$_2$O$_3$ core/shell nanoparticles using anomalous small-angle x-ray scattering *ACS Nano* **7** 921

[302] Manna P, Yusuf S, Basu M and Pal T 2011 The magnetic proximity effect in a ferrimagnetic Fe$_3$O$_4$ core/ferrimagnetic γ-Mn$_2$O$_3$ shell nanoparticle system *J. Phys. Condens. Matter* **23** 506004

[303] Liu Z, Li M, Pu F, Ren J, Yang X and Qu X 2012 Hierarchical magnetic core–shell nanoarchitectures: non-linker reagent synthetic route and applications in a biomolecule separation system *J. Mater. Chem.* **22** 2935

[304] Peng X, Chen H, Huang J, Mao H and Shin D M 2011 Targeted magnetic iron oxide nanoparticles for tumor imaging and therapy *Biomedical Engineering—From Theory to Applications* (Rijeka: InTech)

[305] Arruebo M, Fernández-Pacheco R, Ibarra M R and Santamaría J 2007 Magnetic nanoparticles for drug delivery *Nano Today* **2** 22

[306] Durán J D, Arias J L, Gallardo V and Delgado A V 2008 Magnetic colloids as drug vehicles *J. Pharm. Sci.* **97** 2948

[307] Cao S W, Zhu Y J, Ma M Y, Li L and Zhang L 2008 Hierarchically nanostructured magnetic hollow spheres of Fe$_3$O$_4$ and gamma-Fe$_2$O$_3$: preparation and potential application in drug delivery *J. Phys. Chem.* C **112** 1851

[308] Wahajuddin and Arora S 2012 Superparamagnetic iron oxide nanoparticles: magnetic nanoplatforms as drug carriers *Int. J. Nanomed.* **7** 3445

[309] Banerjee S S and Chen D H 2010 Grafting of 2-hydroxypropyl-beta-cyclodextrin on gum arabic-modified iron oxide nanoparticles as a magnetic carrier for targeted delivery of hydrophobic anticancer drug *Int. J. Appl. Ceram. Technol.* **7** 111

[310] Zhu Y F, Fang Y and Kaskel S 2010 Folate-conjugated Fe$_3$O$_4$@SiO$_2$ hollow mesoporous spheres for targeted anticancer drug delivery *J. Phys. Chem.* C **114** 16382

[311] Talelli M, Rijcken C J F, Lammers T, Seevinck P R, Storm G, van Nostrum C F and Hennink W E 2009 Superparamagnetic iron oxide nanoparticles encapsulated in biodegradable thermosensitive polymeric micelles: toward a targeted nanomedicine suitable for image-guided drug delivery *Langmuir* **25** 2060

[312] Hasenpusch G *et al* 2012 Magnetized aerosols comprising superparamagnetic iron oxide nanoparticles improve targeted drug and gene delivery to the lung *Pharm. Res.* **29** 1308

[313] Wan Q *et al* 2013 Self-assembled magnetic theranostic nanoparticles for highly sensitive MRI of minicircle DNA delivery *Nanoscale* **5** 744

[314] Liu S, Xing R, Lu F, Rana R K and Zhu J-J 2009 One-pot template-free fabrication of hollow magnetite nanospheres and their application as potential drug carriers *J. Phys. Chem.* C **113** 21042

[315] Cao S-W, Zhu Y-J, Ma M-Y, Li L and Zhang L 2008 Hierarchically nanostructured magnetic hollow spheres of Fe$_3$O$_4$ and Fe$_2$O$_3$: preparation and potential application in drug delivery *J. Phys. Chem.* C **112** 1851

[316] Chen F H, Zhang L M, Chen Q T, Zhang Y and Zhang Z J 2010 Synthesis of a novel magnetic drug delivery system composed of doxorubicin-conjugated Fe$_3$O$_4$ nanoparticle cores and a PEG-functionalized porous silica shell *Chem. Commun.* **46** 8633

[317] Kayal S and Ramanujan R V 2010 Doxorubicin loaded PVA coated iron oxide nanoparticles for targeted drug delivery *Mat. Sci. Eng.* C **30** 484

[318] Zhu X, Yuan J, Leung K, Lee S, Sham K, Cheng C, Au D, Teng G, Ahuja A and Wang Y 2012 Hollow superparamagnetic iron oxide nanoshells as a hydrophobic anticancer drug carrier: intracelluar pH-dependent drug release and enhanced cytotoxicity *Nanoscale* **4** 5744

[319] Kim S, Kim J H, Jeon O, Kwon I C and Park K 2009 Engineered polymers for advanced drug delivery *Eur. J. Pharm. Biopharm.* **71** 420

[320] Zhang J and Misra R D K 2007 Magnetic drug-targeting carrier encapsulated with thermosensitive smart polymer: core–shell nanoparticle carrier and drug release response *Acta Biomater.* **3** 838

[321] Patel M, Patel R and Patel J 2010 Chitosan mediated targeted drug delivery system: a review *J. Pharm. Pharm. Sci.* **13** 536

[322] Yang X, Grailer J J, Rowland I J, Javadi A, Hurley S A, Matson V Z, Steeber D A and Gong S 2010 Multifunctional stable and pH-responsive polymer vesicles formed by heterofunctional triblock copolymer for targeted anticancer drug delivery and ultrasensitive MR imaging *ACS Nano* **4** 6805

[323] Chen Y C, Liao L C, Lu P L, Lo C L, Tsai H C, Huang C Y, Wei K C, Yen T C and Hsiue G H 2012 The accumulation of dual pH and temperature responsive micelles in tumors *Biomater.* **33** 4576

[324] Zou P, Yu Y K, Wang Y A, Zhong Y Q, Welton A, Galban C, Wang S M and Sun D X 2010 Superparamagnetic iron oxide nanotheranostics for targeted cancer cell imaging and pH-dependent intracellular drug release *Mol. Pharm.* **7** 1974

[325] Peng X H, Qian X M, Mao H, Wang A Y, Chen Z, Nie S M and Shin D M 2008 Targeted magnetic iron oxide nanoparticles for tumor imaging and therapy *Int. J. Nanomed.* **3** 311

[326] Chen Y J, Tao J A, Xiong F, Zhu J B, Gu N, Zhang Y H, Ding Y and Ge L A 2010 Synthesis, self-assembly, and characterization of PEG-coated iron oxide nanoparticles as potential MRI contrast agent *Drug Dev. Ind. Pharm.* **36** 1235

[327] Chow A M, Chan K W Y, Cheung J S and Wu E X 2010 Enhancement of gas-filled microbubble R-2* by iron oxide nanoparticles for MRI *Magn. Reson. Med.* **63** 224

[328] John R, Rezaeipoor R, Adie S G, Chaney E J, Oldenburg A L, Marjanovic M, Haldar J P, Sutton B P and Boppart S A 2010 *In vivo* magnetomotive optical molecular imaging using targeted magnetic nanoprobes *Proc. Natl Acad. Sci.* **107** 8085

[329] Hadjipanayis C, Machaidze R, Kaluzova M, Wang L, Schuette A, Chen H, Wu X and Mao H 2010 EGFRvIII antibody-conjugated iron oxide nanoparticles for magnetic resonance imaging-guided convection-enhanced delivery and targeted therapy of glioblastoma *Cancer Res.* **70** 6303

[330] Basly B, Felder-Flesch D, Perriat P, Billotey C, Taleb J, Pourroy G and Begin-Colin S 2010 Dendronized iron oxide nanoparticles as contrast agents for MRI *Chem. Commun.* **46** 985

[331] Wu Y L, Ye Q, Foley L M, Hitchens T K, Sato K, Williams J B and Ho C 2006 *In situ* labeling of immune cells with iron oxide particles: an approach to detect organ rejection by cellular MRI *Proc. Natl Acad. Sci.* **103** 1852

[332] Tsai Z T, Wang J F, Kuo H Y, Shen C R, Wang J J and Yen T C 2010 *In situ* preparation of high relaxivity iron oxide nanoparticles by coating with chitosan: a potential MRI contrast agent useful for cell tracking *J. Magn. Magn. Mater.* **322** 208

[333] Asanuma T *et al* 2010 Super paramagnetic iron oxide MRI shows defective kupffer cell uptake function in non-alcoholic fatty liver disease *Gut* **59** 258

[334] Branca R T, Cleveland Z I, Fubara B, Kumar C S S R, Maronpot R R, Leuschner C, Warren W S and Driehuys B 2010 Molecular MRI for sensitive and specific detection of lung metastases *Proc. Natl Acad. Sci.* **107** 3693

[335] Zhang Z L, Dharmakumar R, Mascheri N, Fan Z Y, Wu S Y and Li D B 2009 Comparison of superparamagnetic and ultrasmall superparamagnetic iron oxide cell labeling for tracking green fluorescent protein gene marker with negative and positive contrast magnetic resonance imaging *Mol. Imaging* **8** 148

[336] Bulte J W M and Kraitchman D L 2004 Iron oxide MR contrast agents for molecular and cellular imaging *NMR Biomed.* **17** 484

[337] Joshi H M, De M, Richter F, He J, Prasad P and Dravid V P 2013 Effect of silica shell thickness of Fe_3O_4-SiO_x core–shell nanostructures on MRI contrast *J. Nanopart. Res.* **15** 1448

[338] Mahmoud W E, Bronstein L M, Al-Hazmi F, Al-Noaiser F and Al-Ghamdi A A 2013 Development of Fe/Fe_3O_4 core–shell nanocubes as a promising MRI contrast agent *Langmuir* **29** 13095

[339] Zeng L, Ren W, Xiang L, Zheng J, Chen B and Wu A 2013 Multifunctional Fe_3O_4-TiO_2 nanocomposites for magnetic resonance imaging and potential photodynamic therapy *Nanoscale* **5** 2107

[340] Smolensky E D, Neary M C, Zhou Y, Berquo T S and Pierre V C 2011 Fe_3O_4@organic@Au: core–shell nanocomposites with high saturation magnetisation as magnetoplasmonic MRI contrast agents *Chem. Commun.* **47** 2149

[341] Zhou Y-M, Gong M, Sun Z, Cheng K, Guo Z and Chen Q 2013 Yolk-type Au@Fe_3O_4@C nanospheres for drug delivery, MRI and two-photon fluorescence imaging *Dalton Trans.* **42** 9906

[342] O'Grady K 2009 Progress in applications of magnetic nanoparticles in biomedicine *J. Phys. D: Appl. Phys.* **42** 220301

[343] Roca A G, Costo R, Rebolledo A F, Veintemillas-Verdaguer S, Tartaj P, Gonzalez-Carreno T, Morales M P and Serna C J 2009 Progress in the preparation of magnetic nanoparticles for applications in biomedicine *J. Phys. D: Appl. Phys.* **42** 224002

[344] Thomas L A, Dekker L, Kallumadil M, Southern P, Wilson M, Nair S P, Pankhurst Q A and Parkin I P 2009 Carboxylic acid-stabilised iron oxide nanoparticles for use in magnetic hyperthermia *J. Mater. Chem.* **19** 6529

[345] Kita E *et al* 2010 Ferromagnetic nanoparticles for magnetic hyperthermia and thermoablation therapy *J. Phys. D: Appl. Phys.* **43** 474011

[346] This picture is copied from website: www.ims.demokritos.gr and Rabias I *et al* 2010 Rapid magnetic heating treatment by highly charged maghemite nanoparticles on wistar rats exocranial glioma tumours at micro litre volume *Biomicrofluidics* **4** 024111

[347] Maier-Hauff K *et al* 2007 Intracranial thermotherapy using magnetic nanoparticles combined with external beam radiotherapy: results of a feasibility study on patients with glioblastoma multiforme *J. Neuro. Oncol.* **81** 53

[348] Tasci T O, Vargel I, Arat A, Guzel E, Korkusuz P and Atalar E 2009 Focused RF hyperthermia using magnetic fluids *Med. Phys.* **36** 1906

[349] Yang F, Li Y X, Chen Z P, Zhang Y, Wu J R and Gu N 2009 Superparamagnetic iron oxide nanoparticle-embedded encapsulated microbubbles as dual contrast agents of magnetic resonance and ultrasound imaging *Biomaterials* **30** 3882

[350] Virtanen H, Keshvari J and Lappalainen R 2006 Interaction of radio frequency electromagnetic fields and passive metallic implants—a brief review *Bioelectromagnetics* **27** 431–9

[351] Gonzales-Weimuller M, Zeisberger M and Krishnan K M 2009 Size-dependant heating rates of iron oxide nanoparticles for magnetic fluid hyperthermia *J. Magn. Magn. Mater.* **321** 1947

[352] Liu X L, Fan H M, Yi J B, Yang Y, Choo E S G, Xue J M, Fan D D and Ding J 2012 Optimization of surface coating on Fe_3O_4 nanoparticles for high performance magnetic hyperthermia agents *J. Mater. Chem.* **22** 8235

[353] Mohammad F, Balaji G, Weber A, Uppu R M and Kumar C S S R 2010 Influence of gold nanoshell on hyperthermia of superparamagnetic iron oxide nanoparticles *J. Phys. Chem. C* **114** 19194

[354] Balivada S *et al* 2010 A/C magnetic hyperthermia of melanoma mediated by iron(0)/iron oxide core/shell magnetic nanoparticles: a mouse study *BMC Cancer* **10** 119

[355] Shao D D, Xu K K, Song X J, Hu J H, Yang W L and Wang C C 2009 Effective adsorption and separation of lysozyme with PAA-modified Fe_3O_4@silica core/shell microspheres *J. Colloid Interface Sci.* **336** 526

[356] Chen F, Shi R B, Xue Y, Chen L and Wan Q H 2010 Templated synthesis of monodisperse mesoporous maghemite/silica microspheres for magnetic separation of genomic DNA *J. Magn. Magn. Mater.* **322** 2439

[357] Du C L, Du W, Wang B, Feng W Y, Wang Z and Zhao Y L 2010 Bioseparation and bioassay based on iron oxide nanomaterials properties *Chin. J. Anal. Chem.* **38** 902

[358] Wu H D, Qian H, Yu Z J and Ye W H 2010 An effective magnetic separation technique for antibody based on thiophilic paramagnetic polymer beads *Acta Polym. Sin.* 1238

[359] Latham A H and Williams M E 2008 Controlling transport and chemical functionality of magnetic nanoparticles *Acc. Chem. Res.* **41** 411

[360] Chang J H, Lee J, Jeong Y, Lee J H, Kim I J and Park S E 2010 Hydrophobic partitioning approach to efficient protein separation with magnetic nanoparticles *Anal. Biochem.* **405** 135

[361] Wang C G and Irudayaraj J 2010 Multifunctional magnetic-optical nanoparticle probes for simultaneous detection, separation, and thermal ablation of multiple pathogens *Small* **6** 283

[362] Reza R T, Perez C A M, Martinez A M, Baques D B and Garcia-casillas P E 2010 study of the particle size effect on the magnetic separation of bovine serum albumin (BSA) *Sensor Lett.* **8** 476

[363] Arsianti M, Lim M, Marquis C P and Amal R 2010 Assembly of polyethylenimine-based magnetic iron oxide vectors: insights into gene delivery *Langmuir* **26** 7314

[364] Bao F, Yao J-L and Gu R-A 2009 Synthesis of magnetic Fe_2O_3/Au core/shell nanoparticles for bioseparation and immunoassay based on surface-enhanced Raman spectroscopy *Langmuir* **25** 10782

[365] Xie H-Y, Zhen R, Wang B, Feng Y-J, Chen P and Hao J 2010 Fe_3O_4/Au core/shell nanoparticles modified with Ni^{2+}-nitrilotriacetic acid specific to histidine-tagged proteins *J. Phys. Chem.* C **114** 4825

[366] Chen H, Deng C and Zhang X 2010 Synthesis of Fe_3O_4@SiO_2@PMMA core–shell–shell magnetic microspheres for highly efficient enrichment of peptides and proteins for MALDI-ToF MS analysis *Angew. Chem. Int. Edn* **49** 607

[367] Shao M, Ning F, Zhao J, Wei M, Evans D G and Duan X 2012 Preparation of Fe_3O_4@SiO_2@layered double hydroxide core–shell microspheres for magnetic separation of proteins *J. Am. Chem. Soc.* **134** 1071

[368] Haun J B, Yoon T J, Lee H and Weissleder R 2010 Magnetic nanoparticle biosensors *Wires. Nanomed. Nanobi.* **2** 291

[369] Perez J M and Kaittanis C 2008 *Nanoparticles in Biomedical Imaging* vol 102 ed J W M Bulte and M M J Modo (New York: Springer) p 183

[370] Perez J M, Josephson L and Weissleder R 2004 Use of magnetic nanoparticles as nanosensors to probe for molecular interactions *Chem. Bio. Chem.* **5** 261

[371] Grimm J, Perez J M, Josephson L and Weissleder R 2004 Novel nanosensors for rapid analysis of telomerase activity *Cancer Res.* **64** 639

[372] Wang Y, Dostalek J and Knoll W 2011 Magnetic nanoparticle-enhanced biosensor based on grating-coupled surface plasmon resonance *Anal. Chem.* **83** 6202

[373] Depalo N, Carrieri P, Comparelli R, Striccoli M, Agostiano A, Bertinetti L, Innocenti C, Sangregorio C and Curri M L 2011 Biofunctionalization of anisotropic nanocrystalline semiconductor-magnetic heterostructures *Langmuir* **27** 6962

[374] Li J P, Zhu W Y and Wang H Z 2009 Novel magnetic single-walled carbon nanotubes/methylene blue composite amperometric biosensor for DNA determination *Anal. Lett.* **42** 366

[375] Perez-Lopez B and Merkoci A 2011 Magnetic nanoparticles modified with carbon nanotubes for electrocatalytic magnetoswitchable biosensing applications *Adv. Funct. Mater.* **21** 255

[376] Stanley S A, Gagner J E, Damanpour S, Yoshida M, Dordick J S and Friedman J M 2012 Radio-wave heating of iron oxide nanoparticles can regulate plasma glucose in mice *Science* **336** 604

[377] Nouira W, Maaref A, Siadat M, Errachid A and Jaffrezic-Renault N 2011 Conductometric biosensors based on layer-by-layer coated paramagnetic nanoparticles for urea detection *Sensor Lett.* **9** 2272

[378] Teymourian H, Salimi A and Hallaj R 2012 Low potential detection of NADH based on Fe_3O_4 nanoparticles/multiwalled carbon nanotubes composite: fabrication of integrated dehydrogenase-based lactate biosensor *Biosens. Bioelectron.* **33** 60

[379] Sandhu A, Handa H and Abe M 2010 Synthesis and applications of magnetic nanoparticles for biorecognition and point of care medical diagnostics *Nanotechnology* **21** 442001

[380] Tan X C, Zhang J L, Tan S W, Zhao D D, Huang Z W, Mi Y and Huang Z Y 2009 Amperometric hydrogen peroxide biosensor based on horseradish peroxidase immobilized on Fe_3O_4/chitosan modified glassy carbon electrode *Electroanal.* **21** 1514

[381] Yang L Q, Ren X L, Tang F Q and Zhang L 2009 A practical glucose biosensor based on Fe_3O_4 nanoparticles and chitosan/nafion composite film *Biosens. Bioelectron.* **25** 889

[382] Sun X, Li Q Q, Wang X Y and Du S Y 2012 Amperometric immunosensor based on gold nanoparticles/Fe_3O_4-FCNTS-CS composite film functionalized interface for carbofuran detection *Anal. Lett.* **45** 1604

[383] Li J P, Li S H and Yang C F 2012 Electrochemical biosensors for cancer biomarker detection *Electroanal.* **24** 2213

[384] Bellan L M, Wu D and Langer R S 2011 Current trends in nanobiosensor technology *Wires. Nanomed. Nanobi.* **3** 229

[385] Burtea C *et al* 2011 *In vitro* biomedical applications of functionalized iron oxide nanoparticles, including those not related to magnetic properties *Contrast Media. Mol. I.* **6** 236

[386] Li H, Wei Q, He J, Li T, Zhao Y F, Cai Y Y, Du B, Qian Z Y and Yang M H 2011 Electrochemical immunosensors for cancer biomarker with signal amplification based on ferrocene functionalized iron oxide nanoparticles *Biosens. Bioelectron.* **26** 3590

[387] Zhuo Y, Yuan P X, Yuan R, Chai Y Q and Hong C L 2009 Bienzyme functionalized three-layer composite magnetic nanoparticles for electrochemical immunosensors *Biomater.* **30** 2284

[388] Li J J, Yuan R, Chai Y Q and Che X 2010 Fabrication of a novel glucose biosensor based on Pt nanoparticles-decorated iron oxide-multiwall carbon nanotubes magnetic composite *J. Mol. Catal. B—Enzym.* **66** 8

[389] Singh R, Verma R, Sumana G, Srivastava A K, Sood S, Gupta R K and Malhotra B D 2012 Nanobiocomposite platform based on polyaniline-iron oxide-carbon nanotubes for bacterial detection *Bioelectrochem.* **86** 30

[390] Ariga K, Ji Q M, McShane M J, Lvov Y M, Vinu A and Hill J P 2012 Inorganic nanoarchitectonics for biological applications *Chem. Mater.* **24** 728

[391] Chan T and Gu F 2012 Development of a colorimetric, superparamagnetic biosensor for the capture and detection of biomolecules *Biosens. Bioelectron.* **42C** 12

[392] Arrabito G and Pignataro B 2012 Solution processed micro- and nano-bioarrays for multiplexed biosensing *Analyt. Chem.* **84** 5450

[393] Monosik R, Stred'ansky M and Sturdik E 2012 Application of electrochemical biosensors in clinical diagnosis *J. Clin. Lab. Anal.* **26** 22

[394] Devadasu V R, Bhardwaj V and Kumar M N V R 2013 Can controversial nanotechnology promise drug delivery? *Chem. Rev.* **113** 1686

[395] Mitragotri S and Lahann J 2009 Physical approaches to biomaterial design *Nat. Mater.* **8** 15

[396] Amstad E, Textor M and Reimhult E 2011 Stabilization and functionalization of iron oxide nanoparticles for biomedical applications *Nanoscale* **3** 2819

[397] Reddy L H, Arias J L, Nicolas J and Couvreur P 2012 Magnetic nanoparticles: design and characterization, toxicity

and biocompatibility, pharmaceutical and biomedical applications *Chem. Rev.* **112** 5818

[398] Wu W, Jiang C Z and Roy V A L 2015 Recent progress in magnetic iron oxide-semiconductor composite nanomaterials as promising photocatalysts *Nanoscale* **7** 38

[399] Rivet C J, Yuan Y, Borca-Tasciuc D A and Gilbert R J 2012 Altering iron oxide nanoparticle surface properties induce cortical neuron cytotoxicity *Chem. Res. Toxicol.* **25** 153

[400] Mahmoudi M, Hofmann H, Rothen-Rutishauser B and Petri-Fink A 2012 Assessing the *in vitro* and *in vivo* toxicity

of superparamagnetic iron oxide nanoparticles *Chem. Rev.* **112** 2323

[401] Laurent S, Forge D, Port M, Roch A, Robic C, Elst L V and Muller R N 2010 Magnetic iron oxide nanoparticles: synthesis, stabilization, vectorization, physicochemical characterizations, and biological applications *Chem. Rev.* **110** 2574

[402] Terreno E, Delli Castelli D, Viale A and Aime S 2010 Challenges for molecular magnetic resonance imaging *Chem. Rev.* **110** 3019